



HAL
open science

Electronic refrigeration using superconducting tunnel junctions

Sukumar Rajauria

► **To cite this version:**

Sukumar Rajauria. Electronic refrigeration using superconducting tunnel junctions. Superconductivity [cond-mat.supr-con]. Université Joseph-Fourier - Grenoble I, 2008. English. NNT: . tel-00371431

HAL Id: tel-00371431

<https://theses.hal.science/tel-00371431>

Submitted on 27 Mar 2009

HAL is a multi-disciplinary open access archive for the deposit and dissemination of scientific research documents, whether they are published or not. The documents may come from teaching and research institutions in France or abroad, or from public or private research centers.

L'archive ouverte pluridisciplinaire **HAL**, est destinée au dépôt et à la diffusion de documents scientifiques de niveau recherche, publiés ou non, émanant des établissements d'enseignement et de recherche français ou étrangers, des laboratoires publics ou privés.

Thèse
présentée par
Sukumar Rajauria

pour obtenir le titre de Docteur
de l'Université Joseph Fourier - Grenoble I
en Physique

**Electronic refrigeration using
superconducting tunnel junctions**

Soutenue publiquement le 14 novembre 2008 à Grenoble devant le Jury:

Cristián Urbina, Président
Jukka Pekola, Rapporteur
Sophie Guéron, Rapportrice
Philippe Gandit, Examineur
Anjan Gupta, Examineur
Hervé Courtois, Codirecteur de thèse
Bernard Pannetier, Directeur de thèse

Thèse préparée à l'Institut Néel
CNRS - UJF - Grenoble

Acknowledgements

'Ideas move fast when their time comes'. I thank God for running the clock and for giving us the joy, laughter, strength and passion to follow our dreams. I am thankful that my stay in Grenoble has been immensely enriched by unforgettable friends and colleagues, whom I shall always cherish.

I thank to Bernard Pannetier for giving this opportunity. He is an institution of knowledge in himself. His teaching, experimental skill and intuition as a physicist is immense which I hope to emulate some day. His persistence in understanding the phenomena motivated/pushed me to work hard to find out the explanation. Bernard, thank you for being the nurturing adviser.

I would like to thank Hervé Courtois, whose door was always open for me whenever I ran into trouble spot or had a question about any idea. He allowed me to have an independent thought, but still steered me in the right direction whenever he thought I needed it. From lab to dam, from physics facts to life, from experiments to running...I learned, you survived, thank you.

Frank Hekking, thank you for being my unofficial *guru*, for explaining the most basic and also very sophisticated of theoretical nuance...and making it real. Thank you for all long and extremely learning discussion.

This thesis is a result of numerous collaboration with whom I worked extensively through the course of my research. T. Fournier, T. Crozes, B. Fernandez and C. Lemonias for nano-fabrication. P. Brosse helped me in cryogenics and electronics shop for the electronics of my experiment. Ph. Gandit for many discussions and experiments done in his dilution refrigerator. A. Vasenko and M. Houzet for many fruitful discussions. P. S. Luo for many discussions on white board and also for the delicious vegetarian Chinese food. E. Favre-Nicolin for the initial encouraging results on micro-coolers. I am happy and thankful to have had the opportunity to explore and learn from all of you. A special thank to all the secretaries of Nano department for being very patient with me, especially with my French language and still giving their beautiful smile.

I am thankful to C. Urbina, J. Pekola, S. Guéron, Ph. Gandit and A. Gupta for accepting the invitation for my PhD defense. A special thank to Anjan for his constant support and encouragement over the years and for numerous conversation that have shaped my horizon in more ways than I am consciously aware of and also coming all the way from India to attend my defense.

As someone said *'A journey is easier when you travel together'*. I have always believed that interdependence is more valuable than independence. I would like to thank all the

members of second floor in CRTBT for creating such a splendid setting. Aurélien, Cécile, Julien, Franck - Rudi, Florent, Thomas, Ioan, Loren, Laetitia and Olivier, I thank you all for having shared many experiences and thoughts with me. I always felt as if I am in a family away from a family. Laetitia, Ioan and Thomas, I learnt more from you more than I could have imagined for, thank you for the truly infectious enthusiasm. Aurélien and Franck, thank you for everything - for laughter, cheering and teasing...for being a friend. I have the feeling that I have known all of you all my life. Dada, Jitu, Boss and Pranjit, thank you for being extremely supportive, funny and for making me a good chef.

I have been fortunate to come across many funny and good friends, without whom life would be bleak. A special thank goes to Bhaskar, Sunny and Rahul, whom I have known for more than 15 years now and showed to be kind, mostly helpful and trustful friends. Ashish, Mona, Lala and Abhishek thank you for all the help, generosity and encouragement during all these years.

I am very grateful to my parents, sister and jiju - whom have always encouraged and supported me to dreams, to have passion and for care freeness...thank you.

Merci beaucoup!

Contents

1	Introduction	7
1.1	Historical background	7
1.2	Motivation for this work	10
2	Cooling effect in S-I-N-I-S tunnel junction	17
2.1	Introduction	17
2.2	Quasiparticle tunnel current in a N-I-S junction	18
2.2.1	Tunnel Hamiltonian	18
2.2.2	Tunnel current across N-I-S junction: golden rule	18
2.3	Heat transfer in the mesoscopic tunnel junction	21
2.3.1	Heat transfer in Normal metal - Insulator - Normal metal junction	21
2.3.2	Heat transfer in Normal metal - Insulator - Superconductor junction	23
2.4	Cooling using a pair of N-I-S junction	25
3	Andreev current in a S-I-N junction	27
3.1	Introduction	27
3.2	Andreev reflection	27
3.2.1	Andreev reflection: BTK model	28
3.3	Phase-coherent Andreev reflection - Historical introduction	31
3.3.1	Excess current in superconductor-semiconductor junction	31
3.3.2	Qualitative explanation of zero bias anomaly	32
3.3.3	Flux modulation in NS-QUIDS	32
3.4	Quantitative model: Hekking and Nazarov	33
3.5	Current - voltage relation in disordered N-I-S junctions	39
3.5.1	Phase-coherent Andreev current	39
3.5.2	Cooperon solution in quasi 1-D diffusive wire	40
3.5.3	Full expression for the Andreev current	40
3.5.4	Temperature dependence of the Andreev current	42
3.5.5	Relevant cut-off length of Andreev pair	42
3.5.6	Non-uniform tunnel barrier	45
3.6	Heat contribution due to phase-coherent Andreev current	47

4	Sample fabrication and experimental techniques	49
4.1	Introduction	49
4.2	Nano-fabrication	49
4.2.1	Bilayer resist coating	50
4.2.2	Electron beam lithography, the EBL	50
4.2.3	Development of resist	51
4.2.4	Metal deposition	52
4.2.5	Lift-off	56
4.3	Example: Fabrication procedure of the individual samples	56
4.4	Measurement apparatus	58
5	Inherent thermometer in a S-I-N-I-S cooling junction	63
5.1	Introduction	63
5.2	External electronic thermometer	63
5.2.1	Experiment with an external thermometer	65
5.3	Inherent electron thermometer in cooler junction	67
5.3.1	Introduction	67
5.3.2	Sample with no external thermometer	68
5.3.3	Experiments	69
5.3.4	Quasi-equilibrium in the S-I-N-I-S cooling junction	71
5.3.5	Comparison with experiments	74
5.4	Assumption to extract electronic temperature	76
5.4.1	Energy states in superconductor energy gap	77
5.4.2	Tunnel current due to second order processes	79
5.5	Extraction of electron temperature	80
5.6	Conclusion	83
6	Electron and phonon cooling in micro-coolers	85
6.1	Introduction	85
6.2	The thermal model	86
6.2.1	Thermal model taken for cooling device	87
6.2.2	Non equilibrium phonon distribution	88
6.3	Experiments on a S-I-N-I-S cooler	91
6.4	Thermal model in a S-I-N-I-S cooler	92
6.5	Electron and Phonon cooling in the S-I-N-I-S junction	94
6.6	Conclusion	97
7	Andreev current-induced dissipation	99
7.1	Introduction	99
7.2	Experimental observation of phase-coherent Andreev current	100
7.2.1	Introduction	100
7.2.2	Experiment on Probe junction	100
7.2.3	Phase-coherent Andreev current in Probe junction	101

7.2.4	The Fit parameters for the phase-coherent Andreev current	103
7.3	Cooler junction at low temperature	105
7.3.1	The behavior of the cooler junction in the presence of an Andreev current	106
7.4	The Andreev current induced dissipation	109
7.5	Thermal model with Andreev dissipation	111
7.6	Conclusion	113
7.6.1	Taper coherence	114
7.6.2	The ultimate cooling device	115
8	Quasiparticle diffusion based heating in S-I-N-I-S coolers	117
8.1	Introduction	117
8.2	Quasiparticle diffusion along the superconducting strip	118
8.2.1	Introduction	118
8.2.2	Phenomenological model	118
8.2.3	Connection to experimental parameters	120
8.2.4	Exact solution	121
8.3	Parasitic power in the cooler	122
8.3.1	Quasiparticle back-tunneling	122
8.3.2	Reabsorption of 2Δ phonons	123
8.3.3	Comparison of parasitic back-tunneling and phonon reabsorption power	124
8.4	Preliminary experimental connection with theory	124
9	Conclusions and perspectives	127
A	Normal state tunnel conductance	131
B	Phase-coherent Andreev current in a N-I-S junction	135
C	Publications	141

Chapter 1

Introduction

1.1 Historical background

Photons of the Cosmic microwave background CMB radiations have the lowest temperature in the Nature [1]. It has a thermal black body spectrum at a temperature of 2.73 K. Low temperature physics has already surpassed it by several orders of magnitude. The credit for the embarkation of the golden era goes to the Dutch scientist Heike Kamerlingh Onnes who liquified the helium-4 at 4.2 K in 1908. It opened the doors for Kelvin range of science, for instance superconductivity, electronic magnetism etc. This achievement also started the tremendous work to attain extremely low temperatures. Several designs of cryostat and devices used for producing sub-kelvin temperature have been realized including demagnetization refrigerators, dilution refrigerators etc. An overall overview on very low temperature cooling techniques is summarized in Ref. [2]. The most popular technique in many laboratories to attain the millikelvin range is the dilution refrigerator. It is based on the continuous dilution of rare isotope ^3He by the common isotope ^4He .

In the mid 90's the integrated circuit technology progressed fast to miniaturize electronic devices. Soon the overall size of the device reduced to the micron-scale. It led to the birth of mesoscopic physics. Mesoscopic physics refers to the dynamics of structures larger than a nanometer (one billionth of the meter) but smaller than the micron (one millionth of the meter). The physical properties of a mesoscopic system reveal the information on the quantum nature of electrons. The phenomenon due to the quantum nature of electrons are summarized as quantum tunneling, single electron effects and many others.

The blend of endeavors in low temperature physics and also the advancement in the integrated circuit technology started the search for on-chip solid state refrigerator [3]. Solid state cooling systems use generally a thermoelectric device, consisting of a semiconductor based bi-metal junction, a heat sink, and DC power. A typical solid state cooling system is a sandwich-type structure filled with bismuth telluride particles and doped to obtain P-N junctions. When a current is passed through the junction of the two different conductors, a temperature change is achieved. There are no moving parts and no refrigerants. Solid state cooling systems are very good for small and quiet applications.

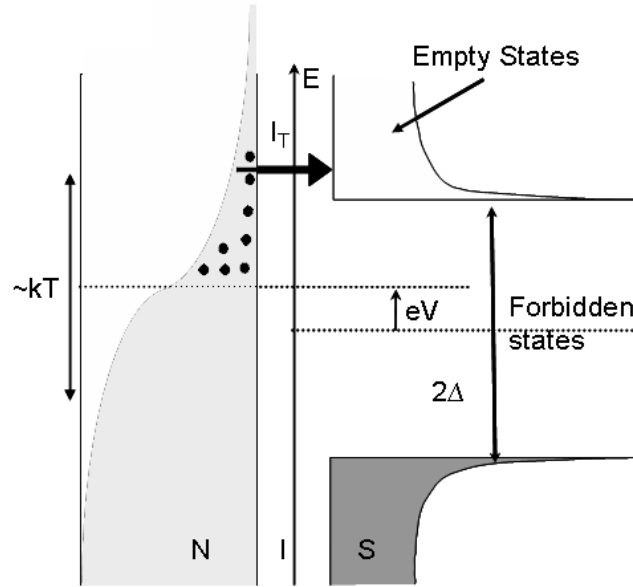


Figure 1.1: *Density of states vs energy schematic of a N-I-S junction showing single quasiparticles transfer across the junction.*

Most solid state heat pumps operate utilizing the Peltier effect. It was first discovered by J.C.A. Peltier in 1834 and is based on the thermoelectric effect. Here, the current flow in between the two different materials kept at the same initial temperature force the heat from one to the other. The amount of heat transported per unit time is proportional to the Peltier coefficient (Π) of the two materials. For most pure nonmagnetic metals $\Pi = kT^2/eT_F$, T_F being the Fermi temperature. For typical metals, Π is around $50 \mu\text{V}$ at room temperature, and for semi-conductor it is around one volt with linear dependence on the temperature. Peltier coolers derived from the semiconductor has cooling power up to 100 W at room temperature. Based on thermoelectric coolers, the Peltier coolers can get a maximum temperature difference of about 70 K. Soon Peltier cooler became popular in the semi-conductor industry. However, these coolers are unable to reach sub kelvin temperature.

In the sub-kelvin range, the solid state cooler is based on a quantum mechanical tunneling based normal metal (N) - insulator (I) - superconductor (S) junction. The refrigerator based on N-I-S junction is the main topic of this thesis. Fig. 1.1 shows the semiconductor model schematic of a tunnel barrier (I) in between a BCS superconductor (S) and a normal metal (N). For $T > 0$, the electrons in the N-metal get excited to occupy the state above the Fermi level, which smears the electronic Fermi distribution. The amount of smearing is proportional to the thermal energy ($\sim kT$) of the system. The presence of superconducting gap (Δ) in the density of states of the superconductors leads to an energy selective tunneling. With a sub-gap bias ($V < \Delta/e$), only the most energetic electrons from the normal metal can tunnel out of it, leaving behind the electrons with less energy. The weak

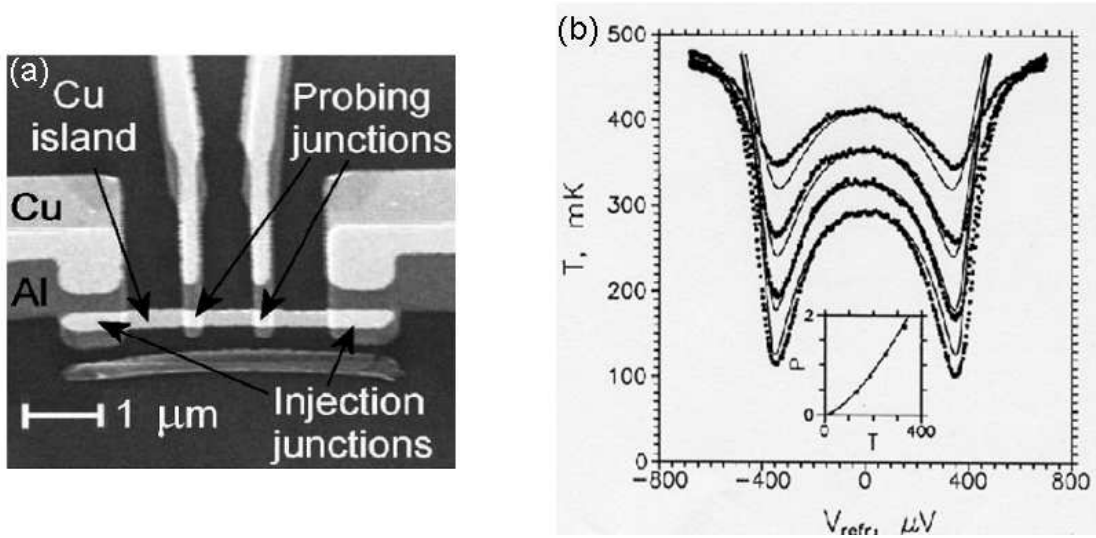


Figure 1.2: *Left: First S-I-N-I-S based cooler. Right: Typical electron cooling curve for different bath temperature. Adapted from Ref. [5].*

electron-phonon coupling in a N-metal at sub-Kelvin temperature and the extraction of hot quasiparticles out of the N-metal, lead to the electronic cooling of the N - metal. The first cooler based on a single N-I-S junction dates back to 1994 by Nahum et. al. [4], using a Al/AlO_x/Cu tunnel junction. Although the cooling power and efficiency was minimal, it inspired many research groups to make it more efficient for practical applications. A significant improvement was done by Leivo et. al. [5], where they exploited the symmetric cooling power of the N-I-S junction. They arranged the two N-I-S junctions in series configuration (i.e. S-I-N-I-S). The double junction configuration doubled the cooling power and also gave a better thermal isolation of the Cu island. The electrons cooled down from bath temperature of 300 mK to around 100 mK. Fig. 1.2 a shows a typical S-I-N-I-S cooler with the central Cu island (N) connected to the two Al electrode (S) via tunnel barrier (I) called the injection junctions. In addition to it, there are two additional N-I-S junctions (probe junction) acting as a thermometer. For a sub-gap bias, the electrons cool down, reaching the lowest value around the optimum bias of $V \approx 360 \mu\text{V}$ (see Fig. 1.2b). On further increasing the bias, the temperature of the electrons in the N-island increases due to the injection of heat into the metal.

The coolers based on S-I-N-I-S junction cool down the electrons in the central N - island. The phonons in the N-metal can be cooled down via electron-phonon coupling. The practical application of such coolers requires more efficient phonon cooling. One effective solution is to exploit thermally isolated thin membranes on which the N region is extended. Here, the micro-cooler junction cools down electrons and the phonons of the metal. The latter will subsequently refrigerate the membrane phonons via Kapitza coupling. The first demonstration [6] of the lattice cooling exploited the phonon cooling to cool down the silicon nitride (Si₃N₄) membrane. The membrane cooled down by only

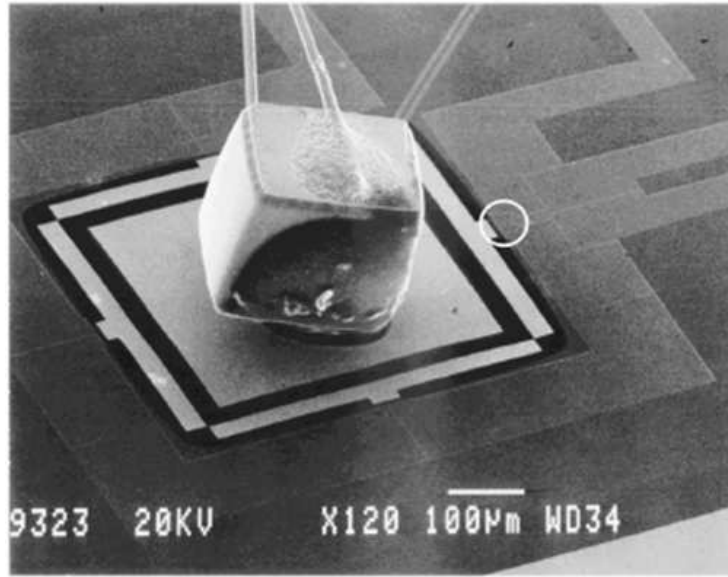


Figure 1.3: *Scanning electron micrograph of a working prototype of a N-I-S refrigerator with attached neutron transmutation doped (NTD) germanium resistance thermometer [8].*

2% from the bath temperature of 200 mK. It was further improved by fabricating the Si_3N_4 membrane with the self-suspended bridges [7]. The bridges isolate the suspended membrane from the substrate and the phonon propagation is essentially two dimensional.

Recently Clark et. al. [8] demonstrated the first practical realization of complete S-I-N-I-S based coolers (Fig. 1.3). Here four pairs of N-I-S junctions are used to cool down a suspended Si_3N_4 membrane. On the membrane, they glued a neutron transmutation doped (NTD) Ge thermometer and cooled it down to 240 mK from the bath temperature of 320 mK.

1.2 Motivation for this work

The above encouraging work motivated us to start a new project in Grenoble to develop a new cryogenic device based on S-I-N-I-S junctions. This thesis is the continuation of the preliminary experiments done at the CRTBT [9].

The quasiparticle tunneling out of a N-metal contribute to sub-gap current across the N-I-S junction. The electrical properties has been well studied previously. Recently it was demonstrated that the extraction of quasiparticles leads to cooling of electrons in the N metal. This demonstration was done using an externally embedded thermometer junction (probe junction in Fig. 1.2). However, it motivated us to work for an alternate mechanism to extract the electronic temperature without any thermometer. To enhance cooling and the efficiency of such devices, it is important to understand the different heat paths in such devices. Consequently, it motivated us to work on thermal model which takes into account different heat paths. To achieve an ultimate cooling, we realized the importance to

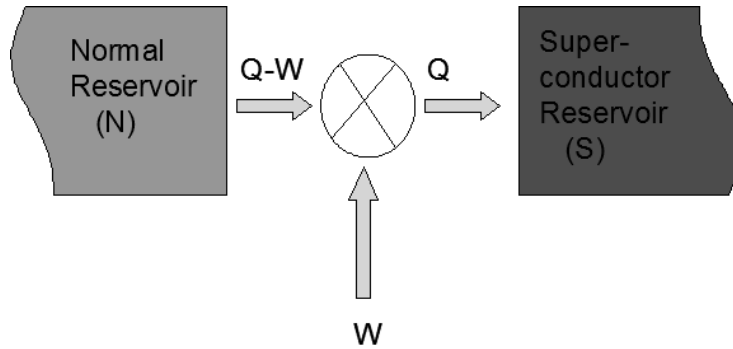


Figure 1.4: *Carnot heat engine diagram for a N-I-S device.*

understand the limitation in cooling using N-I-S junction. Such understanding motivated us to perform experiments in the dilution refrigerator. In the following, we summarize the important findings in this thesis.

This device can be thought of as a heat engine, where the heat is transferred from the normal metal to the superconductor, when the work is done on the system (see Fig. 1.4). An attempt is made in chapter 2 to bring this analogy closer. It is shown qualitatively that the smearing of Fermi distribution and superconductor gap leads to the selective tunneling of hot quasiparticles from N to S. It leads to the electronic cooling of the N-metal. The heat transfer in such hybrid devices is different from the all normal N-I-N junction. In N-I-N junctions the work done by the external source V^2/R_N is deposited equally in the two normal reservoirs.

A N-I-S junction is extremely sensitive to the electronic distribution of the normal metal, therefore can be used as a thermometer. The experimental demonstration of the cooling of N metal electrons using N-I-S junctions is usually done with an external N-I-S thermometer (chapter 5). Soon we realized the importance of a reliable and easy thermometry of the cooling N-island. A thermometer measures the temperature of electrons in N metal, which is located on a hot chip. All the experiments discussed in the previous section use an external double N-I-S junction as a thermometer. The thermometer junction helped in direct demonstration of electrons cooling in N-metal electrons but it made the whole design of the cooling device cumbersome (probe junction in Fig. 1.2). The problems get even more aggravated for the tri-layer geometry or for mounting microcoolers on the membranes. For instance in Ref. [8] a prototype of practical refrigerator, there was no thermometer to measure the electronic temperature of the device.

In this thesis (chapter 5), we have done experiments on micro-coolers with no external thermometer (Fig. 1.5). We have done the precise investigation on the direct current-voltage characteristic obtained from the cooler junction. The N-metal is assumed to be at quasi-equilibrium with the electrons following the Fermi distribution. We have used the kinetic equations to re-define the electronic distribution in the central N-metal. On comparison with the experiments we concluded that the electrons can be considered as being at thermal equilibrium. The electronic temperature of the N metal electrons is extracted

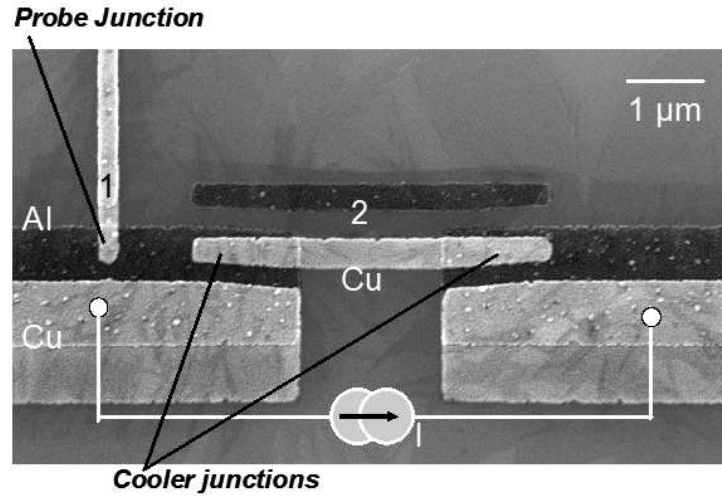


Figure 1.5: *Scanning electron micrograph of a cooler with no external thermometer on the central N-island.*

directly from the current-voltage characteristic of the cooler junction. The temperature $T_e(V)$ in the sub-gap region is obtained by superimposing the experimental I-V curve on a series of isotherm curves, see Fig. 1.6. Every crossing point gives the electronic temperature T_e in the normal metal at a particular bias. This sample design with no external thermometer attains a higher ratio of volume/area of N-metal in comparison with the previous design, which can contribute to a better cooling of the island.

The theoretical and experimental understanding of heat transfer in the cooling device is extremely interesting. The electron - phonon coupling in the normal metal is vanishingly small at low temperature. The decoupling and extraction of hot quasiparticles out of the N metal lead to cooling of the electron cloud in the N-metal. A complete thermal model and its effect on the N metal phonon distribution is important for understanding an efficient cooling. We have devised a quantitative thermal model (chapter 6), by taking into account the electron - phonon coupling in the N metal and the Kapitza coupling between the phonons of the central N metal and the substrate.

Some questions remain: What is the minimum electronic temperature that can be achieved from the N-I-S cooler? At a very low temperature ($T_{bath} < 200$ mK), the thermal transport in such N-I-S tunnel junctions appears to be still little understood. For instance, an apparent reversal of the normal metal temperature evolution was observed in various experiments [10, 11] and related to a non-BCS density of states of the superconductor [11]. A clear understanding of this behavior is still missing.

In a tunnel junction between a normal metal (N) and a superconductor (S), the charge transfer occurs mainly through two different mechanisms. The tunneling of a single quasiparticle is possible for electrons or holes with an energy E (compared to the Fermi level E_F) larger than the superconductor gap (Δ). At low energy, the charge transfer occurs through the Andreev reflection [12, 13]. In the normal metal, an electron (a hole) impinging on

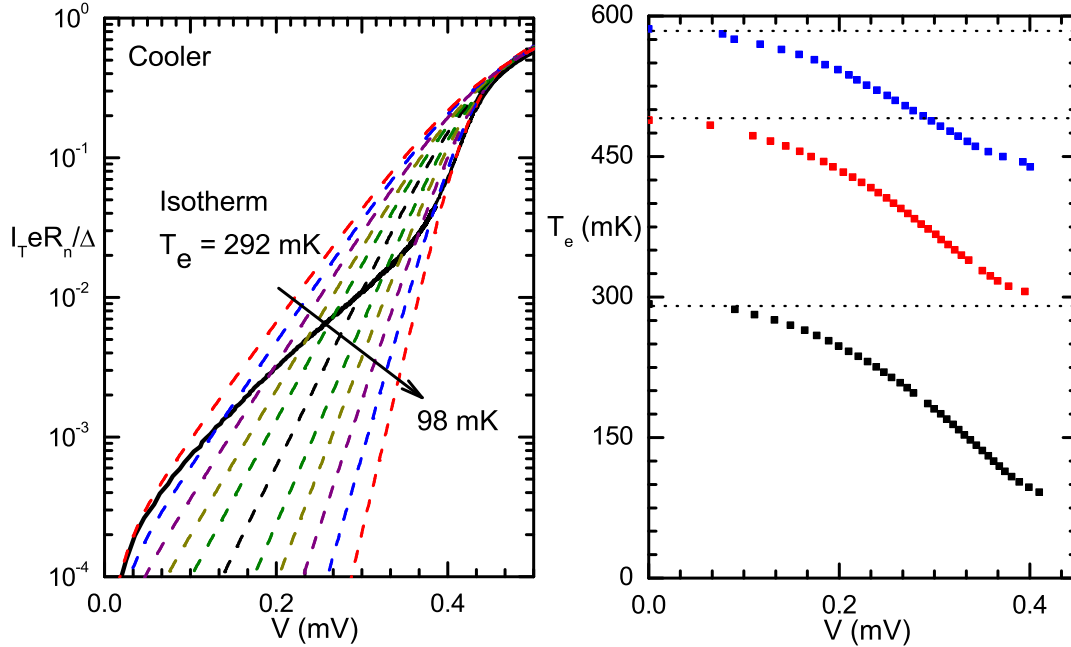


Figure 1.6: *Left: Experimental current-voltage characteristic (full line, black) superposed on a series of calculated isotherm characteristic from $T_e = 292$ mK (top) to $T_e = 98$ mK (bottom). Every crossing point gives the electronic temperature T_e in the central N metal at a particular bias. Right: Extracted normal metal electronic temperature as a function of the cooler bias at different cryostat temperatures.*

the superconducting interface is reflected as a hole (an electron), enabling the transfer of a Cooper pair into (out of) the superconductor (see Fig. 1.8). The probability for an incident quasi-particle to follow an Andreev reflection, a specular reflection or a tunnel transfer is given in the ballistic regime (no disorder) by the Blonder - Tinkham - Klapwijk (BTK) [14]. For a N-I-S tunnel junction with an insulator (I) of intermediate or low transparency, the Andreev reflection probability is predicted to be vanishingly small. Taking into account the quasi-particles confinement in the vicinity of the interface, this is no longer true. This confinement can be induced by the disorder or the presence of a second barrier in the normal metal. A single quasiparticle then experiences several collisions with the interface [15, 16]. The actual Andreev reflection transmission coefficient corresponds to the coherent addition of many individual transmission probabilities. Therefore, the Andreev sub-gap current significantly exceeds the ballistic case prediction [17] and can be modulated by a magnetic flux [18].

A quasi-particle current in a N-I-S junction indeed carries both a charge current and a

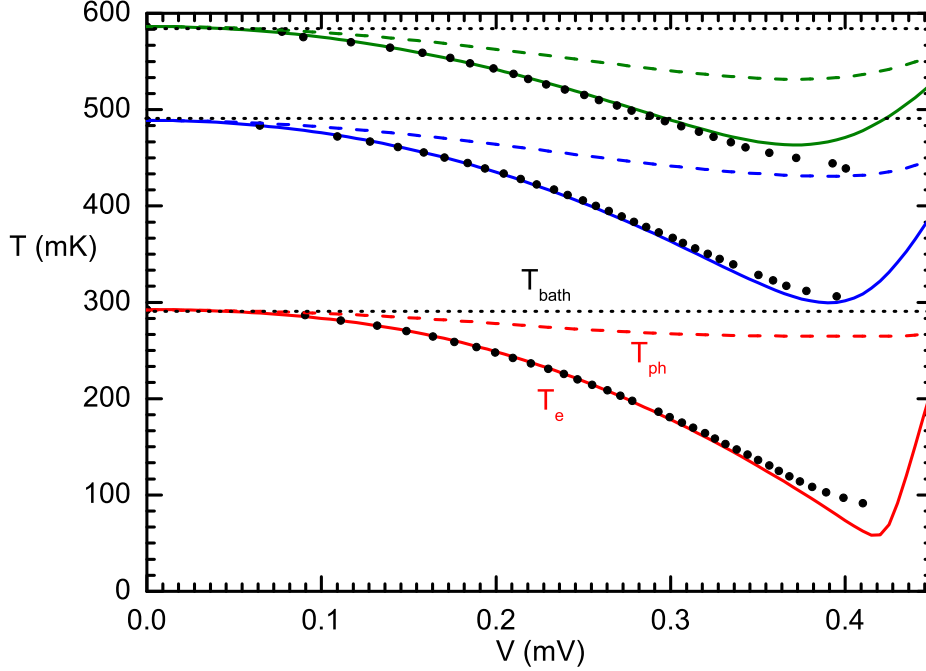


Figure 1.7: *Electron and phonon temperature as a function of cooler bias voltage at different cryostat temperatures. The dots are the experimental points. The complete and dotted line shows the calculated electron and phonon temperatures respectively, obtained from the thermal model for $\Sigma = 2 \text{ nW} \cdot \mu\text{m}^{-3} \cdot \text{K}^{-5}$ and $K \cdot A = 66 \text{ pW} \cdot \text{K}^{-4}$.*

heat current; this cools the electronic population of the normal metal. We have done an experimental and theoretical study of the heat transport in a S-I-N-I-S junction, focusing on the very low temperature regime. The heat contribution due to the phase-coherent Andreev current (I_A) is mostly neglected. The naive reason is as the energies of the involved electron and hole are located symmetrically around E_F , the Andreev reflection does not carry heat through the interface at zero bias. However at a finite bias, the two electrons coming from the N-metal have finite energy, which gets dissipated in the normal metal before tunneling into the superconductor as a Cooper pair (see Fig. 1.8). We provide a fully quantitative analysis of the heat transfer in the system, which shows that although the Andreev current is a small effect in terms of charge current, the heat it creates has a dominating influence on the heat balance. Theoretical understanding of the charge and heat contribution due to the phase coherent Andreev current has been done here in chapter 3. The experiments on the cooler junction at very low temperature are discussed in chapter 7. Fig. 1.9 shows the comparison of the experiment (complete line) and the thermal model (dotted line) at different cryostat temperatures. Here we have included the work $I_A \cdot V$

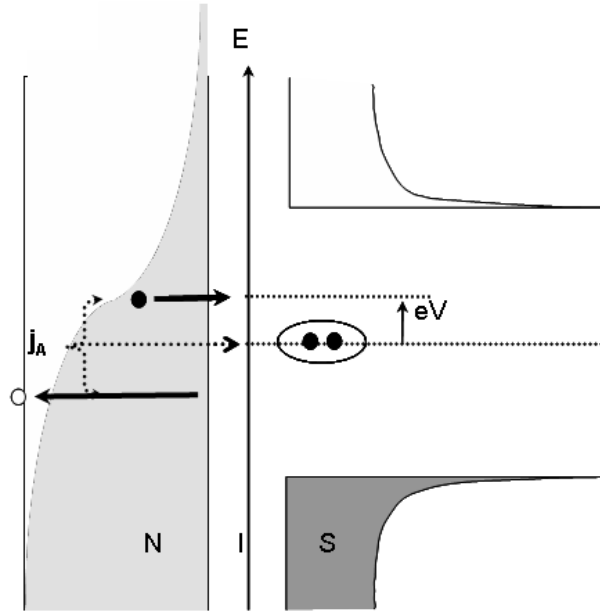


Figure 1.8: *Density of states vs energy schematic of a N-I-S junction showing Andreev reflection across the junction.*

done on the central metallic island by the current source. The agreement is good for the sub-gap bias and at every accessible cryostat temperature.

An important question still remains: What is the limitation in cooling electrons in the S-I-N-I-S junction? In the N-I-S cooler, the driving current takes hot quasiparticles from the normal metal to the superconductor. It leads to lowering of the electronic temperature in the N metal, which reaches its minimum at an optimum bias ($\sim \Delta$). The electronic cooling at an optimal bias ($\approx \Delta$) is poorly understood (see Fig. 1.7 at $V \approx 0.4$ mV). Cooling effect is accompanied by the injection of hot quasiparticles in the superconducting electrodes. The injected quasiparticles have a small group velocity and get accumulated near the junction in superconductor, leading to two undesirable mechanisms : quasiparticles backscattering and re-absorption of 2Δ phonons in the normal metal strip.

In chapter 8, an attempt is made to understand the phenomena involving the non equilibrium quasiparticles diffusion in the superconducting electrodes of a S-I-N tunnel junction. We have proposed a phenomenological model based on the recombination and pair breaking mechanism in the superconductor. The model includes a normal metal trap junction which relaxes the quasiparticles to the bath temperature. We have shown that the diffusion equation has a complete analytic solution. Our model gives the spatial profile of the effective quasiparticle temperature in the S-strip. Numerical implications of heating of superconductor on the cooled N - metal electrons are discussed. Our model will be useful to test accurately the influence of the material and geometrical parameters (diffusion coefficient, tunnel conductance, trapping junction, thicknesses) and therefore will be helpful to improve the ultimate cooling of S-I-N-I-S devices.

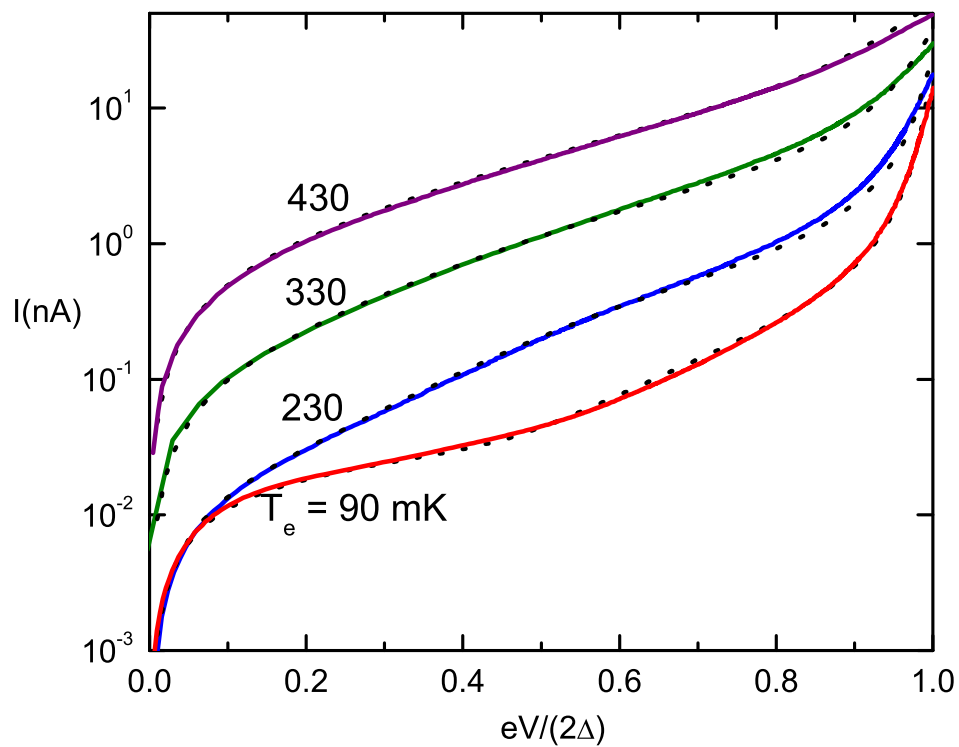


Figure 1.9: *Current voltage characteristic of the cooler junction at different cryostat temperatures together with the calculated best fit from the full thermal model including the charge and heat contribution due to Andreev current.*

Chapter 2

Cooling effect in S-I-N-I-S tunnel junction

2.1 Introduction

This chapter is devoted to the charge and heat transport in hybrid superconductor - normal metal tunnel junctions. We mainly focus on the transport properties in the sub-gap region i.e. the temperature and the applied bias voltages are smaller than the BCS superconductor gap energy (Δ).

Tunneling in hybrid structures is known for many years already to be a sensitive tool enabling to probe the energy dependence of the density of states (DoS). Combining an ordinary normal metal in which the DoS is approximately constant close to the Fermi level, with a superconductor whose DoS is energy dependent gives a non-trivial phenomenon. For sub-gap bias voltage ($eV < \Delta$), due to the absence of single quasiparticle states within the superconductor energy gap, the electronic transport across the normal metal (N) - superconductor (S) decreases exponentially with lowering the temperature. The tunnel current across the junction is mainly due to tunneling of high-energy quasiparticles ($E > \Delta$) from the normal metal to the superconductor. Giaever pioneered this technique and confirmed experimentally the energy dependent DoS as predicted by the microscopic theory of superconductivity [19, 20].

In this chapter, we shall illustrate the peculiar behavior of sub-gap transport in a N-I-S tunnel junction. Since tunnel junctions are amenable to the simple calculations using perturbation theory, we will obtain an analytical expression of the tunnel current across a N-I-S junction. Here, we will restrict to a first order perturbation calculation. In section 2.2, we will obtain the subgap current and conductance across the N-I-S junction in the clean limit, i.e. the effect of impurity scattering shall be ignored. The heat transport in such hybrid devices shall be discussed in section 2.3. Here, we will begin with the heat transport in N-I-N junctions and subsequently discuss the N-I-S junctions. An attempt will be made to do the schematic comparison of such nano-devices with the heat engines.

2.2 Quasiparticle tunnel current in a N-I-S junction

2.2.1 Tunnel Hamiltonian

To describe the transfer of electrons across N-I-S junctions, we follow the tunnel Hamiltonian formalism. The basic idea is to say that there exists a non-zero probability of charge transfer by quantum mechanical tunneling of electrons between two electrodes separated by a tunnel barrier. The probability of transfer of charge decreases exponentially with the barrier separation and these aspects can be absorbed in a phenomenological matrix element $t_{k,p}$. Thus, the tunnel Hamiltonian can be written as [21]:

$$\hat{H}_T = \sum_{k,p,\sigma,\sigma'} t_{k,p;\sigma,\sigma'} \hat{a}_{k,\sigma}^\dagger \hat{b}_{p,\sigma'} + t_{k,p;\sigma,\sigma'}^* \hat{b}_{p,\sigma'}^\dagger \hat{a}_{k,\sigma}, \quad (2.1)$$

where the subscript k refers to electrode on the right and p refers to the other. σ and σ' refer to the electron spin in the respective electrode. The operator $\hat{a}_{k,\sigma}^\dagger$ ($\hat{a}_{k,\sigma}$) creates (annihilates) an electron with the quantum number k and spin σ in the right electrode, similarly \hat{b}^\dagger (\hat{b}) in the left electrode. Physically, the explicit terms on the right hand side in Eq. 2.1 refer to the transfer of an electron from metal p to metal k , whereas the conjugate term corresponds to the reverse process. In this thesis, for simplicity we assume that the spin is conserved during tunneling, hence the amplitude in Eq. 2.1 is independent of the spin indices. Furthermore, we ignore the dependence of t on the quantum numbers k and p and substitute $t_{k,p} = t_0$. The total Hamiltonian of the junction is written as the sum of the three parts, $\hat{H} = \hat{H}_L + \hat{H}_R + \hat{H}_T$.

2.2.2 Tunnel current across N-I-S junction: golden rule

Fig. 2.1 shows the semiconductor model schematic of the density of states (DoS) as a function of energy in a N-I-S junction at a non-zero temperature. The normal metal is represented as a continuous distribution of independent-particle energy states with density $N(0)$, including the energies well below the Fermi level. The superconductor is represented by an ordinary semiconductor with a density of independent particle states but with an energy gap (Δ), where there are no single quasiparticle states.

At $T = 0$ K, all the states up to the Fermi energy are filled and for $T > 0$ K, the occupation number in the respective electrode is given by the Fermi distribution function $f(E) = 1/(1 + e^{E/kT})$. The value of $f(E)$ ranges from 0 to 1. In order to calculate the tunnel current across the N-I-S junction, we use the perturbation theory. The total rate of tunneling across the N-I-S junction is given by $\Gamma = \Gamma_{N \rightarrow S} - \Gamma_{S \rightarrow N}$. According to Fermi's golden rule, the rate of tunneling from the normal metal to the superconductor can be written as

$$\Gamma_{N \rightarrow S} = \sum_{k,p,\sigma} \frac{2\pi}{\hbar} |t_0|^2 f_N(E_k) [1 - f_S(E_p)] \delta(E_k - E_p), \quad (2.2)$$

with $f_i(E) = [1 + e^{\beta_i(E - \mu_i)}]$ being the Fermi function of the electrode $i =$ normal metal

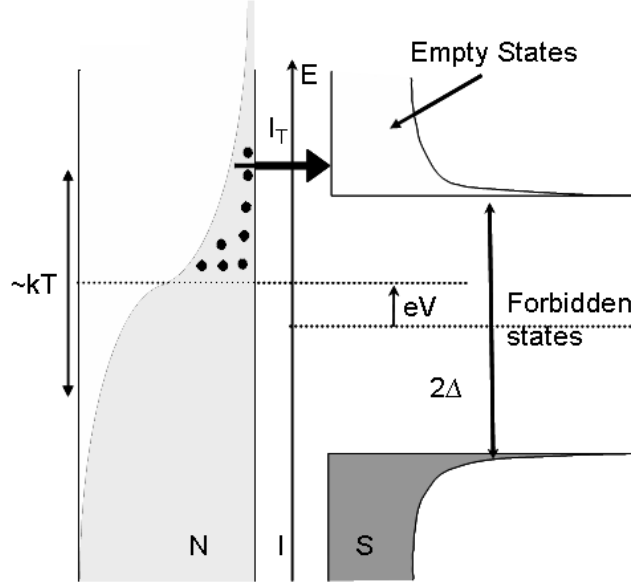


Figure 2.1: *Density of states vs energy schematic of a N-I-S junction showing single quasiparticles transfer across the junction.*

(N) and superconductor (S) electrode kept at the electrochemical potential μ_i and β_i is defined as $1/kT_i$. Here the Fermi functions ensure that tunneling is allowed only when the initial state in the left electrode is occupied and the final state in right is empty. The delta function $\delta(E_k - E_p)$ is to ensure the energy conservation during tunneling.

The sum over k in right side of Eq. 2.2 can be replaced by an integral over the continuous spectrum $\sum_{k,(p)} \dots \rightarrow \int dE N_{N,(S)}(E) \dots$, where $N_{N,(S)}$ is the density of states per spin and per unit of energy in the respective electrode. Thus we get

$$\begin{aligned} \Gamma &= \frac{4\pi t_0^2}{\hbar} \int dE_1 dE_2 N_N(E_1) N_S(E_2) [f(E_1) - f(E_2)] \delta(E_1 - E_2 + eV) \\ &= \frac{4\pi t_0^2}{\hbar} \int dE N_N(E - eV) N_S(E) [f_N(E - eV) - f_S(E)], \end{aligned} \quad (2.3)$$

with eV being the electrochemical potential difference between the normal metal and the superconductor (Fig. 2.1).

The total current across the N-I-S junction is given by $I_{N-I-S} = e\Gamma$. Thus we get:

$$I(V) = \frac{4\pi e t_0^2}{\hbar} \int N_N(E - eV) N_S(E) [f_N(E - eV) - f_S(E)] dE. \quad (2.4)$$

The normalized density of states in the superconductor can be written as:

$$N_S(E) = N_N(E) \frac{|E|}{\sqrt{E^2 - \Delta^2}}. \quad (2.5)$$

Thus, we get

$$I(V) = \frac{4\pi et_0^2}{\hbar} \int N_N(E - eV)N_N(E) \frac{|E|}{\sqrt{E^2 - \Delta^2}} [f_S(E - eV) - f_N(E)] dE. \quad (2.6)$$

Normal state conductance :

If both sides of the tunnel barrier are normal metals with a constant DoS, equal to the value N_0 then the integration in Eq. 2.4 can be written as:

$$\begin{aligned} I(V) &= \frac{4\pi et_0^2 N_0^2}{\hbar} \int [f(E - eV) - f(E)] dE \\ &= \left[\frac{4\pi et_0^2 N_0^2 e}{\hbar} \right] V = G_N V, \end{aligned} \quad (2.7)$$

with G_N being the normal state conductance of the junction. The above result is straightforward, corresponding to the ohmic nature of the junction.

On substituting Eq. 2.7 in Eq. 2.6, the single quasiparticle current across a N-I-S junction can be written as:

$$I(V) = \frac{1}{eR_N} \int_{-\infty}^{\infty} N_N(E - eV)N_N(E) \frac{|E|}{\sqrt{E^2 - \Delta^2}} [f_N(E - eV) - f_S(E)] dE. \quad (2.8)$$

Now, employing the symmetric DoS in the superconductor, $N_S(-E) = N_S(E)$ and $f(-x) = 1 - f(x)$, we get

$$I(V) = \frac{1}{eR_N} \int_0^{\infty} N_S(E) [f_N(E - eV) - f_N(E + eV)] dE. \quad (2.9)$$

Note that Eq. 2.9 is insensitive to the temperature of the superconductor electrode and depends only on the superconductor gap. At low temperature $T < 0.3T_c$, the gap attains almost the zero temperature value, $\Delta(T) \simeq \Delta(0)$.

Fig. 2.2 shows the calculated isotherm tunnel current across the N-I-S junction for three different normal metal electrons temperatures. The sub-gap current depends strongly on the electronic temperature. Pictorially one can understand from Fig. 2.1 that higher temperature means that there are more electrons above the Fermi energy, which tunnel across the junction. For $eV > \Delta$, all the isotherms merge together to the resistive normal state of the junction.

For $\Delta \gg kT_N$ and $0 \ll eV < \Delta$, the current through N-I-S junction can be written as [22]:

$$I(V) \simeq \frac{\Delta}{eR_n} \sqrt{\frac{\pi \cdot kT_e}{2\Delta}} \exp\left[-\frac{eV - \Delta}{kT_e}\right]. \quad (2.10)$$

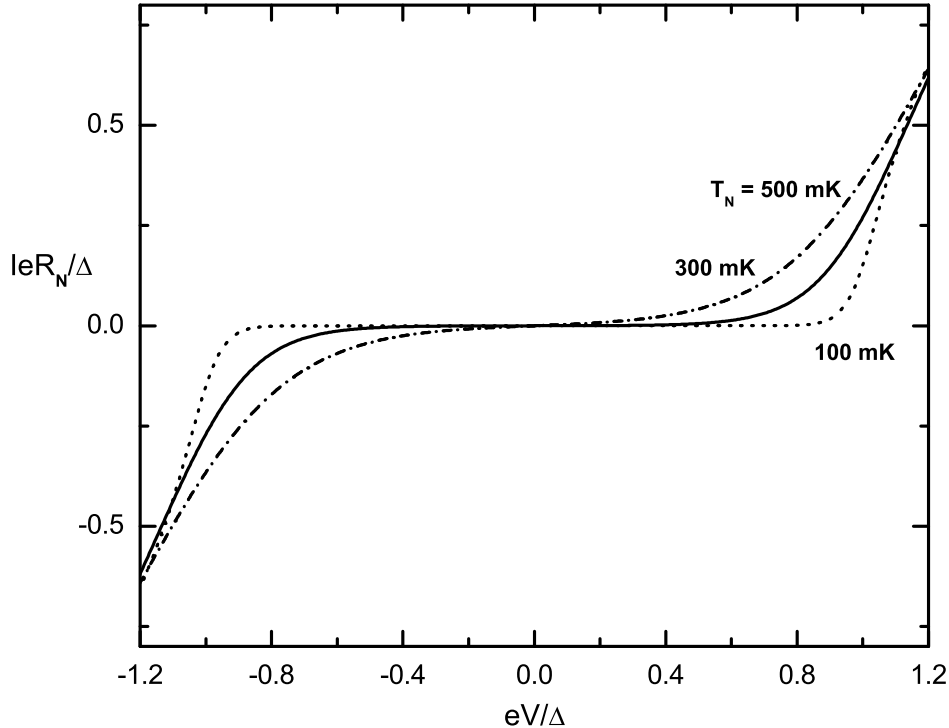


Figure 2.2: *Calculated characteristic curve for a N-I-S junction for three different temperature with $\Delta = 0.21$ meV.*

2.3 Heat transfer in the mesoscopic tunnel junction

In the previous section, we discussed the charge current across the hybrid tunnel junction based devices. However, it remains to understand the heat current distribution due to tunneling in the tunnel junction. In section 2.3.1, we shall first consider the heat transfer in a normal metal-based tunnel junction and then in section 2.3.2 we shall consider the heat transfer in the N-I-S tunnel junction.

2.3.1 Heat transfer in Normal metal - Insulator - Normal metal junction

We consider two normal metals (N1, N2) connected through a tunnel barrier with a bias voltage across it and with the chemical potential difference (μ). We calculate the energy transfer through the tunnel barrier between the two normal metals. The energy transfer rate (heat flux) upon electron tunneling from electrode N1 to N2 can be written as:

$$\dot{Q}_{N1 \rightarrow N2} = \frac{1}{e^2 R_N} \int_{-\infty}^{\infty} E f(E) [1 - f(E + eV)] dE,$$

with R_N being the tunnel resistance across the junction. This describes the tunneling of an electron from electrode N1 under the action of an applied bias V into the electrode 2. Similarly, the heat flux in the reverse process is given by

$$\dot{Q}_{N2 \rightarrow N1} = \frac{1}{e^2 R_N} \int_{-\infty}^{\infty} E f(E + eV) [1 - f(E)] dE.$$

Thus the heat flow out of N1 (\dot{Q}_{N1}) is given by,

$$\dot{Q}_{N1} = \frac{1}{e^2 R_N} \int_{-\infty}^{\infty} E [f(E) - f(E + eV)] dE = -\frac{V^2}{2R_N}.$$

Here the negative sign signifies that $\frac{V^2}{2R_N}$ is the energy per unit time deposited in electrode N1 by the load.

Similarly for electrode N2, we get

$$\dot{Q}_{N2} = \frac{1}{e^2 R_N} \int_{-\infty}^{\infty} (E + eV) [f(E + eV) - f(E)] dE = -\frac{V^2}{2R_N}.$$

The total heat energy of the N1-I-N2 system is given by:

$$\boxed{\dot{Q}_{N1}(V) + \dot{Q}_{N2}(V) = -\frac{V^2}{R_N}}. \quad (2.11)$$

as it should; $\frac{V^2}{R_N}$ is the energy per unit time put in by the load.

The work done on the normal reservoir N1 is given by:

$$W_{N1} = \frac{1}{e^2 R_N} \int_{-\infty}^{\infty} \mu [f_{N1}(E) - f_{N2}(E - eV)] dE = -\frac{\mu \cdot V}{e R_N}.$$

Similarly, the work done on reservoir N2 is given by:

$$W_{N2} = \frac{1}{e^2 R_N} \int_{-\infty}^{\infty} \mu [f_{N2}(E - eV) - f_{N1}(E)] dE = \frac{(\mu + eV) \cdot V}{e R_N}.$$

The total work done on the N1-I-N2 device is given by:

$$\boxed{W_{N1} + W_{N2} = \frac{V^2}{R_N}}. \quad (2.12)$$

It shows that total work done by an external source is V^2/R_N . By inspection on Eq. 2.11 and Eq. 2.12 we can draw a Carnot engine-like diagram for the N1-I-N2 device (see Fig. 2.3). It shows that the work done by the source (V^2/R_N) is deposited equally in the two reservoirs (N1 and N2).

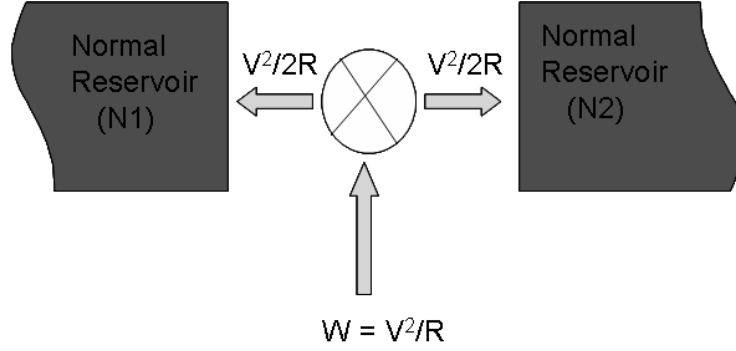


Figure 2.3: *Carnot heat engine diagram for N1-I-N2 device: The work done by the source is equally distributed among the two normal reservoirs.*

2.3.2 Heat transfer in Normal metal - Insulator - Superconductor junction

The principle of N-I-S cooling devices (Fig. 2.1) is based on the energy-selective extraction of high-energy quasiparticles out of the normal metal. The existence of the forbidden single particle energy states within the superconductor gap results in the fact that only electrons with energy $E > \Delta$ tunnel from the normal metal to the superconductor.

Here, we shall discuss the heat transfer across a N-I-S junction. We consider that the two metals have a chemical potential difference eV such that $\mu_N = \mu_S + eV$, where $\mu_{N,S}$ is the chemical potential of the normal metal and the superconductor respectively. The energy transfer rate from the normal metal to the superconductor can be written as:

$$\dot{Q}_{N \rightarrow S} = \frac{1}{e^2 R_N} \int_{-\infty}^{\infty} (E - eV) N_N(E - eV) N_S(E) f_N(E - eV) [1 - f_S(E)] dE,$$

as electrons tunneling out of normal metal carry the energy $(E - eV)$. Similarly, the reverse process corresponds to a rate:

$$\dot{Q}_{S \rightarrow N} = \frac{1}{e^2 R_N} \int_{-\infty}^{\infty} (E - eV) N_N(E - eV) N_S(E) [1 - f_N(E - eV)] f_S(E) dE.$$

The net heat transfer out of N is given by: $\dot{Q}_N = \dot{Q}_{N \rightarrow S} - \dot{Q}_{S \rightarrow N}$. We get,

$$\dot{Q}_N = \frac{1}{e^2 R_N} \int_{-\infty}^{\infty} (E - eV) N_N(E - eV) N_S(E) [f_N(E - eV) - f_S(E)] dE.$$

To simplify the calculation we approximate the Fermi function: $f(E) \approx e^{-\beta E}$, where $\beta = 1/kT$ such that $\beta\Delta \gg 1$. Assuming $T_S = T_N$ and constant density of states in the

normal metal. We get,

$$\begin{aligned}\dot{Q}_N &= \frac{1}{e^2 R_N} 2(\cosh[\beta eV] - 1) \int_0^\infty E N_S(E) e^{-\beta E} dE \\ &\quad - \frac{1}{e^2 R_N} 2eV \sinh[\beta eV] \int_0^\infty N_S(E) e^{-\beta E} dE.\end{aligned}\quad (2.13)$$

The second term on the right side is $I_T.V$ with I_T being the the tunnel current across the N-I-S junction.

Now we calculate the net heat transfer out of S. The energy transfer rate from the normal metal to the superconductor can be written as:

$$\dot{Q}_{N \rightarrow S} = \frac{1}{e^2 R_N} \int_{-\infty}^\infty E N_N(E - eV) N_S(E) f_N(E - eV) [1 - f_S(E)] dE.$$

Similarly, the reverse process corresponds to a rate:

$$\dot{Q}_{S \rightarrow N} = \frac{1}{e^2 R_N} \int_{-\infty}^\infty E N_N(E - eV) N_S(E) [1 - f_N(E - eV)] f_S(E) dE.$$

The net heat transfer out of S is given by: $\dot{Q}_S = \dot{Q}_{S \rightarrow N} - \dot{Q}_{N \rightarrow S}$. We get,

$$\dot{Q}_S = \frac{1}{e^2 R_N} \int_{-\infty}^\infty E N_S(E) [f_S(E) - f_N(E - eV)] dE.$$

Using the same approximation on the Fermi function, we get:

$$\dot{Q}_S = -2 \frac{1}{e^2 R_N} [\cosh(\beta eV) - 1] \int_0^\infty E N_S(E) e^{-\beta E} dE \quad (2.14)$$

The total heat energy of the N-I-S device is $\dot{Q}_{NIS} = \dot{Q}_N + \dot{Q}_S$. Using Eq. 2.13 and Eq. 2.14, we get:

$$\dot{Q}_{NIS} = -2eV \frac{1}{e^2 R_N} \sinh(\beta eV) \int_0^\infty N_S(E) e^{-\beta E} dE = -I_T.V \quad (2.15)$$

The work done by the source on the superconductor is given by:

$$\begin{aligned}W_S &= \frac{1}{e^2 R_N} \int_{-\infty}^\infty \mu N_S(E) [f_S(E) - f_N(E - eV)] dE \\ &\approx -\frac{2\mu}{e^2 R_N} \sinh(\beta eV) \int_0^\infty N_S(E) e^{-\beta E} dE.\end{aligned}\quad (2.16)$$

The work done by the source on the normal metal is given by:

$$\begin{aligned}W_N &= \frac{1}{e^2 R_N} \int_{-\infty}^\infty (\mu + eV) N_S(E) [f_N(E - eV) - f_S(E)] dE \\ &\approx \frac{2(\mu + eV)}{e^2 R_N} \sinh(\beta eV) \int_0^\infty N_S(E) e^{-\beta E} dE.\end{aligned}\quad (2.17)$$

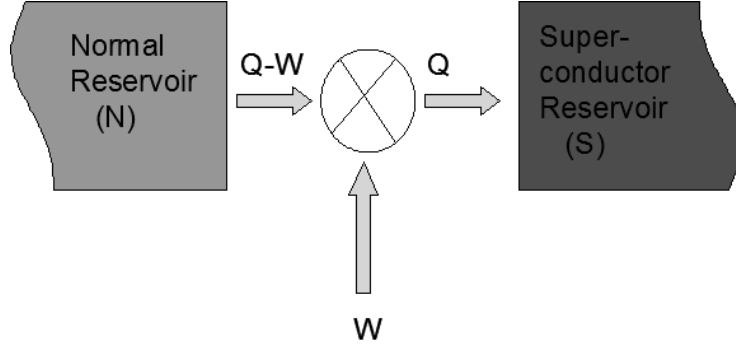


Figure 2.4: *Carnot heat engine diagram for a N-I-S device.*

The total work done by the source on the N-I-S device is: $W = W_N + W_S$. Using Eq. 2.16 and Eq. 2.17, the total work done is given by,

$$W = 2eV \frac{1}{e^2 R_N} \sinh(\beta eV) \int_0^\infty N_S(E) e^{-\beta E} dE = I_T \cdot V \quad (2.18)$$

Using the above definition of the work and energy transfer across the junction, the heat engine schematic of the N-I-S device for a sub-gap bias voltage, can be given by Fig. 2.4. In comparison with the N-I-N device, the external source in the N-I-S device takes heat out of the normal metal (for $eV < \Delta$) and dissipates heat in the superconductor.

2.4 Cooling using a pair of N-I-S junction

The heat current P_{cool} out of the normal metal into an individual N-I-S junction is given by:

$$P_{cool} = \frac{1}{e^2 R_n} \int_{-\infty}^{\infty} (E - eV) n_s(E) [f_n(E - eV) - f_s(E)] dE, \quad (2.19)$$

Fig. 2.5 shows the calculated P_{cool} for a N-I-S tunnel junction versus bias voltage at different temperatures ($T = T_e = T_s$). When P_{cool} is positive, it implies the removal of heat from the N electrode, i.e., hot excitations are transferred to the superconductor. For each temperature, there is an optimal voltage that maximizes P_{cool} and, by decreasing the temperature, that causes the heat current results to be peaked around Δ/e . In the low temperature limit $T_e \leq T_s \ll \Delta/k_B$, it is possible to give an approximate expression for the optimal bias voltage V_{opt} ,

$$V_{opt} \approx \Delta - 0.66 k_B T_e / e.$$

For $V = V_{opt}$, the current through the N-I-S junction can be approximated as

$$I \approx 0.48 \frac{\Delta}{e R_n} \sqrt{k_B T_e / \Delta}.$$

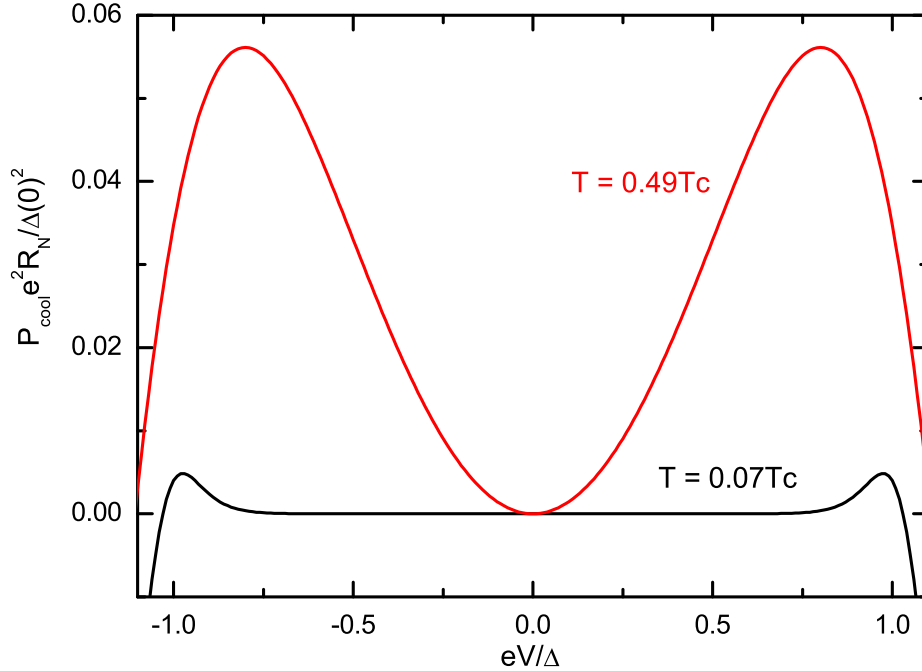


Figure 2.5: Calculated cooling power P_{cool} of a N-I-S junction vs bias voltage for different temperatures $T=T_e=T_s$.

The N-I-S junction coefficient of performance is

$$\eta(V) = \frac{P_{cool}}{I(V) \cdot V}.$$

For $V \approx \Delta/e$ and in the low-temperature limit, $\eta \approx 0.7(T_e/T_c)$.

It is also worth noticing P_{cool} is a symmetric function to applied bias. One can exploit this symmetric P_{cool} by taking a pair of N-I-S junctions in series and arranged in a symmetric configuration i.e., as a S-I-N-I-S that leads to a much stronger cooling effect. Therefore at fixed voltage across the S-I-N-I-S junction, quasielectrons are extracted from the N region through one junction, while at the same time quasiholes are filled in the N region below the superconducting gap from the other junction.

Chapter 3

Andreev current in a S-I-N junction

3.1 Introduction

This chapter is concerned with the Andreev reflection [12, 13] process, which is a high order tunnelling phenomenon in Superconductor - Normal metal junctions. As discussed in Chapter 2, the first order perturbation calculation up to t_0^2 , where t_0 is the transfer matrix element, gives a zero tunnel current for energy below the superconducting gap Δ . High-energy quasiparticles in the normal metal cannot tunnel within the superconductor gap since there are no single quasiparticle states within the superconducting gap. However, the higher order tunnel processes does contribute to the tunnel current. At second order, the tunnel process allows the transfer of two-electrons from the normal metal to form a Cooper pair in the superconductor.

In this chapter, we begin with the main properties of Andreev reflection. The influence of the Andreev reflection on the current voltage characteristic of a N-I-S junction shall be discussed in the framework of a ballistic interface as worked out by Blonder, Tinkham and Klapwijk (BTK) [14]. This formalism is applicable for an arbitrary barrier from a perfect contact to a tunnel barrier [23].

In section 3.4, the disorder in the electrodes is included in the device. In such a situation, the phase-coherent Andreev current strongly dominates the subgap conductance of the hybrid N-I-S junctions [17, 24]. Based on the formalism by Hekkking and Nazarov [16], we calculate this current for our sample geometry. In Section 3.6, an attempt is made to understand the heat contribution of the phase-coherent Andreev current [25] and to derive the relationship with the Andreev heat.

3.2 Andreev reflection

It was noted by Saint James [13] and also by Andreev [12] in 1964 that an electron is reflected from a superconductor in an unusual way. The incident electron in the normal metal (N) is retro-reflected as a hole, while a Cooper pair is transmitted in the Superconductor (S). This is called Andreev reflection. Fig. 3.1 shows the schematic of Andreev

reflection, where the electron coming from N undergoes Andreev reflection at the junction interface.

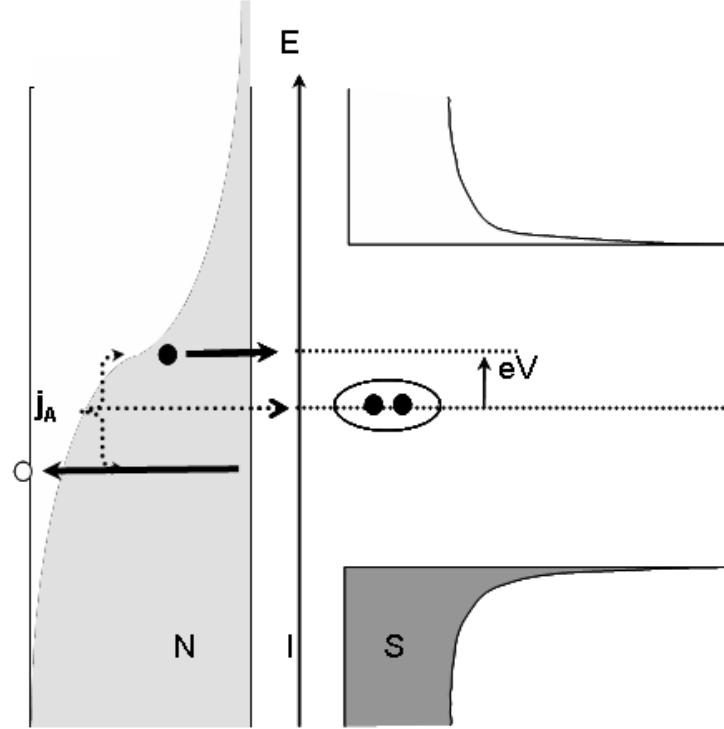


Figure 3.1: *Density of states vs energy schematic of a N-I-S junction showing a two-electrons tunneling process. An incident electron from N with $E < \Delta$ strikes the N-S interface. It is retro-reflected as a hole and as a result a Cooper pair is transmitted in S.*

The hall mark properties of the Andreev reflection have been discussed in Ref. [26, 27]. The Andreev reflection conserves the spin, charge, energy and momentum. In the normal metal, the reflected hole traces back the same trajectory as the incident electron. As a consequence, this two-electrons pair in N metal is also called an "Andreev pair" [28] as their existence is not because of the attractive interaction in the N but due to the Andreev reflection at the N-S interface.

3.2.1 Andreev reflection: BTK model

For a ballistic N-S interface, Blonder, Tinkham and Klapwijk (BTK) formulated a transport theory taking into account both the specular reflection and the Andreev reflection at the interface. The BTK model successfully explained the experiments done in 80's on N-S junctions for an arbitrary transparency [23]. It describes the cross-over in the behavior of the conductance of the junction as a function of the tunnel barrier transparency. The authors showed that for the highly transparent junctions the sub-gap conductance is twice the normal state conductance i.e. $G_{NS} = 2G_{NN}$ and in low transparency junctions, the

sub-gap conductance vanishes i.e. $G_{NS} \rightarrow 0$.

BTK considered a scattering potential located at the N-S interface $V(x) = H\delta(x)$. The strength of the barrier is indicated by the parameter $Z = H/\hbar v_F$. The parameter Z is related to the normal state transmissivity (T) of the interface as:

$$T = \frac{1}{1 + Z^2}$$

The total transmission for particle transfer is proportional to $1 - B(E) + A(E)$, where $A(E)$ and $B(E)$ are the probability for the Andreev reflection and the specular reflection respectively. Fig. 3.2 shows the transmission and reflection coefficients at the N-S interface for different barrier strengths from $Z = 0$ (a transparent barrier) to $Z = 3$ (a tunnel barrier). Here $C(E)$ and $D(E)$ are the transmission probability without and with branch crossing respectively. The probability A of the Andreev reflection at the Fermi energy is

$$A = \frac{1}{1 + 2Z^4}$$

For a transparent barrier ($Z = 0$) the probability of Andreev reflection is maximum in the sub-gap region i.e. $A = 1$ and $B = 0$. This means that in the sub-gap region, for each incoming electron, there is a reflected hole and a Cooper pair is transferred into the superconductor. Above the gap bias $A = B = 0$, the usual quasi-particle tunneling is relevant.

For an opaque barrier ($Z = 3$) the probability of the Andreev reflection is minimum. Indeed the specular reflection of the incident incoming electron is maximum i.e. $A \simeq 0$ and $B \simeq 1$. Increasing the barrier strength increases the specular reflection, thus reducing the transmission probability.

The BTK model gives a good agreement in the case of a macroscopic N-S junction but it does not take into account the disorder in the electrodes. As we will see in the next section the disorder plays a crucial role, and contributes significantly to the sub-gap conductance of N-S hybrid junctions.

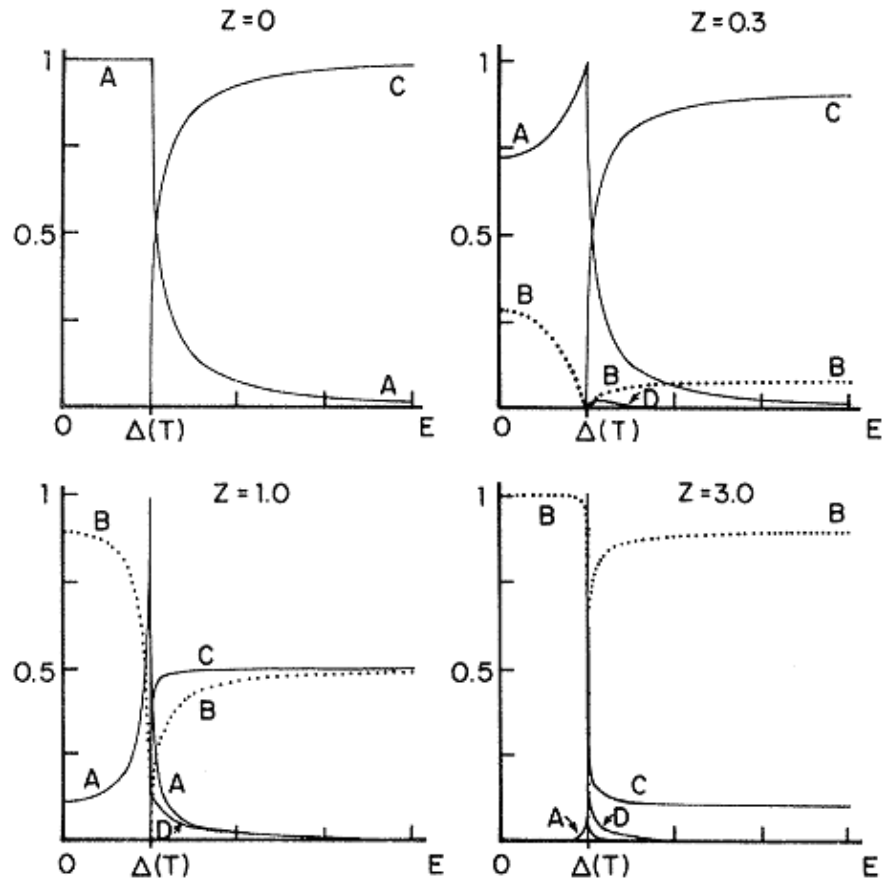


Figure 3.2: Plots of transmission and reflection coefficients at the N-S interface for different barrier strength $Z = 0$ (transparent) to 3 (tunnel). The coefficient A gives the probability of Andreev reflection; B gives the probability of ordinary reflection; C gives the transmission probability without branch crossing and D gives the probability of transmission with branch crossing [14].

3.3 Phase-coherent Andreev reflection - Historical introduction

In the late 80's, tremendous effort took place to miniaturize the devices, that led to the emergence of mesoscopic physics. In the early 90's, Kastalsky et. al. [17] demonstrated the enhancement of differential conductance at low bias on the Superconductor - Semiconductor junction. This zero-bias anomaly was clearly incompatible with the BTK theory. This discovery triggered an extensive work both experimentally [18, 24] and theoretically [15, 16, 29] to understand it.

3.3.1 Excess current in superconductor-semiconductor junction

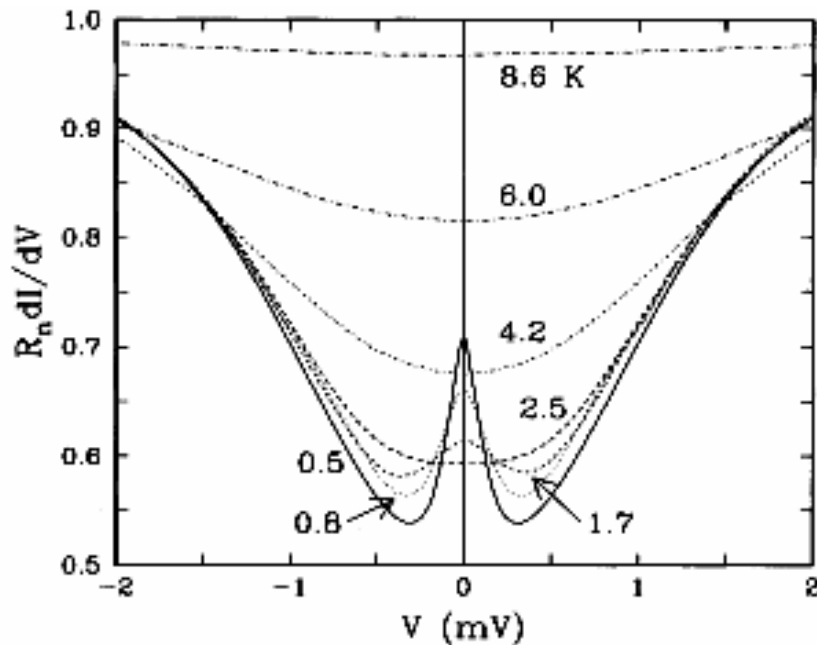


Figure 3.3: Normalized differential conductance - bias voltage characteristic at different temperatures for Nb - InGaAs junction [17].

Fig. 3.3 shows this anomaly in the differential conductance of a Nb - InGaAs junction as a function of bias voltage for different cryostat temperature. The BTK model predicts that for a N-I-S junction the sub-gap conductance decreases with a decrease in the temperature. This is same as observed in the experiment from 8.5 to 2.5 K. However on further lowering the temperature the differential conductance no longer decreases at zero bias. On the contrary, the peak in the differential conductance at low bias increases. The enhancement of the differential conductance at zero bias and for low temperature was incompatible with the BTK model.

3.3.2 Qualitative explanation of zero bias anomaly

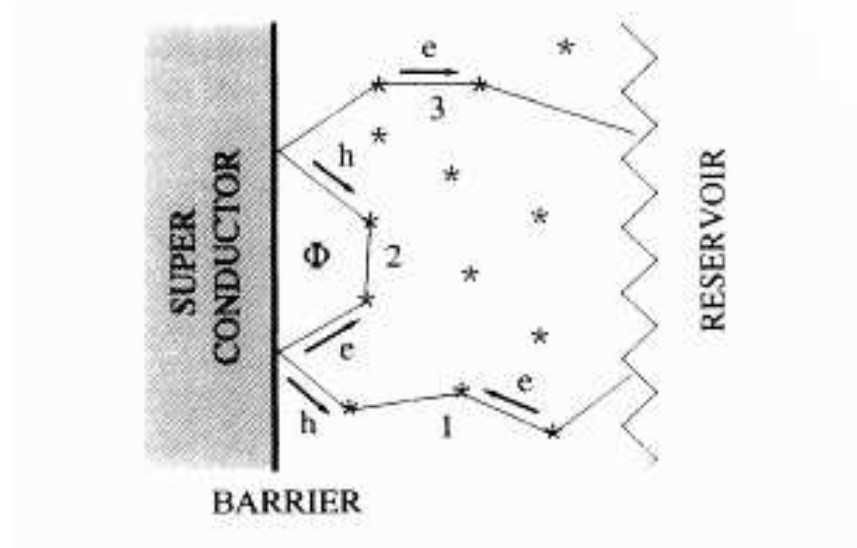


Figure 3.4: *Van Wees et. al. qualitative model of the excess conductance in a S-I-N tunnel junction at low temperature. It consists of three sections: the pure superconductor, the pure normal metal reservoir and the section near the junction with impurities.*

Van Wees et. al. [15] gave the first qualitative picture of zero-bias anomaly by considering the quantum coherence of the electron and the disorder in the electrodes. Fig. 3.4 shows the schematic of the N-S junction with disorder/impurities in the electrodes. The electron with energy $E < \Delta$ is incident from N towards the barrier. Since there is no single quasiparticle state within the superconducting gap, the electron gets mainly specularly reflected from the barrier. The probability of Andreev reflection is very small. The specularly reflected electron undergoes elastic scattering from impurities (asterisk in Fig. 3.4) leading to trajectories re-directed towards the barrier. The two-electron tunneling amplitude at each point on the barrier is immune to the phase-randomization induced by the disorder and therefore adds coherently for the transfer of the electron pairs. Therefore, disorder increases the probability of transfer of electron pair across the N-S junction.

3.3.3 Flux modulation in NS-QUIDS

Pothier et. al. [18] demonstrated the constructive coherence in the N-S junction with a fork geometry (see Fig. 3.5). In the NS-QUID the iterative tunneling involves two different parts of the barrier with a superconducting phase difference θ . An external magnetic field is used to tune the phase θ . For instance at $\theta = \pi$, the electron pairs undergo destructive interference and the sub-gap conductance decreases. The NS-QUID measures the phase-coherent Andreev current as a function of the imposed superconducting phase difference and explicitly shows the constructive and destructive interference due to phase-coherent Andreev current in a N-I-S tunnel junction.

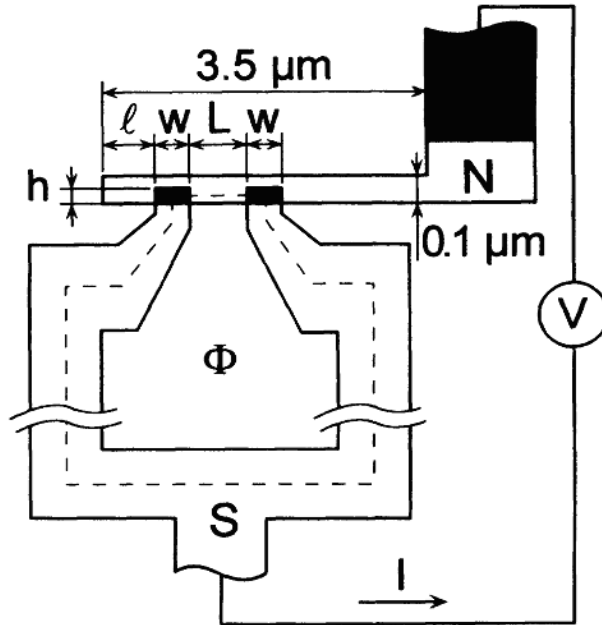


Figure 3.5: *Pothier et. al. experiment on a NS-QUID. A normal metal (Cu) overlaps an oxidized superconducting (Aluminium) fork-shaped electrode.*

Fig. 3.6 shows the enhancement of the sub-gap current in the device at a very low temperature. The left top inset shows the current - voltage characteristic of the junction without (complete line) and with (dashed line) external magnetic field (100 mT) at $T = 27$ mK. The bottom right inset shows the magnetic field dependence of the current. The conductance was periodic with respect to the magnetic flux in the closed loop.

This experiment clearly illustrated the existence of phase-coherent Andreev current in which the disorder in the normal metal electrode confines the electrons near the junctions. The enhancement in current is much larger than the prediction from the ballistic BTK model [14]. Moreover the current was strongly modulated by the external magnetic field. The experiment was in excellent agreement to the theory but needed a fitting re-scale factor of around 2.

3.4 Quantitative model: Hekking and Nazarov

The qualitative explanation of enhancement of differential conductance in the N-I-S junction considered the highly transparent interface in between the two metals. It means that the resistance R_T of the boundary is small or comparable to the normal state resistance. But the experimental situation is on the contrary, with the sub-gap conductivity much lower than the normal state conductivity. The Andreev current in a N-S structure can be obtained from the linearized Usadel equation. This has been done by Volkov [30]. However

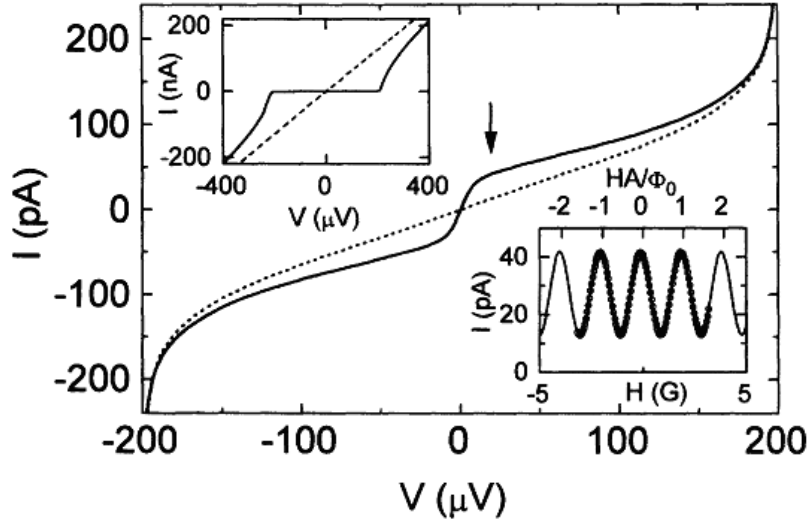


Figure 3.6: *Pothier et. al. experiment on a NS-QUID. Current - voltage characteristic obtained across the junction at 27 mK with (complete line) and without (dotted line) magnetic field. The bottom right inset shows the modulation of current as a function of magnetic field. The top left inset shows the direct I-V at $H = 0$ (solid line) and $H = 0.1$ T (dashed line).*

in the following we shall follow the tunnel hamiltonian approach as worked out in Ref. [16] to calculate the phase-coherent Andreev current across the N-I-S junction.

The first quantitative analysis on the enhancement due to phase-coherent Andreev current was done by Hekking and Nazarov [16]. For clarity, the detailed calculation has been included in Appendix B. The total Hamiltonian of the the N-S junction is given by:

$$\hat{H} = \hat{H}_N + \hat{H}_S + \hat{H}_T.$$

The subscript N and S refer to the normal and superconductor Hamiltonian respectively. \hat{H}_N and \hat{H}_S are described by the electron operator a and a^\dagger in case of N and by quasiparticle operators γ and γ^\dagger for the superconductor. The transfer of electrons across the tunnel barrier is described by the tunnel Hamiltonian \hat{H}_T [21]. The tunnel Hamiltonian can be written as:

$$\hat{H}_T = \sum [t_{k,p} \hat{a}_{k,\sigma}^\dagger \hat{b}_{p,\sigma} + t_{k,p}^* \hat{b}_{p,\sigma}^\dagger \hat{a}_{k,\sigma}],$$

with $t_{k,p}$ being the phenomenological matrix element associated with the transfer of charge across the barrier; the subscript k and p refers to normal metal and superconductor electrode. Using the second order perturbation theory in \hat{H}_T , we can calculate the total amplitude of the transfer of electron pairs from N to S:

$$A_{N \rightarrow S} = \sum_p t_{k_2, p}^* t_{k_1, p}^* [v_p a_{k_2 \uparrow}^\dagger \left[\frac{1}{E_p - \xi_{k_1}} + \frac{1}{E_p - \xi_{k_2}} \right] u_p a_{k_1 \downarrow}^\dagger]. \quad (3.1)$$

with ξ_k and ς being the electron energies for the normal metal and the the superconductor respectively. The quasiparticle energies are $E_p = \sqrt{\Delta^2 + \varsigma^2}$. The denominators in Eq. 3.1 reflect the fact that a virtual state is formed when the first electron enters the superconductor as a quasiparticle. This is subsequently coupled with an another quasiparticle to form a Cooper pair. The total rate of tunneling from N to S is then given by the golden rule:

$$\Gamma_{N \rightarrow S} = 2 \times \frac{2\pi}{\hbar} \times \sum_{k_1, k_2} [|A_{N \rightarrow S}|^2 f(\xi_{k_1}) f(\xi_{k_2}) \delta(\xi_{k_1} + \xi_{k_2} + 2eV)]. \quad (3.2)$$

where the factor 2 is due to the other possibility of the spin and $f(\xi_k)$ is the Fermi function in the normal metal. A similar representation can be written for the electron transfer from S to N ($\Gamma_{S \rightarrow N}$).

Eq. 3.2 requires the knowledge of the dependence $t_{k, p}$ on the wave vectors k and p . In order to make a connection with the standard diagrammatic techniques for diffusive systems, we will re-write the tunnel matrix element in real space coordinates. The tunnel matrix element $t_{k, p}$ can be written in terms of the complete set of functions for the disordered electrodes:

$$t_{k, p} = \int d^3 r d^3 r' \phi_p(r) \phi_k^*(r') t(r, r'), \quad (3.3)$$

where $\phi_p(r)$ forms a complete set of one-electron wave functions in the electrodes, and $t(r, r')$ describes the tunneling from a point r in the superconductor to r' in the normal metal. Further, we define the propagator from r' to r : $K_\xi(r, r') = \sum_k \delta(\xi - \xi_k) \phi_k(r) \phi_k^*(r')$ (see Appendix A). We assume that tunneling predominantly occurs between the neighboring points at the barrier, thus $t(r, r') = t(r) \delta(r - r') \delta(z - z_b)$, where z_b is a point on the barrier and also inserting the identity $1 = \int d\xi d\xi' d\varsigma d\varsigma' \delta(\xi - \xi_{k_1}) \delta(\xi' - \xi_{k_2}) (\varsigma - \varsigma_{p1}) (\varsigma' - \varsigma_{p2})$, we get:

$$\Gamma_{N \rightarrow S} = \frac{4\pi}{\hbar} \int d\xi d\xi' d\varsigma d\varsigma' f(\xi) f(\xi') \delta(\xi + \xi' + 2eV) [v_\varsigma u_\varsigma v_{\varsigma'} u_{\varsigma'}] \left[\frac{1}{\xi + eV - E_p} + \frac{1}{\xi' + eV - E_p} \right] \Xi_{N \rightarrow S}(\varsigma, \varsigma'; \xi, \xi'), \quad (3.4)$$

where we define the quantity

$$\Xi_{N \rightarrow S}(\varsigma, \varsigma'; \xi, \xi') = \int_{\text{barrier}} d^2 r_1 d^2 r_2 d^2 r_3 d^2 r_4 t^*(r_1) t^*(r_2) t(r_3) t(r_4) K_\xi(r_2, r_4) K_{\xi'}(r_1, r_3) K_\varsigma(r_1, r_2) K_{\varsigma'}(r_3, r_4). \quad (3.5)$$

Fig. 3.7 represents the physical meaning of Eq. 3.4 by depicting it diagrammatically. The cross r_i for $i = 1, \dots, 4$ corresponds to the point of tunneling to either side of the barrier with amplitude $t(r_i)$. The solid lines correspond to that of propagator K which depicts

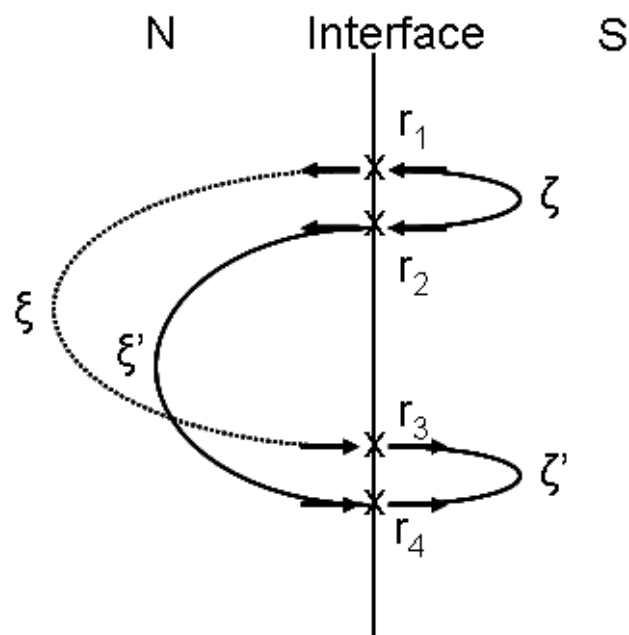


Figure 3.7: Diagram corresponding to Eq. 3.4. Electrons tunnel at point r_1 and r_3 (marked by crosses) across the N-S junction. Solid lines show the propagation of the electron with energy ξ and ξ' in the normal metal (N) and energy ζ and ζ' in the superconducting (S). Crosses at r_2 and r_4 corresponds to the tunneling points in the barrier.

the propagation of the electron due to disorder. The two-electrons tunnel into the normal metal from the superconductor with an energy ς at r_1 and r_2 , propagate in the normal metal with an energy ξ and ξ' . The diagram also takes into account the time-reversed process.

One can compare Eq. 3.4 with the BTK model, if the area of the junction (S) is comparable to λ_F^2 (with λ_F being the Fermi wavelength). In such situation, all the crosses (Fig. 3.7) on the barrier are separated by a few Fermi wavelengths such that the components of momentum k_{\parallel} and p_{\parallel} parallel to the barrier are quantized, leading to the discrete number of channels. Assuming that the scattering is negligible, the electrons have a ballistic motion in electrodes. The sub-gap conductance (Using Eq. 3.4) is given by $G_{NS} = G_{NN}^2 R_Q / (k_F^2 S)$ with G_{NN} the normal state conductance of the tunnel barrier, $R_Q = h/2e^2$ the quantum resistance and G_{NS} the sub-gap conductance due to two-electron tunneling. The effective number of channels contributing to transport $N_{eff} = G_{NN}^2 R_Q / G_{NS}$. For such a case, the contribution depends on the properties of the tunnel barrier only. This gives a result which coincides with the BTK theory. In the opposite limit, the electrons move diffusively in the junction region. Due to interference between incoming and backward electron waves, N_{eff} will decrease, whereby increasing the conductance due to two-electron tunneling. This is the 'phase-coherent Andreev current'.

Based on Fig. 3.7, the two-electrons tunneling across the N-S junction can be driven by three possibilities. Fig. 3.8 depicts the three possible cases.

Possibility 1: The interference contribution originating from the normal metal. It means that crosses in Fig. 3.7 are defined as: $r_1 \approx r_2$ and $r_3 \approx r_4$. Fig. 3.8(a) depicts this situation.

Possibility 2: The interference contribution originating from the superconductor. It means that crosses in Fig. 3.7 are defined as: $r_1 \approx r_3$ and $r_2 \approx r_4$. Fig. 3.8(b) depicts this situation.

Possibility 3: The interference contribution originating from both the normal metal and the superconductor. It is essentially the total contribution due to the interference discussed individually above. Fig. 3.8(c) depicts this situation.

The average over impurities in the respective electrodes can be done by averaging the products of propagators in Eq. 3.4. It means that the impurity averaging leads to definition of Cooperon. The Cooperon is a long-ranged space-dependent quantity with a characteristic length scale $|\vec{r}_1 - \vec{r}_2|$ given by $\sqrt{\hbar D/E}$, which satisfies the equation

$$-\hbar D \Delta P_{\epsilon}(\vec{r}_1 - \vec{r}_2) - i\epsilon P_{\epsilon}(\vec{r}_1 - \vec{r}_2) = \delta(\vec{r}_1 - \vec{r}_2), \quad (3.6)$$

with D being the diffusion coefficient. It can be related to the propagators K as:

$$\langle K_{\xi}(\vec{r}_1, \vec{r}_2) K_{\xi'}(\vec{r}_2, \vec{r}_1) \rangle = \frac{\nu_0}{2\pi} [P_{\xi-\xi'}(r_1 - r_2) - P_{\xi'-\xi}(\vec{r}_1 - \vec{r}_2)].$$

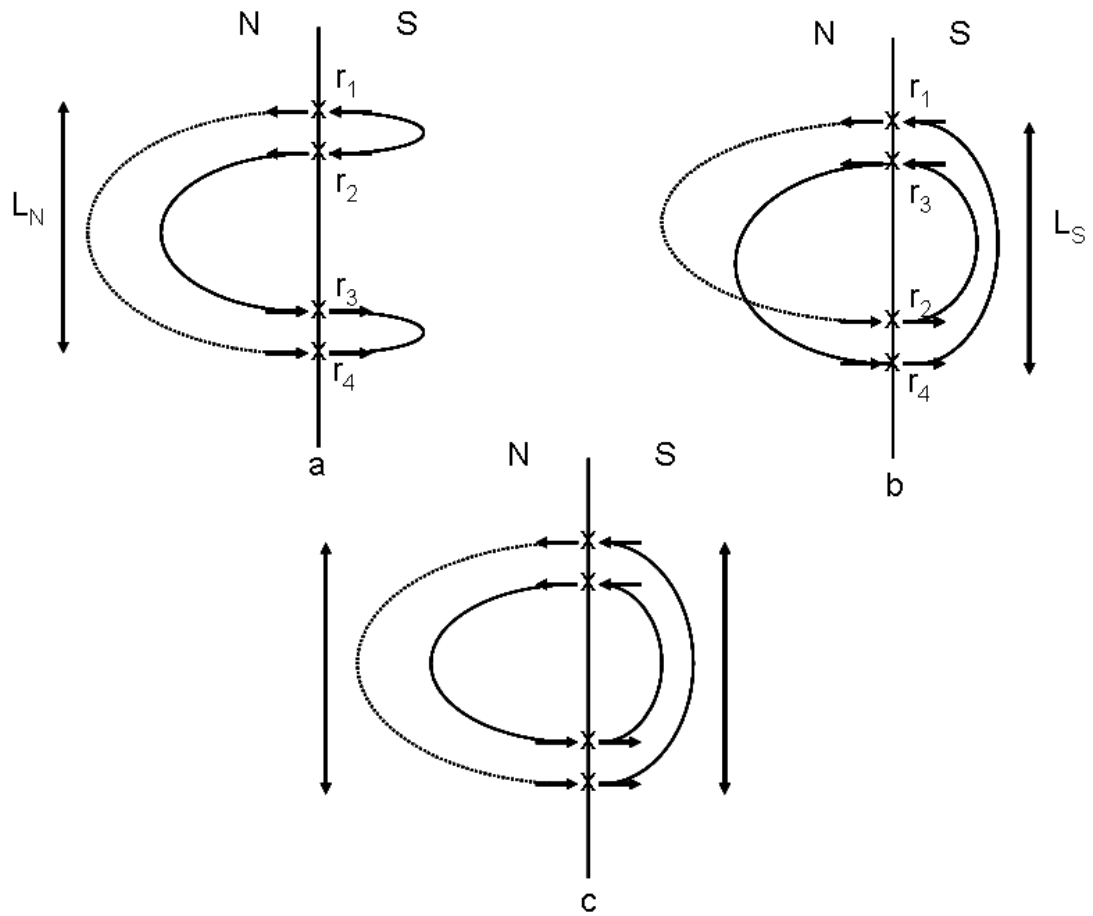


Figure 3.8: Contribution to the sub-gap conductivity due to interference in (a) the normal electrode, (b) the superconducting electrode, and (c) both electrodes.

3.5 Current - voltage relation in disordered N-I-S junctions

In the following, we calculate the phase-coherent Andreev current for our sample geometry. In section 3.5.1 we have re-calculated the phase-coherent current based on Hekking and Nazarov formalism. In the next section (3.5.2), we solved the differential equation involving the Cooperon for our considered geometry. In the last section 3.5.3, we have calculated the full expression of the phase-coherent Andreev current. In comparison to Ref. [16], our expression is valid for $\Delta > eV \gg kT$ and the prefactor is obtained more precisely.

3.5.1 Phase-coherent Andreev current

The total phase-coherent Andreev current is given by $I_{N_{ave},NIS} = 2e(\Gamma_{N \rightarrow S} - \Gamma_{S \rightarrow N})$, due to the transfer of electrons in a N-I-S junction by taking into account the averaging over the disorder in the normal electrode. It is given by:

$$I_{N_{ave},NIS} = \frac{8\pi}{2\pi\hbar} \frac{e\nu_0^3}{k_F^4} F_3(k_F l) \int d^2 R [t(R)]^4 \int d\xi d\zeta d\zeta' (f(\xi) - f(\xi + 2eV)) [v_\zeta u_\zeta] [v_{\zeta'} u_{\zeta'}] \left[\frac{1}{\xi + eV - E_p} + \frac{1}{\xi' + eV - E_p} \right] \int d^2 r [P_{2\xi+2eV}(r) + P_{2\xi-2eV}(r)], \quad (3.7)$$

with $F_3(k_F l)$ being the dimensionless integral defined as :

$$F_3(k_F l) = \int d^2 u d^2 v \frac{\sin[u]}{u} e^{\frac{-u}{2k_F l}} \frac{\sin[v]}{v} e^{\frac{-v}{2k_F l}}. \quad (3.8)$$

A similar expression can be obtained for the total current, $I_{S_{ave},NIS}$ due to two-electron tunneling in a N-I-S junction by taking into account the averaging over the disorder in the superconducting electrode.

$$I_{S_{ave},NIS} = \frac{8\pi}{2\pi\hbar} \frac{\nu_0^3}{k_F^4} F_3(k_F l) \int d^2 R [t(R)]^4 \int d\xi d\zeta d\zeta' (f(\xi) - f(\xi + 2eV)) [v_\zeta u_\zeta] [v_{\zeta'} u_{\zeta'}] \left[\frac{1}{\xi + eV - E_p} + \frac{1}{\xi' + eV - E_p} \right] \int d^2 r [P_{\zeta-\zeta'}(r) + P_{\zeta-\zeta'}(r)]. \quad (3.9)$$

The total phase-coherent Andreev current through the N-I-S tunnel junction is the sum of Eq. 3.7 and Eq. 3.9, which constitutes the central result of this section. It clearly shows the importance of the phase-coherence transport due to disorder in a N-S tunnel junction. The interference effects have been taken into account by averaging the possible scattering events inside the electrode, which is in the Cooperon. Therefore, the subgap transport in the N-I-S tunnel junction depends on both the properties of the barrier and the disorder in the electrodes over a phase-coherence length. In the next section, we will calculate the total phase-coherent Andreev current for our sample design.

3.5.2 Cooperon solution in quasi 1-D diffusive wire

As seen in the previous section, the Cooperon solution (Eq. 3.6) depends on the disorder in electrode and in turn on the layout of the sample. Here, we calculate the total phase-coherent Andreev current for a quasi 1D diffusive wire, with a cross-section area A_{cross} , connected to a superconducting electrode by a point-contact tunnel junction at $\vec{r} = 0$. The spectral current related to Cooperon can be obtained by solving Eq. 3.6 for a 1D case such that $L_{N,S} \gg A_{cross}^{1/2}$.

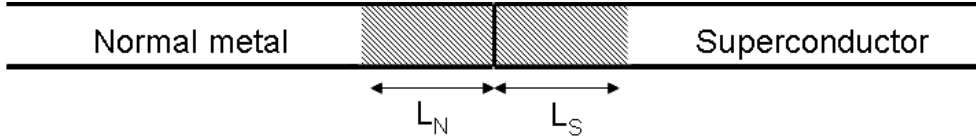


Figure 3.9: *Layout of the design considered. Here the normal metal (N) is connected to a superconductor (S).*

Thus Eq. 3.6 can be written as:

$$-\hbar D d^2 \frac{P_\epsilon(x_1, x_2)}{dx_1^2} - i\epsilon P_\epsilon(x_1, x_2) = \delta(x_1 - x_2).$$

The above diffusion equation is solved for the boundary condition $dP/dx = 0$ at the barrier, indicating no current. Upon Fourier transform, we obtain the Cooperon in momentum representation,

$$P(k, \epsilon) = \frac{1}{\hbar D k^2 - i\epsilon - \hbar/\tau_\phi},$$

with τ_ϕ being introduced as a cut-off time to the Cooperon diffusion in the electrode. The Cooperon can be transformed back in the real space and time

$$P(x, t) = \frac{\theta(t)}{2A_{cross}\hbar} \sqrt{\frac{\pi}{Dt}} \exp\left[-\frac{x^2}{4Dt} - \frac{t}{\tau_\phi}\right]. \quad (3.10)$$

3.5.3 Full expression for the Andreev current

Now we will calculate the Andreev current for the given geometry with the Cooperon defined as above. The local barrier tunnel conductance by considering the averaging over the disorder can be written as (see Appendix A):

$$g_{NN}(R) = \frac{4\pi e^2 \nu(0)^2 F_1(k_F l)}{\hbar k_F^2} [t(R)]^2.$$

Now, we consider a uniform tunnel barrier such that G_{NN} is the total normal state conductance across the junction. G_{NN} is defined as:

$$G_{NN} = \int d^2 R g_{NN}(0) = \frac{4\pi e^2 \nu(0)^2 S F_1(k_F l)}{\hbar k_F^2} t_0^2. \quad (3.11)$$

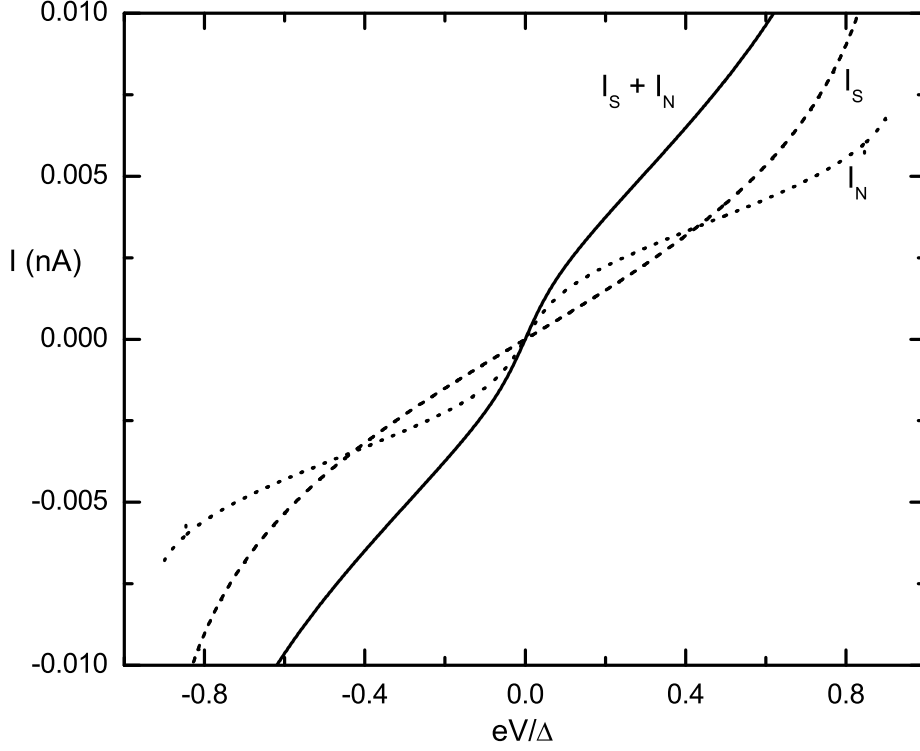


Figure 3.10: Calculated Andreev current - voltage characteristics for quasi 1D diffusive normal metal wire connected to a superconductor as a function of bias voltage. The dot - dashed line corresponds to interference originating from the superconductor ($I_{S_{ave},NIS}$ from Eq. 3.14). The dotted line corresponds to interference originating from normal metal ($I_{N_{ave},NIS}$ from Eq. 3.13). Complete line : $I_A(V) = I_{N_{ave},NIS} + I_{S_{ave},NIS}$. Parameters : $R_{NN} = 2 \text{ k}\Omega$, $\Delta = 0.2 \text{ meV}$, $T = 50 \text{ mK}$, $A_{cross} = 50 \text{ nm} \times 0.3 \text{ }\mu\text{m}$, $D = 80 \text{ cm}^2/\text{s}$, $\tau_\phi = 300 \text{ ps}$.

The total phase-coherent Andreev current across N-I-S junction ($eV < \Delta$) is the sum of Eq. 3.7 and Eq. 3.9:

$$I(V) = I_{N_{ave},NIS} + I_{S_{ave},NIS} \quad (3.12)$$

$$I_{N_{ave},NIS} = \frac{G_{NN}^2 \hbar F_3(k_F l) \Delta^2}{8\nu_0 e^3 [F_1(k_F l)]^2 \sqrt{D}} \frac{1}{2A_{cross} \hbar} \int d\xi [f(\xi/2 - eV) - f(\xi/2 + eV)] \times \frac{1}{[\Delta^2 - \xi^2/4]} \left[\frac{1}{\sqrt{\frac{1}{\tau_\phi} - \frac{i\epsilon}{\hbar}}} + \frac{1}{\sqrt{\frac{1}{\tau_\phi} + \frac{i\epsilon}{\hbar}}} \right] \quad (3.13)$$

$$I_{S_{ave},NIS} = \frac{4G_{NN}^2 \hbar^{3/2} F_3(k_F l) \Delta^2}{2^{5/2} \nu_0 e^3 [F_1(k_F l)]^2 \sqrt{D}} \frac{1}{2A_{cross} \hbar} \int d\xi \frac{f(\xi/2 - eV) - f(\xi/2 + eV)}{[\Delta^2 - \xi^2/4]^{5/4}} \quad (3.14)$$

These equations constitute the central result of this section. Here, we have calculated the phase-coherent Andreev current by doing the averaging over the disorder on either side of the barrier namely, normal metal and the superconductor. The above results are valid for $\Delta > eV \gg kT$. It is worth noticing that both the contributions diverge near the threshold voltage (Δ) indicating the breakdown of the perturbation theory.

Let us discuss the relevant length scale of the diffusion of the Andreev pairs in the electrodes. Fig. 3.10 shows the different components in the phase-coherent Andreev current arising due to disorder in the normal metal and the superconducting electrode along with the total current due to the two processes. For simplicity, we have taken the diffusion coefficient to be identical in the normal metal and the superconductor. The parameters for calculation are similar to that of our sample. We have taken the phase-coherence length as the cut-off length for the diffusion of the Cooperon. The part emerging from the normal metal is more sensitive to the disorder and adds to the zero bias anomaly.

3.5.4 Temperature dependence of the Andreev current

The total current across the N-I-S tunnel junction is the sum of single quasiparticle current (I_T) and the phase-coherent Andreev current (I_A), so that $I_{N-I-S} = I_T + I_A$. For $\Delta \gg kT_e$ and $0 \ll eV < \Delta$, the quasiparticle current contribution to the total current can be written as:

$$I(V) \simeq I_0 \exp\left[\frac{eV - \Delta}{kT_e}\right]. \quad (3.15)$$

where $I_0 = \frac{\Delta}{eR_n} \sqrt{\frac{\pi kT_e}{2\Delta}}$. Thus, quasiparticle current reduces exponentially with temperature. At very low temperature, the quasiparticle current contribution almost goes to zero for sub-gap bias voltage. In comparison, the phase-coherent Andreev current depends mostly on the transparency of the junction rather than on temperature.

Fig. 3.11 shows the comparison of the quasiparticle current and the phase-coherent Andreev current at a temperature of 300 and 100 mK respectively. For Andreev current we consider the disorder on either side of the junction so that, $I_A(V) = I_{N_{ave},NIS} + I_{S_{ave},NIS}$.

For $T = 300$ mK, the quasiparticle current is always greater than the phase-coherent Andreev current. For $T = 100$ mK, in most of the region the quasiparticle current is much smaller than the phase-coherent Andreev current. For bias close to the gap, quasiparticle current subjugates Andreev current due to the tunneling of high-energy quasiparticles.

3.5.5 Relevant cut-off length of Andreev pair

For the two-electrons to interfere constructively, they should have zero phase difference between them. At zero voltage, energy (compared to E_F) indeed it happens, so that the

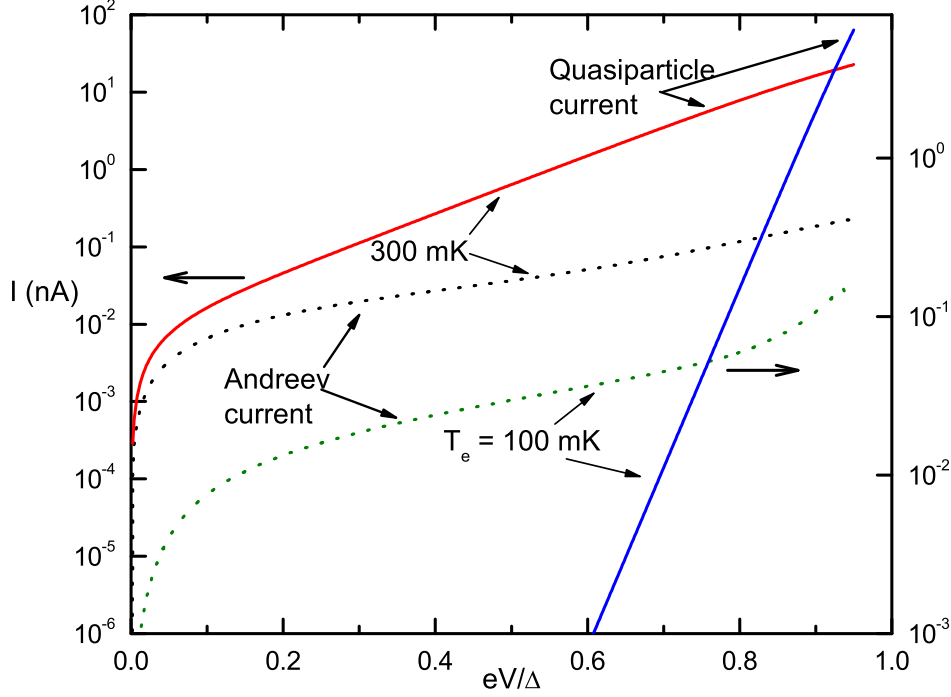


Figure 3.11: *Calculated current-voltage characteristic of the N-I-S junction at $T_e = 300$ and 100 mK. The complete lines show the contribution due to quasiparticle current and the dotted lines show the phase-coherent Andreev current. Parameters : $R_{NN} = 2$ k Ω , $\Delta = 0.2$ meV, $A_{cross} = 50$ nm \times 0.3 μ m, $D = 80$ cm²/s, $\tau_\phi = 300$ ps.*

phase acquired by the electron is canceled by the hole, which retraces the same trajectory as that of the incident electron.

However, the Andreev reflection is a perfect retro-reflection only for the electrons at the Fermi energy [31]. Fig. 3.12 shows the retro-reflection of the incident electron above the Fermi energy. For an incident electron above the Fermi level $E_F + \epsilon$, $k_F + \delta k/2$, the reflected hole is given by $E_F - \epsilon$, $-k_F + \delta k/2$. This leads to a wavevector mismatch between the incident electron and the reflected hole which is linear in energy : $\delta k = 2\epsilon/\hbar v_F$. If the two-electrons originating from the superconductor have an energy E , then after diffusion over a distance L_E from the interface, the phase-shift becomes π and the two-electrons no longer undergoes constructive interference. This energy dependent length scale is given by:

$$L_E = \sqrt{\frac{\hbar D}{E}},$$

with D being the diffusion coefficient in the metal. The resulting L_E at $E = 0$, leads to

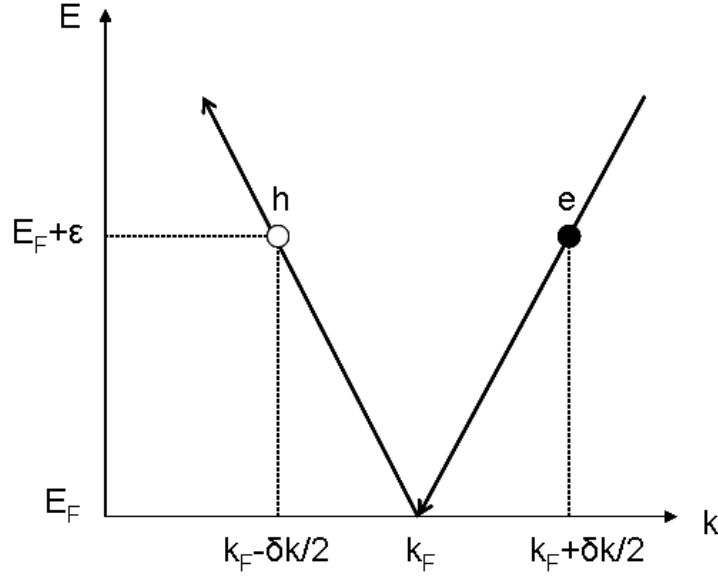


Figure 3.12: Schematic of the Andreev reflection process. An extra electron with an extra energy ϵ compared to the Fermi energy E_F of the superconductor hits the interface of the two electrodes from the N side. The reflected hole-like particle and the incident electron have a slight wave-vector mismatch δk .

long range coherence responsible for re-entrance effect [32]. For a thermal distribution, the length scale is determined by the thermal energy kT of the single electron. The resulting phase-coherence length is given by:

$$L_T = \sqrt{\frac{\hbar D}{kT}}, \quad (3.16)$$

is much larger than the mean free path. It leads to electron pairs adding coherently up to a distance L_N and hence enhances the sub-gap conductivity near zero bias.

It is also worth noticing that L_N diverges for $T, V = 0$, since the two tunneling electrons have the same energy, and thus their relative phase is conserved over the infinite distances. However, the associated low-energy divergence of the sub-gap conductance is spurious and will be cut naturally by two mechanisms. *Firstly* the natural decoherence mechanism in the metal such as electron-electron interactions, electron-phonon interactions and magnetic impurities will induce decoherence [33]. Thus, the Cooperon propagation is cut by the so-called phase-coherence length, L_ϕ . *Second*, if the length of the wire is smaller than the dephasing length, it provides a cut-off for the diffusion.

Fig. 3.13 shows the differential conductance of the quasi 1D wire as a function of voltage bias. Here, we have taken the phase-coherence length as the cut-off length for the diffusion of the Cooperon. It corresponds to three different phase-coherence times namely 1000 ps, 300 ps and 1 ps. As seen, the enhancement in the differential conductance at low bias due to the phase-coherent Andreev current decreases as we decrease the phase-coherence time.

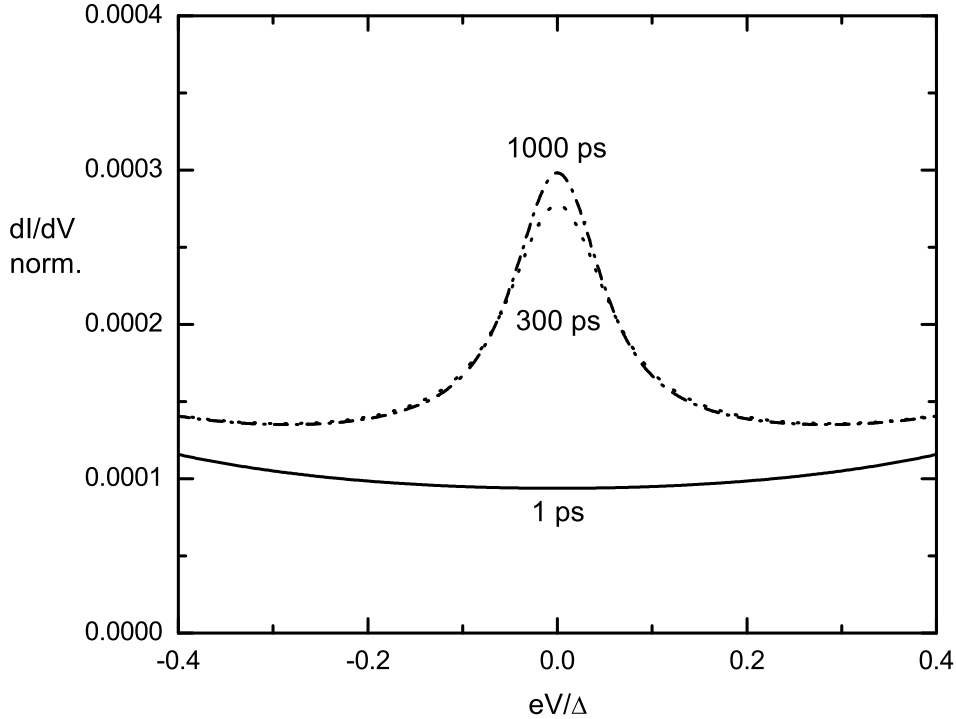


Figure 3.13: Calculated differential conductance as a function of bias voltage across the N-I-S junction for different phase-coherence times. The calculated parameters are the same as in Fig. 3.10.

As will be seen in chapter 7 of this thesis, the phase coherence time τ_ϕ for our sample is around 150 ps.

3.5.6 Non-uniform tunnel barrier

In the above quantitative analysis of the phase-coherent Andreev current, we assumed the uniformity of the tunnel barrier across the junction. Although the barrier is only few nm thick, in practice the tunnel barrier can be non-uniform (see Fig. 3.14).

We assume the oxide in between the electrode to be a tunnel barrier but of variable thickness along the junction area. The variable oxide thickness leads to points in the barrier which have exponentially higher probability for the transfer of the charge across the junction in comparison to other points.

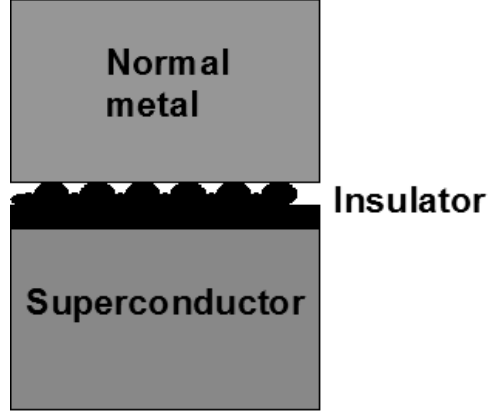


Figure 3.14: *Layout of the design considered with an non-uniform barrier.*

The impurity averaged Andreev current through N-I-S junction can be written as:

$$I_A = \int dE I(E) [f(\frac{E}{2} - eV) - f(\frac{E}{2} + eV)],$$

where $I(E)$ is the spectral current as

$$I(E) = \frac{h}{8e^3\nu(0)} \int_{\text{barrier}} d^2r_1 d^2r_2 g_{NN}(r_1) g_{NN}(r_2) [P_E(0) + P_{-E}(0)]. \quad (3.17)$$

We consider the contribution to the transfer due to the points which has higher probability for the transfer of charge. Thus the integral over local conductance of the junction in Eq. 3.17 for the two particles can be written as:

$$\begin{aligned} \int d^2r_1 d^2r_2 g_{NN}(r_1) g_{NN}(r_2) &= \sum_{i,j} G_{NN}(R_i) G_{NN}(R_j) \\ &= [\sum_{i=j} G_{NN}(R_i)^2 + \sum_{i \neq j} G_{NN}(R_i) G_{NN}(R_j)]. \end{aligned}$$

The tunnel conductance at N such points is assumed to be same, we get

$$\int d^2r_1 d^2r_2 g_{NN}(r_1) G_{NN}(r_2) = [N G_{NN}^2 + \frac{N(N-1)}{2} G_{NN}^2] = N G_{NN}^2 [1 + \frac{N-1}{2}].$$

Thus Eq. 3.17 can be written as:

$$I(E) = \frac{h}{8e^3\nu(0)} \frac{G_{NN}^2}{N} [1 + \frac{N-1}{2}] [P_E(0) + P_{-E}(0)].$$

Therefore, the enhancement of current across the N-I-S junction due to constructive interference averaging on the impurities will be further re-scaled due to the non-uniform tunnel barrier. It could explain the re-scaling (re-scaling factor > 1) done in the experiment of Pothier et. al. [18] and also in the experiment chapter 7 of this thesis [34].

3.6 Heat contribution due to phase-coherent Andreev current

Andreev current is most of the time in the literature is referred as a dissipationless current [35]. The naive picture behind this folklore is the one which shows the two-electrons tunneling across the junction at the Fermi energy. It gets even more boosted when no voltage drop is measured in a S-N-S junction which allows for the flow of supercurrent [36].

As discussed for a N-I-S tunnel junction the probability of transfer two-electrons is mainly dominated by the interference induced by the disorder in the electrodes [25]. In the following, we will calculate the heat contribution due to the phase-coherent Andreev current. We consider a tunnel barrier between the infinitely long normal metal and superconductor. The heat transfer due to the two-electrons tunneling from N to S is obtained from Eq. 3.2 as:

$$\dot{Q}_{N \rightarrow S} = \frac{4\pi}{\hbar} \sum_{k1, k2} |A_{N \rightarrow S}|^2 (\xi_{k1} + \xi_{k2}) f(\xi_{k1}) f(\xi_{k2}) \delta(\xi_{k1} + \xi_{k2} + 2eV),$$

and that of the reverse process is given by:

$$\dot{Q}_{S \rightarrow N} = \frac{4\pi}{\hbar} \sum_{k1, k2} |A_{N \rightarrow S}|^2 (\xi_{k1} + \xi_{k2}) [1 - f(\xi_{k1})][1 - f(\xi_{k2})] \delta(\xi_{k1} + \xi_{k2} + 2eV).$$

The net heat transfer out of the normal metal is given by $\dot{Q}_{outofN} = \dot{Q}_{N \rightarrow S} - \dot{Q}_{S \rightarrow N}$. Thus we get,

$$\begin{aligned} \dot{Q}_{outofN} &= \frac{4\pi}{\hbar} \sum_{k1, k2} |A_{N \rightarrow S}|^2 (\xi_{k1} + \xi_{k2}) [f(\xi_{k1}) + f(\xi_{k2}) - 1] \delta(\xi_{k1} + \xi_{k2} + 2eV) \\ &= \frac{4\pi}{\hbar} \sum_{k1} |A_{N \rightarrow S}|^2 (-2eV) [f(\xi_{k1}) - f(\xi_{k1} + 2eV)] = -I_{Andreev} \cdot V \quad (3.18) \end{aligned}$$

In the above equation we can replace the sum over $k1$ with the integration over the continuous spectrum, $\sum_k \dots \rightarrow \nu_0^2 \int dE_k N_N(E_k) N_N(E_k + 2eV)$ over the density of states per unit spin.

Eq. 3.18 gives the heat carried by the Andreev current out of normal metal. It is worth noticing that the negative sign gives the direction of heat dissipation. The Andreev current induces dissipation like Joule dissipation and with the heat going in the normal metal.

Using the above definition of the work done by the source on the device, the heat engine schematic of the device can be given by Fig. 3.15. In comparison with the N-I-S schematic in chapter 2, the external source dissipates heat in the normal metal only.

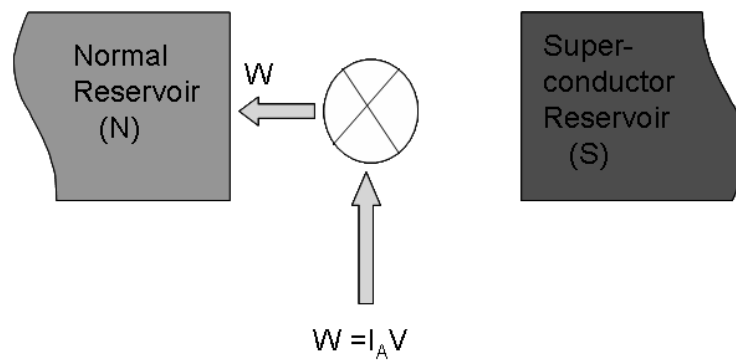


Figure 3.15: *Carnot heat engine diagram for the Andreev current in a N-I-S device.*

Chapter 4

Sample fabrication and experimental techniques

4.1 Introduction

Discovery of various new phenomena in the last two decades in mesoscopic physics is a direct consequence of advances in the fabrication of samples at the nano-scale. Lithographic techniques such as ultra-violet lithography, field emission lithography, enable one to fabricate samples at sub-micron scale, which are highly stable and reproducible. One of the most famous techniques of lithography is electron beam lithography (EBL), which uses a focussed beam of high energy electrons to expose an electron-sensitive resist on the substrate. The resolution of EBL is much higher (50 nm) than the optical lithography due to the short wavelength of high energy electrons. High resolution and reproducibility makes EBL an attractive technique to pattern a sample at sub-micron scale.

In the following, we will describe the various processes involved in the fabrication of our samples. Most of the processes are rather well established now. The various steps involves spinning the resist on the wafer, then exposing it by EBL to pattern the desired mask and then perform a shadow evaporation of various metals with the desired oxidation step. Then we discuss the measurement technique involved in characterizing the samples. A detailed schematic description of the cryostat wiring and the electronic circuit is done.

4.2 Nano-fabrication

Here we will discuss the various steps involved in fabricating most of our devices. For all samples in this thesis, we use a Si wafer with a thick layer (500 nm) of SiO_2 on it. The wafer is first cleaned with plasma oxygen reactive ion etching (RIE) for 1 min.

4.2.1 Bilayer resist coating

Substrate are coated by a conventional bi-layer PMMA. The process is rather well established in which the substrate is coated with a positive resist.

Bottom layer: The substrate is first coated with a PMMA-MAA which is a positive resist, whose role is to sustain the upper layer of resist with a significant undercut. PMMA-MAA is diluted at 90 g/l in 2-ethoxyethanol, filtered with 0.2 μm filters. The PMMA-MAA is spun at 2000 rpm for 60 s. Subsequently, the resist is baked for 5 minutes at 180 degree Celsius on a hot plate. It produces a total thickness ~ 900 nm.

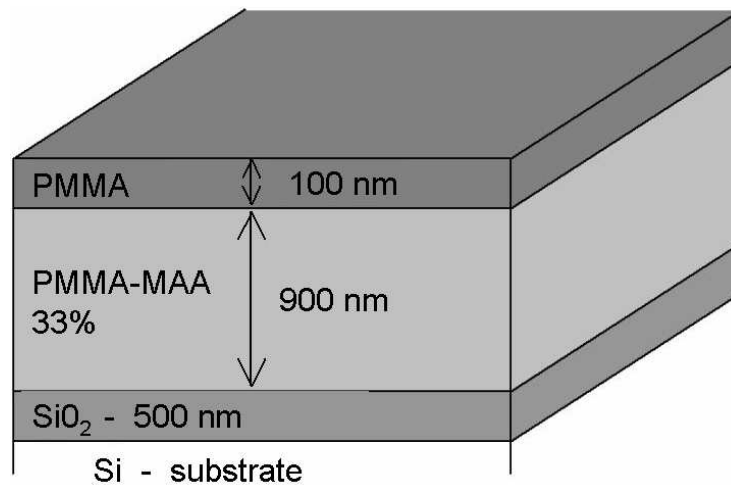


Figure 4.1: Schematic representation of the bilayer resist coating on the top of the substrate. The PMMA-MAA bottom layer is 900 nm thick and the PMMA top layer is 100 nm thick.

Top layer: The upper resist is a PMMA - 4 percent (very high molecular weight), 2 percent in O-xylene constitutes the mask. It is spun at 5000 rpm for 60 s and subsequently baked for 30 minutes at 160 degree Celsius on a hot plate. This resist is baked at slightly lower temperature than the first layer so as to limit the stress between the layers. It is also important to use a rather weak solvent for this layer, to prevent the intermixing of the two layers. It produces the typical thickness ~ 100 nm making the total thickness of the bi-layer of about 1000 nm.

4.2.2 Electron beam lithography, the EBL

The invention of electron beam lithography in late the 60 s and the discovery of a common polymer, the polymethyl methacrylate (PMMA), as e-beam resist led to a rapid success in nano-fabrication. Despite sweeping advances in EBL, PMMA still remains the most common e-beam resist in most of the labs. EBL is preferred over optical lithography since it has no perturbation due to diffraction limit of light and can make features in the nanometer range. It can make masks with high resolution and high reproducibility. The

most important drawback of EBL is low speed, which is crucial for industry but is less important in a laboratory environment.

The principle of the e-beam lithography is based on the interaction of high energy electrons onto the sample coated with an electron sensitive resist. High energy electrons focussed onto the sample penetrate both the polymer (PMMA) and copolymer (PMMA) to make the desired pattern.

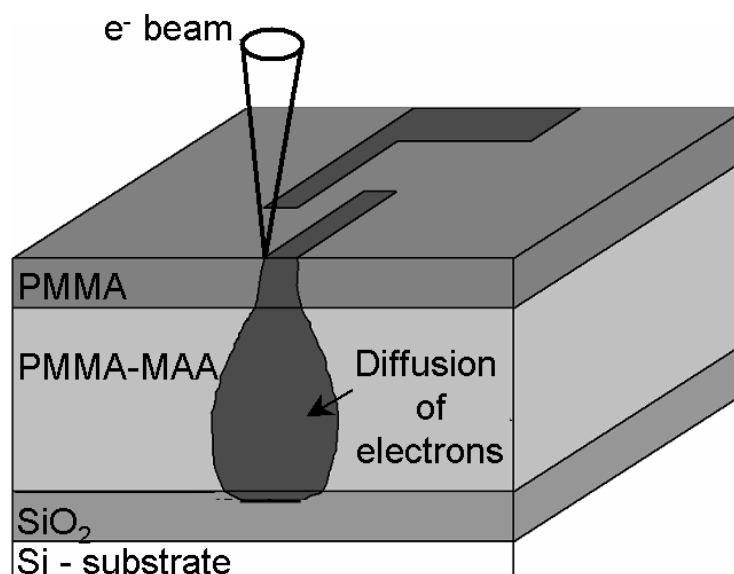


Figure 4.2: Schematic description of the electron beam lithography step. Here, an electron sensitive resist is exposed to a high energy electron beam to form the desired pattern.

Fig. 4.2 shows the schematic description of the involved process. High energy electrons from the beam are absorbed by the resist, leading to the breaking of PMMA and PMMA-MAA polymer chains into fragments of smaller molecular weight, which will be dissolved by the developer in the subsequent process. PMMA-MAA has a broader exposed region in comparison to the top resist. This is due to high sensitivity of PMMA-MAA towards the electron beam in comparison with the top polymer. Also, the electrons backscattering from the substrate leads to an extra profile in the bottom layer.

Most of the samples made in this thesis have been fabricated in a Leo 1530 electron beam lithography with a 20 keV electron beam. It is equipped with a software Elphy from Nano Raith, in which the design of the desired mask are made. EBL has a resolution to a line width of less than 50 nm.

4.2.3 Development of resist

The standard development process for PMMA uses a solution of Methyl Isobutyl Ketone (MIBK) with Iso-Propyl Alcohol (IPA). MIBK is a strong developer of the PMMA so it is diluted with IPA. The development process is typically arrested by the solution of IPA.

IPA is often considered a non-solvent, but in case of PMMA it is appropriately termed as a weak solvent.

A cold mixture of IPA and distilled water can be used as developer. Water by itself cannot develop PMMA, however, when it is in a solution with IPA it becomes a co-solvent. While this development system may have the potential to produce little to no swelling of the resist (unlike MIBK), and very good resolution and line roughness, the needed cold bath was not readily available, and this method of developing was not pursued in this thesis. It is mentioned here for a reason that it may provide a less hazardous and more effective alternative to MIBK.

In this thesis, bilayer polymer and copolymer chains are developed in a 3:1 mixture of Iso-propanol-2 and MIBK (2-propanol : methyl-isobutyl-ketone) for 35 s and then flushed with IPA for 60 s. As a last step, a short anisotropic high pressure oxygen etch is done in a reactive ion etcher to remove the last PMMA-MAA remnants left on the substrate. The suspended mask is now ready for the metal evaporation.

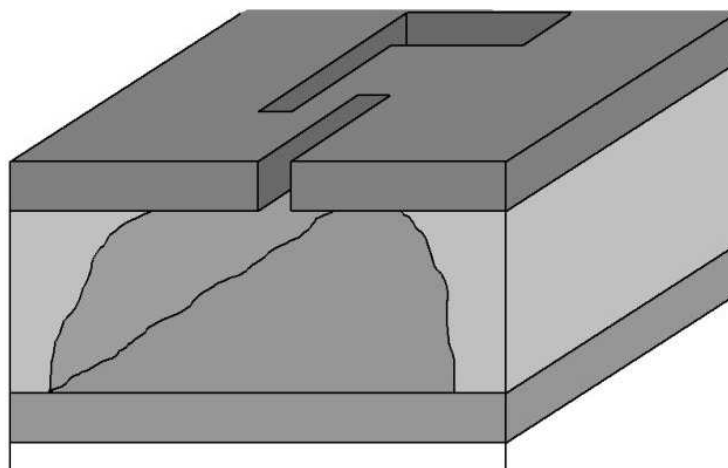


Figure 4.3: *Development process using MIBK/IPA solution.*

4.2.4 Metal deposition

After the completion of the mask, the different metals are deposited accompanied with the in-situ oxidation. Most of the samples discussed in this thesis were made in a ultra high vacuum with a electron gun evaporator at a base pressure of below 10^{-9} Torr. The samples are made with a shadow evaporation technique. In the following, we will discuss the electron gun evaporator and the shadow evaporation.

The sample is placed on a sample holder which is positioned upside down in a ultra high vacuum chamber. On the bottom of the chamber is a movable source with 5 different materials such as: copper, aluminium, niobium, silicon and gold.

All the samples in this thesis are made from Al and Cu. A high energy electron beam is used to evaporate one of the metal. A e-gun evaporator can be used to evaporate material

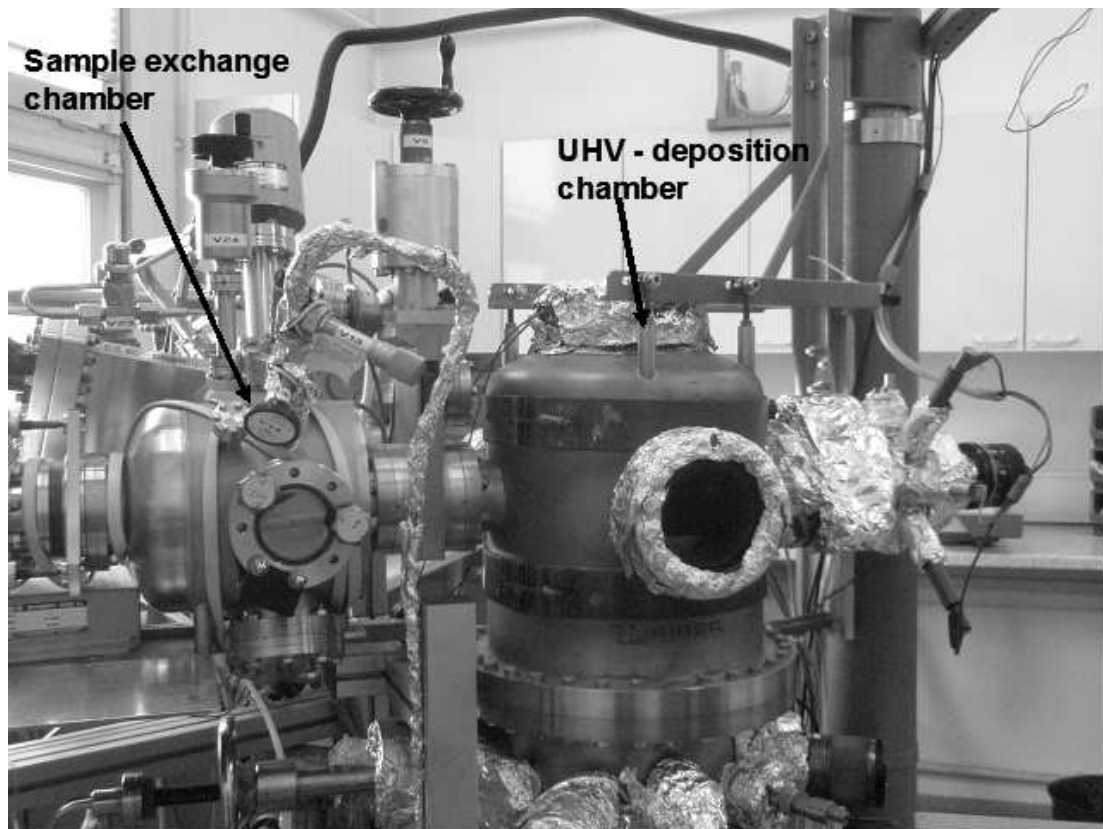


Figure 4.4: *Photograph of the ultra high vacuum deposition chamber used to fabricate the samples.*

with high melting point. Then the materials are deposited at a rate of about 0.2 nm/s with a pressure of deposition chamber lower than 5.10^{-8} Torr.

The shadow evaporation technique exploits the large undercut of the bottom resist of the mask to evaporate two or more different materials. The sample holder can be tilted so that different angles can be used for evaporation without breaking the vacuum.

By evaporating the metals in two steps with a difference in angle θ through a suspended resist mask, the structures are shifted with respect to each other by a distance d given by $d = 2.h.\tan\theta$, where h is the thickness of the resist. In some cases, some additional structures from shadow can be prevented by depositing at sufficient large angle θ . It deposits the material on the side wall of the resist, resulting in a removal during lift off.

Following is the typical process involved during the evaporation of our sample:

Step 1: Deposition of aluminium

First the Al is evaporated through the mask with an angle.

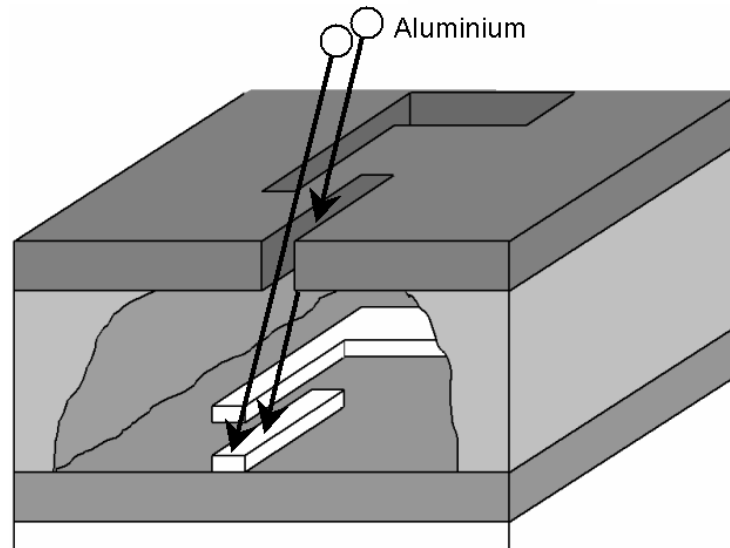


Figure 4.5: *Schematic representation of the Al atoms at an angle through the suspended resist mask.*

Step 2: Oxidation of aluminium electrode

In our samples the quality of tunnel barrier is extremely important. There are many ways to fabricate a tunnel barrier, however the use of aluminium oxide (Al_2O_3) as a tunnel barrier is particularly easy and it has been proven to be a reliable barrier over many years in superconducting tunneling experiments.

In order to prevent the contamination of the other material due to oxidation, we perform the oxidation of our sample in a separate chamber called load-lock. After the first evaporation, the sample is transferred into the load-lock without breaking the vacuum. The pure oxygen is let into the load-lock vacuum chamber for a few minutes and the tunnel barrier is formed on the Al electrode.

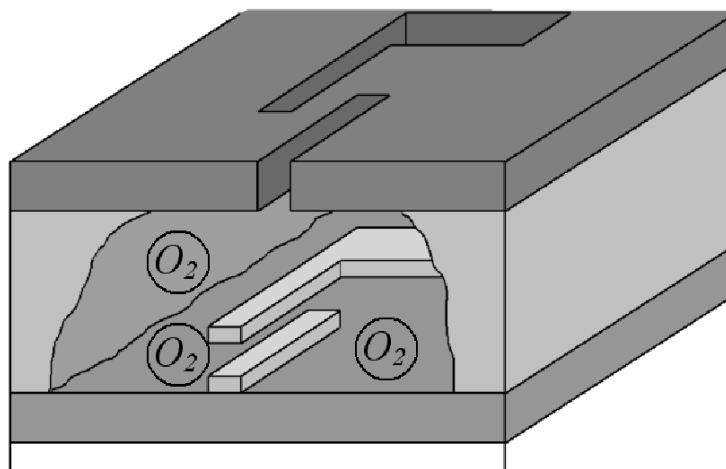


Figure 4.6: *Oxidation of the deposited Al atoms in the presence of pure oxygen.*

The contact resistance of the junction depends mainly on the pressure/amount of the oxygen present inside the chamber and also on the time of oxidation.

Step 3: Evaporation of copper

After the tunnel barrier is formed on the top of Al electrode, the Cu is evaporated at a different angle so as to make a Al-AlO(x)-Cu junction.

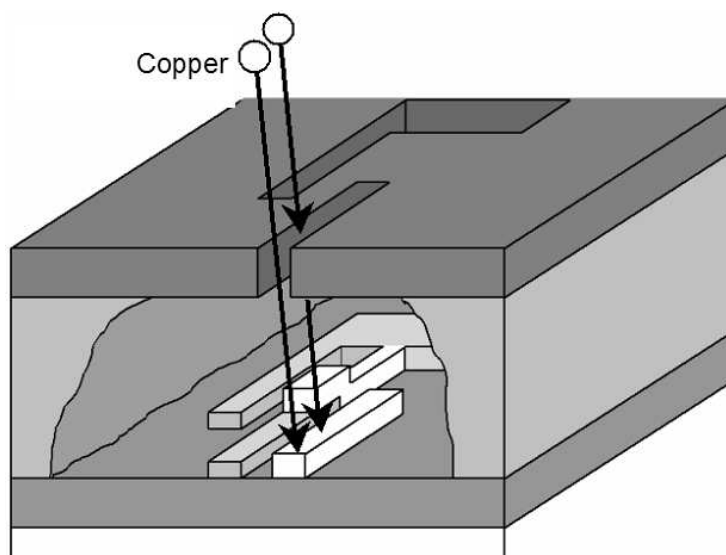


Figure 4.7: *Schematic representation of the evaporation of the Cu atoms at a different angle through the suspended resist mask in order to form a Al-AlO(x)-Cu tunnel junction.*

4.2.5 Lift-off

The last process is the lift off. For our delicate samples, we put the samples in the acetone and wait till all the residual material has lifted off. Then it is flushed with cold Iso-propanol. The use of ultrasonic agitation is avoided as it can destroy the complete sample. Now we use NMP heated at 70 degrees Celsius for the lift off.

4.3 Example: Fabrication procedure of the individual samples

Here I will discuss the fabrication process of two different samples namely the cooler sample and the phonon thermometer. For both of these devices Al is used as a superconductor and Cu as a normal metal. In the cooler sample, we have made several different versions which will be discussed in this thesis. In the following, we will discuss only the main design of the nano-cooler sample. In the following, the description of different processes for the nano-cooler sample shall be discussed.

The aim is to fabricate a cooling device which will cool an isolated normal metal using quasiparticle tunneling. For S-I-N-I-S coolers, the isolated normal metal is a Cu connected to superconducting Al electrodes through tunnel barriers.

The design requirement:

1. The Cu normal metal is an isolated small island connected to the large superconducting reservoirs.
2. To increase the cooling efficiency, the normal metal should have a minimum contact surface to the substrate and also the tunnel junction should have a maximum junction surface/volume ratio.
3. The quality of tunnel barrier is one of the main requirement of our device. The tunnel resistance between the normal metal and the superconductor should not be very high, as it will reduce the cooling power. On the other side, there should not be any defects and pinholes in the barrier. For most of our cooler junctions the achieved transparency is of the order $10^{-5}\Omega.\mu m^2$.

Nano cooler fabrication:

Fig. 4.8 shows the scanning electron micrograph of one of the cooler devices. The device consist of the central Cu island connected to the two large Al line with a tunnel barrier making a Al-AIO(x)-Cu-AIO(x)-Al junction. This is called the cooler as the central N island is electronically cooled due to extraction of quasiparticles through the superconductor tunnel junction. Typically, the central Cu island is 50 nm thick, 4 or 5 μm long and 0.3 μm wide and it is embedded between the two 40 nm thick and 1.5 μm wide superconducting Al electrodes. The tunnel barriers at the symmetric junctions of dimension $1.5 \times 0.3 \mu m^2$ are made by oxidation in 0.2 mBar of oxygen for 3 minutes and this gives a total normal - state resistance R_n in the range 2-3 k Ω . The Al electrode is made wide in comparison to the Cu island, so that Cu obtained from the shadow on either side of Al act as traps.

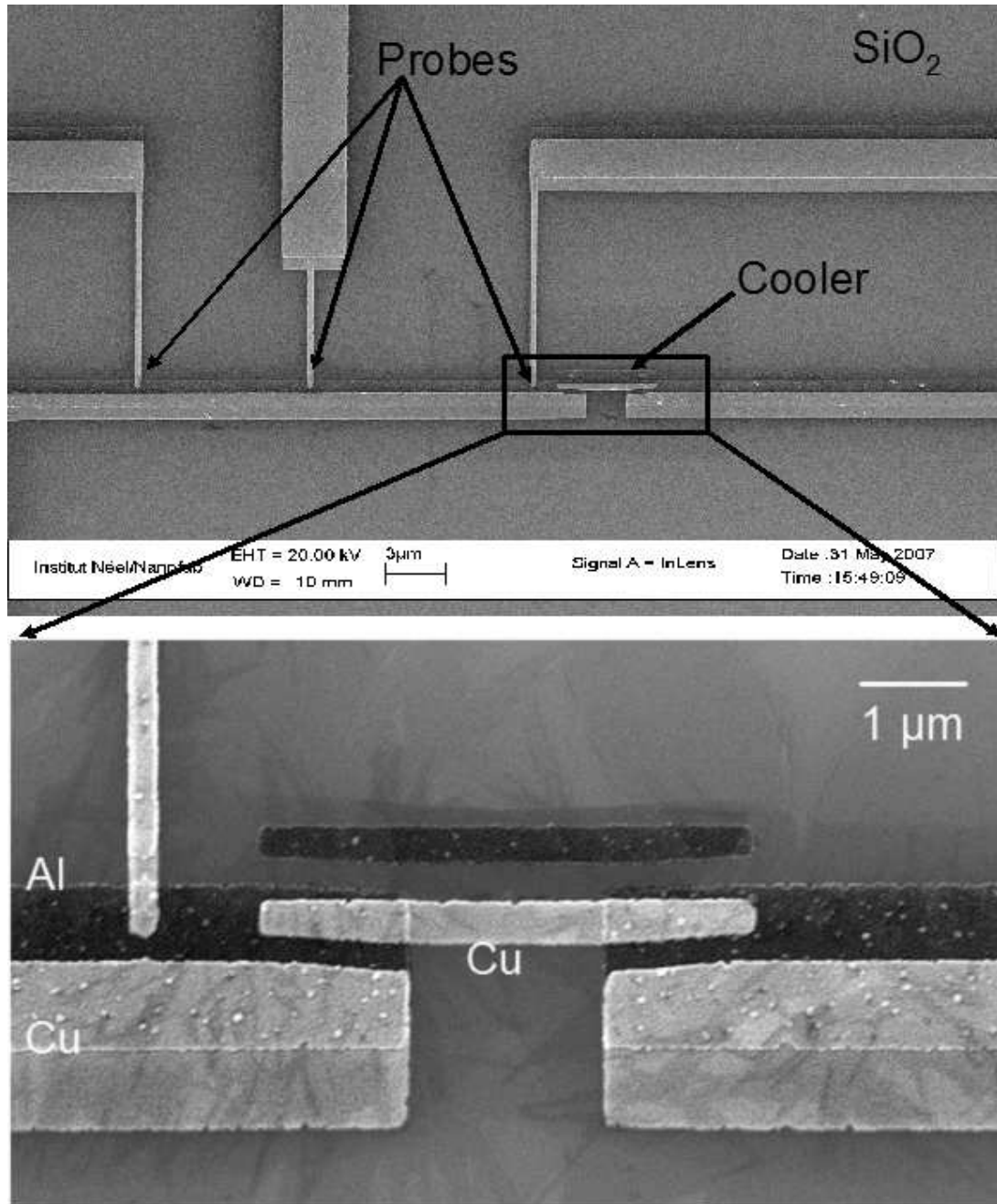


Figure 4.8: Scanning electron micrograph of a cooler sample. Top micrograph shows the entire sample with the 3 Al-AlO(x)-Cu probe junctions. Bottom micrograph shows the zoom of the cooler junction. Here the central Cu island is connected to two superconducting Al reservoirs through a tunnel barrier making a S-I-N-I-S junction.

In addition to the cooler junctions, there are 3 Cu tunnel junction of area $0.3 \times 0.3 \mu\text{m}^2$ on one side of the Al electrode. These are called probe junctions. In comparison to the isolated cooler island, the Cu on the probe junction is connected to a big reservoir. Therefore the Cu on probes are strongly thermalized to the bath temperature of the cryostat.

4.4 Measurement apparatus

In this thesis the nano-cooler devices are measured in a homemade He3 cryostat and a homemade dilution refrigerator [37]. To allow the rapid characterization at room temperature, samples resistance are tested with a two point needle measurement.

The refrigeration in the S-I-N-I-S junction is studied with high accuracy in the sub-gap bias region of about 10^{-4} of the normal state conductance. The current - voltage characteristics of the sample are obtained by two wires measurement. For a large signal/noise ratio from the sample an extra care is taken in the wiring of the cryostat. Fig. 4.9 shows the schematic of the set up. At the top of the cryostat we have a home made room temperature low pass filter box (shown by RLC) with a capacitance of 220 pF and inductance of 470 μH . It acts as a low pass filter and protects the sample from the high frequency noise. Since the current is around few picoAmpere, it is important to filter the electrical noise in the circuit at low temperature. All the wires from the top to the cold plate inside the cryostat are made as unshielded twisted pairs to exclude the electromagnetic interference. The wires from the cold plate to the sample are made to pass through a home-made sample holder (see Fig. 4.9). Inside the sample holder, the wires from the cold plate are connected to the sample via resistive micro co-axial lines (resistance 100 Ohm) and commercial pi-filters which act as a last stage filtering to the sample. A heat link made of thick copper wire is connected from the cold plate to the shield of thermo-coax to thermalize it. The cooler chip is glued with a General Electric resist, which has high thermal conductivity, on a thin gold plated plate, which is a part of the sample holder. The pads of the sample are connected to the pins of the sample holder with a 30 μm diameter Al wire, using a ultrasonic bonding machine. An important feature of the measuring technique is the matrix box (shown in Fig. 4.10) which allows the measurement of as many as 12 different junctions at low temperature. The matrix box is connected in between the electronic box and the refrigerator. The matrix box is a 12×12 line box, where every line can be selected by inserting a specific pin.

Fig. 4.11 shows the circuit diagram of the electronic box. The sample is current biased and the voltage across the sample is measured. The current is obtained by applying a input bias voltage to a bias line consisting of a voltage divider in series with a resistance. According to the desired load line, this resistance can be switched to several values between 100 MOhms and 100 Ohms with a mechanical switch in a shielded box. The current is thus not directly measured, but is calculated from the input voltage. The output voltage across the sample is measured. The voltage drop across the junction in series with the filter is measured as a function bias current in the sample. A series of current-voltage ($I - V$) characteristics are obtained for different current ranges. The offsets in current

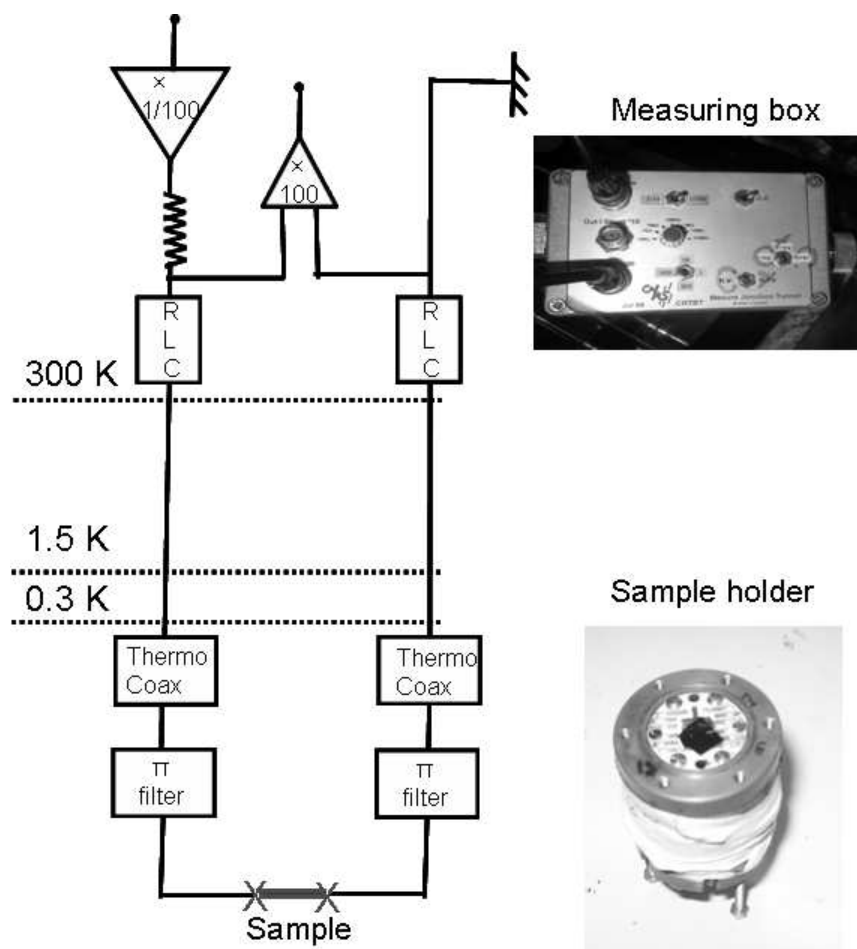


Figure 4.9: Schematic diagram of the set-up. It shows filtering of noise and thermalization scheme of wires at different stages inside the cryostat. The top right shows the measurement box connected at the top of the cryostat. The bottom right shows the sample holder (diameter 40 mm) which has 12 connectors.

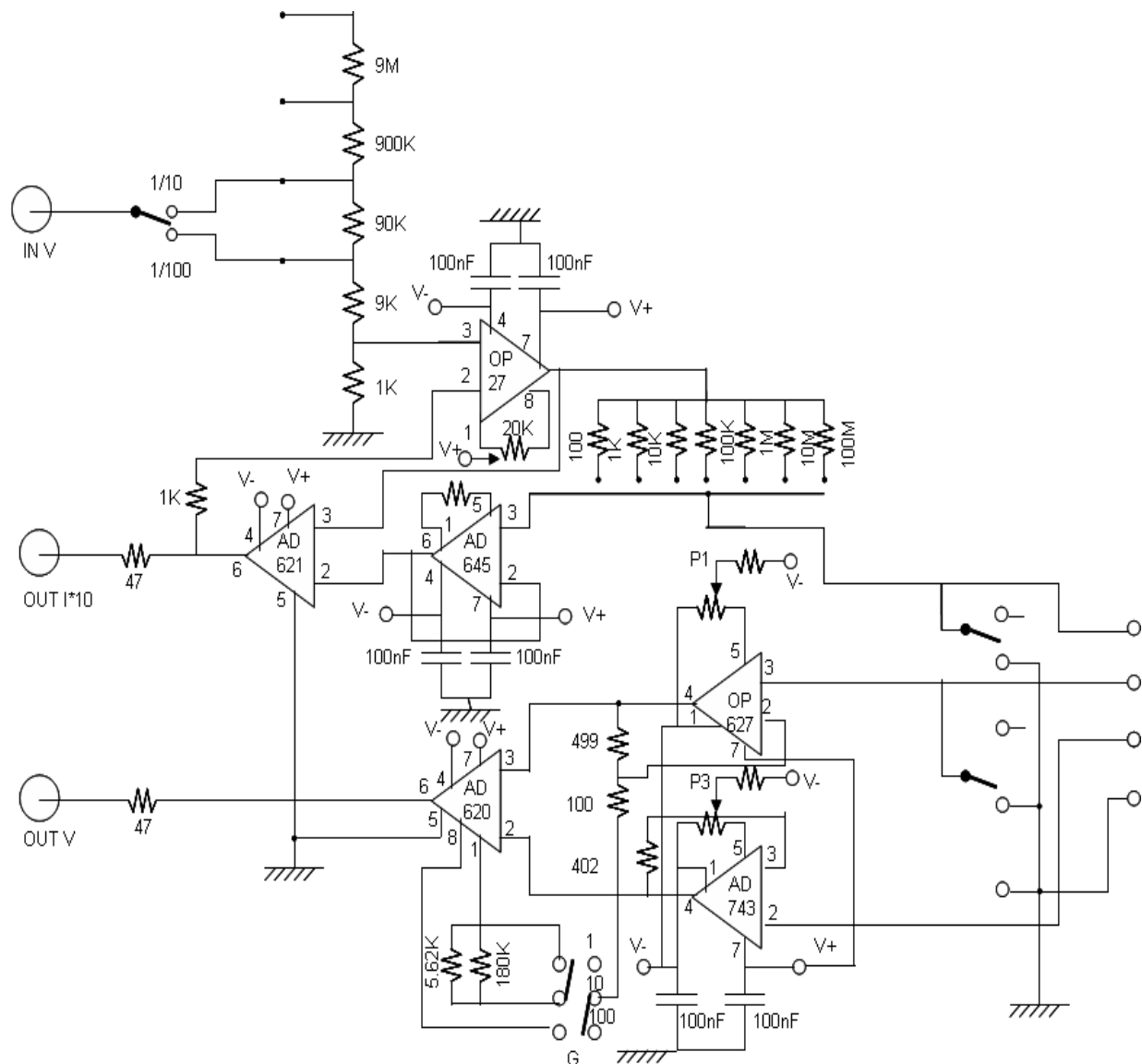


Figure 4.11: *Circuit diagram of the electronics. IN V is used to apply input dc voltage, which is converted into the constant current source. The amplified output voltage is measured at OUT V.*

Chapter 5

Inherent thermometer in a S-I-N-I-S cooling junction

5.1 Introduction

This chapter is concerned with the thermometry of the central normal island in between the two superconducting reservoirs. Accurate temperature determination with high resolution is a demanding field of research. In this chapter, we shall discuss the current-voltage characteristic of a N-I-S junction. We restrict ourself to the contribution of single quasiparticle tunneling across the N-I-S junction. Then we shall discuss the experiment done on S-I-N-I-S cooler junctions with the classical design, which has an external thermometer on the central N island. The external thermometer is a S-I-N-I-S junction. Later, the experiment done on our advanced design is discussed, where there are no external thermometers. Here we will elaborate on the assumption of quasi-equilibrium in the central N island. The kinetic equation is used to re-define the electronic distribution in the N island from complete non-equilibrium to thermal equilibrium electronic distribution. This electron distribution function is compared with the experimental current-voltage characteristic of the cooling island. At the end of this chapter, we present the "nouvelle vague" to extract the electronic temperature from the direct current-voltage characteristic of the cooling junction.

The experiments discussed are samples A, B and C. Samples A and B were cooled down to 275 mK and sample C was measured till the dilution temperature.

5.2 External electronic thermometer

In a N-I-S junction, one has to distinguish between the two tunneling mechanisms: two-electron transfer due to Andreev reflection and the transfer of single quasiparticles. The former is significant only at low bias and at very low temperature, whereas the latter depends strongly on the temperature. In this part, we will discuss only the quasiparticle tunneling in a N-I-S junction.

Rowell and Tsui in 1976 [20] demonstrated experimentally that single quasiparticle

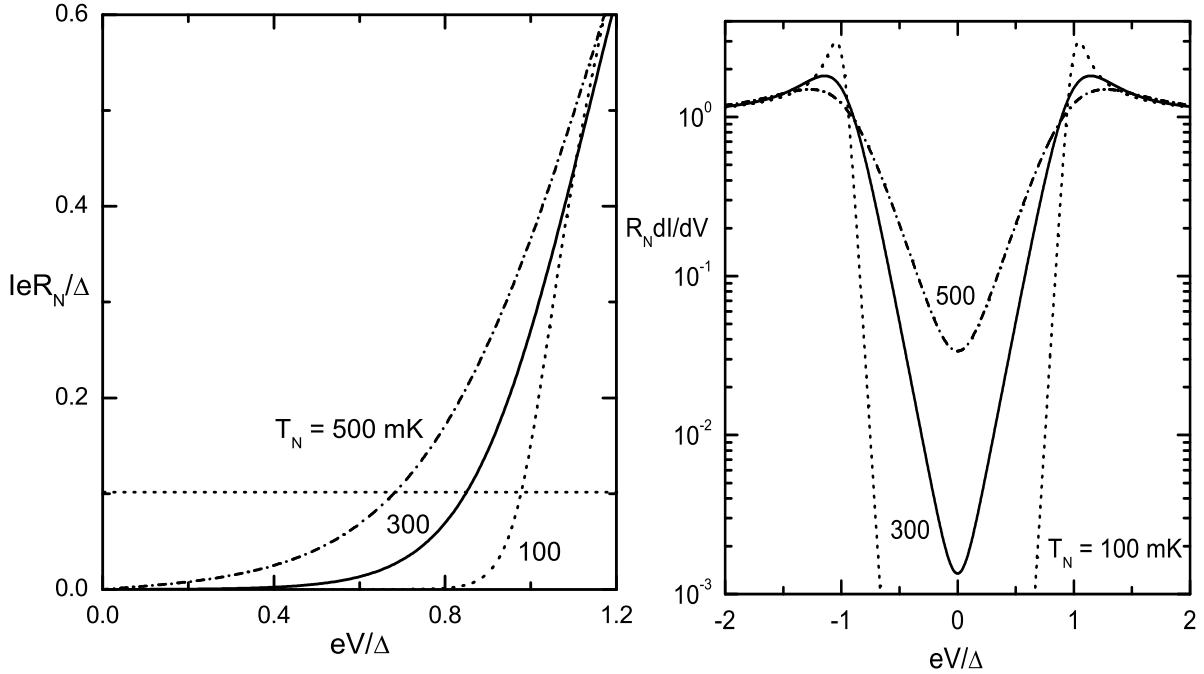


Figure 5.1: Calculated characteristic curves for a N-I-S junction with $\Delta = 0.21$ meV. Left: Sub-gap current for three different isotherms. Right: Differential conductance vs bias plot for the respective isotherms.

tunneling is an extremely sensitive and direct tool of measuring the electron temperature of a normal metal up to values comparable to the energy gap of the superconductor. The current-voltage characteristic across a N-I-S junction is given by :

$$I(V) = \frac{1}{eR_N} \int_0^\infty dEN_S(E)[f_N(E - eV) - f_N(E + eV)]. \quad (5.1)$$

R_N is the normal state conductance, $N_S(E) = |E|/\sqrt{E^2 - \Delta^2}$ is the normalized density of states in the superconductor and $f_N(E)$ is the electron distribution in the normal metal. The quasi-equilibrium limit requires the electrons to follow the Fermi distribution function $f_N(E) = 1/(1 + e^{E/kT_N})$. Note that Eq. 5.1 is insensitive to temperature of the superconductor and depends solely on the electronic distribution in the N-metal. At thermal equilibrium, the electron distribution is given by the Fermi-Dirac distribution.

Fig. 5.1(a) shows the current-voltage isotherm at $T_e = 100$ mK, 300 mK and 500 mK for a N-I-S junction with a gap voltage compatible with aluminium as a superconductor. The sub-gap current depends strongly on the bath temperature of the normal metal. For

$eV > \Delta$, all the curves merge giving the normal state conductance. For $\Delta \gg kT_e$ and $0 \ll eV < \Delta$, the current through a N-I-S junction can be written as [22]:

$$I(V) \simeq I_0 \exp\left[\frac{eV - \Delta}{kT_N}\right], \quad (5.2)$$

where I_0 is the characteristic current given by:

$$I_0 = \frac{\Delta}{eR_n} \sqrt{\frac{\pi \cdot kT_N}{2\Delta}}. \quad (5.3)$$

It means that the slope of the differential conductance (dI/dV) plot as a function of the bias voltage (V) in a logarithmic scale is inversely proportional to the electron temperature. This can be seen in Fig. 5.1(b). The horizontal dotted line shows that employing a constant current $I = I_0$ and measuring the voltage gives a direct measurement of the electronic distribution in the N island. With a thermal distribution given by a Fermi distribution, one can obtain the electronic temperature in the N metal. With R_n and Δ obtained from the experiment, there are no fitting parameters to obtain the electronic temperature of the N-metal from the N-I-S junction based thermometer. Thus the extreme sensitivity of the N-I-S junction to the local electron distribution in N metal makes it an attractive tool for thermometry of the S-I-N-I-S coolers.

5.2.1 Experiment with an external thermometer

Here, we discuss the experiment done on the sample A (shown in Fig. 5.2). The central N-island is connected to two superconductors through a tunnel barrier of large area. These junctions are called "cooler junctions". The two 40 nm thick and 1.5 μm wide superconducting Al electrodes were in-situ oxidized in 0.2 mbar of oxygen for 3 min before the deposition of the central N-metal Cu island which is 14 μm long, 0.3 μm wide and 50 nm thick. The N-island has two small thermometer junctions on it, which are made together with the cooler junction. The thermometer junctions are also two Al tunnel junctions on the Cu island with the area of 0.3 $\mu\text{m} \times 0.3 \mu\text{m}$.

The experiment is done in the following manner:

- (a) The S-I-N-I-S cooler junction is biased for the desired voltage;
- (b) The thermometer is voltage biased with a sub-gap bias and thermometer current is measured as a function of cooler bias voltage;
- (d) The thermometer current-voltage characteristic is fitted with Eq. 5.1 to obtain the electron temperature in the central N-island. Here it is assumed that the central N metal is at quasi equilibrium with the electrons distribution given by a Fermi distribution function.

The red curve and blue curve in Fig. 5.3 shows the differential conductance vs bias plot of the thermometer junction for two different cooler bias. The red curve correspond to "cooler off" state, $V_{cooler} = 0$ mV. The dashed line on the Red curve shows the fit with Eq. 5.1. The fit N-metal electron temperature is 288 mK, which is only slightly higher

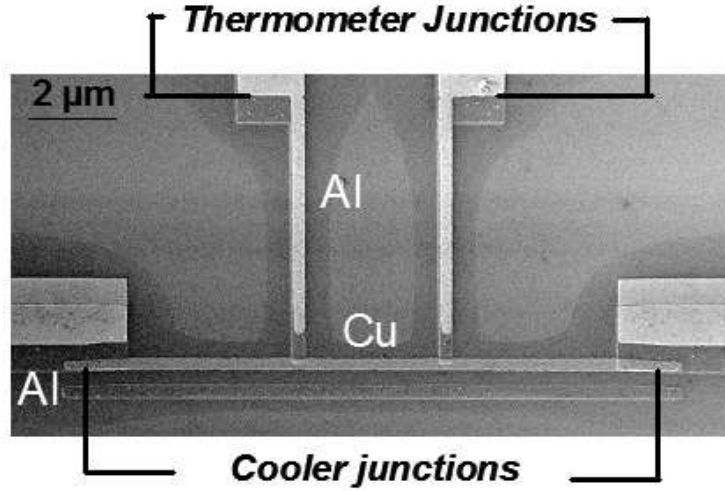


Figure 5.2: *Sample A: Scanning electron micrograph of a cooler with an external thermometer on the central N island. Cooler and thermometer have two Al-AlO(x)-Cu junctions in series. The area of the thermometer junctions is $0.3 \mu\text{m} \times 0.3 \mu\text{m}$ and that of the cooler junctions is $1.5 \mu\text{m} \times 0.3 \mu\text{m}$. The central N island is $14 \mu\text{m}$ long, $0.3 \mu\text{m}$ wide and 50 nm thick.*

than the measured cryostat temperature. This agreement shows the good thermalization of the central N metal electrons to the cryostat temperature.

Now the cooler junction is biased near the optimum voltage, $V_{cooler} = 0.308 \text{ mV}$. The blue curve represents the "cooler on" state. The dashed line on the cooler on state (Blue curve) shows the fit for a N metal electron temperature at 134 mK .

This experiment clearly shows the cooling of the electrons in the central N island when the cooler is sub-gap biased. Here, the electrons in the central N metal have cooled from the bath temperature of 280 mK to about 134 mK .

Fig. 5.4 shows the complete experiment on the device using external thermometer. The thermometer is voltage biased with a bias of 0.35 mV . The thermometer current is measured as a function of the cooler bias for different cryostat temperatures from 275 mK to 345 mK . It decreases as the cooler bias increases to its optimum bias shows the cooling of the N-metal electrons. A further increase in the cooler bias injects heat in the normal metal, shown by the increase in the thermometer current.

External N-I-S thermometers have been in practice since a long time. Nahum et. al. [4] used it to show the first electronic cooling of a Cu island in a micro-cooler. Since then, there has been a lot of advanced version of N-I-S thermometer. Recently, Schmidt et. al. [38] embedded a N-I-S thermometer in a LC resonant circuit to achieve a sub- μs readout times. Jing et. al. [39] used the S-N transparent junction as another possibility to measure the local electronic temperature from the supercurrent across the junction. There has been many other thermometers like Coulomb blockade thermometer [40], Anderson-insulator based thermometer [41, 42] to obtain the local temperature of a normal metal.

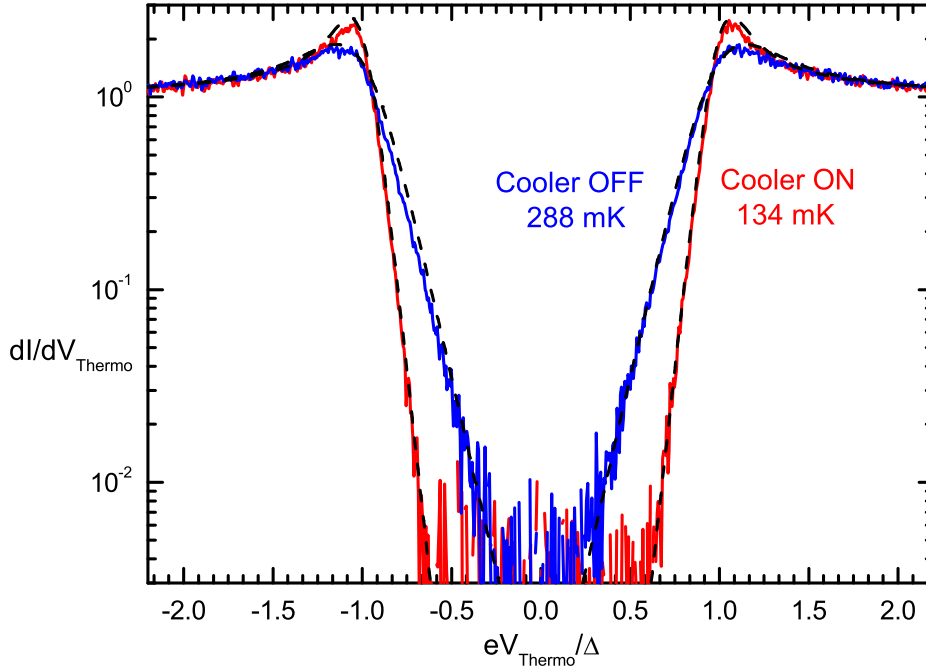


Figure 5.3: *Sample A: Differential conductance characteristic of the thermometer at two different cooler biases. The blue line is the experiment for the cooler junction at 0 mV (Cooler Off). The red line is the experiment for the Cooler biased at 0.308 mV (Cooler On). The dashed lines are the fit to the experiment. The cryostat temperature is 275 mK.*

In the following, we propose a new idea to extract the electronic temperature in the context of S-I-N-I-S cooler junction.

5.3 Inherent electron thermometer in cooler junction

5.3.1 Introduction

In the previous section, we used an external double N-I-S junction as a thermometer to obtain the temperature of the cooling N metal electrons. However, the external thermometer complicates the design of the cooler and inhibits the complete understanding of the cooling junction. In this section, we will discuss the experiments done on a new design with no external thermometer. The electronic temperature is obtained directly from the current voltage characteristic of the cooling junction.

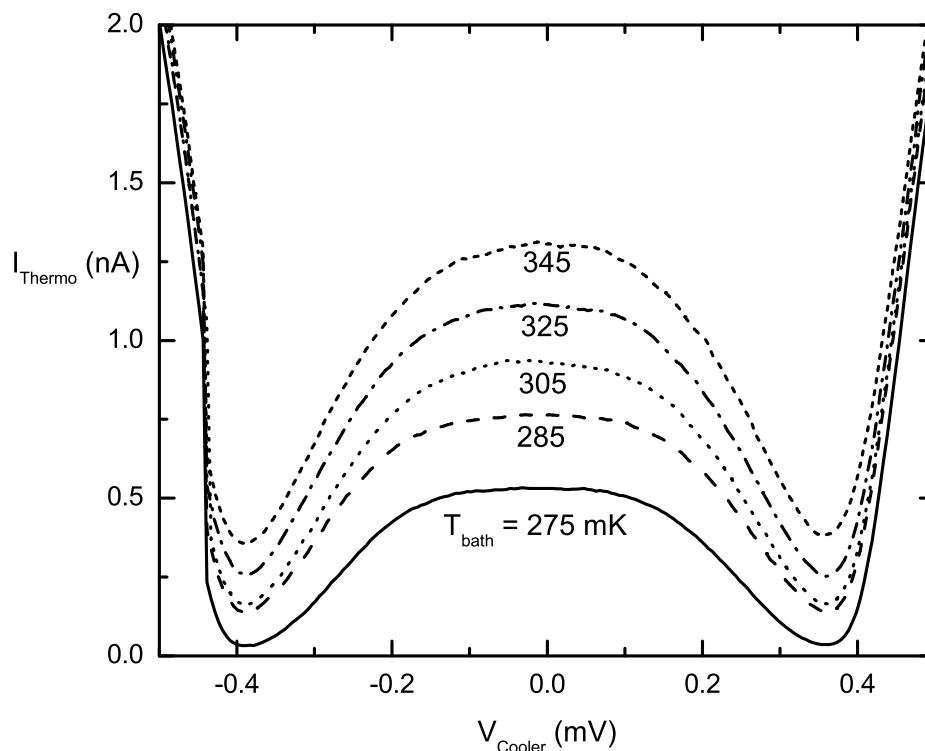


Figure 5.4: *Sample A: Cooling data of the device. Thermometer current as a function of cooler bias voltage at different bath temperatures. The thermometer is voltage biased at 0.35 mV.*

5.3.2 Sample with no external thermometer

Fig. 5.5 shows the scanning electron micrograph of one of the cooler devices of a new design (sample B), where the central Cu island is attached to two superconducting reservoirs through tunnel barriers. The two 40 nm thick and 1.5 μm wide superconducting Al electrodes were in-situ oxidized in 0.2 mbar of oxygen for 3 min before the deposition of the central N-metal Cu island which is 5 (sample B) or 4 μm (sample C) long, 0.3 μm wide and 50 nm thick.

Compared to the previous design (Fig.5.2), there is no external thermometer junction on the central N island. The cooler junctions are the same, the central Cu island is connected to two superconducting reservoirs via tunnel barriers. In addition to the two cooler junctions, we added three Cu tunnel probes (one is shown) of area 0.3 $\mu\text{m} \times 0.3 \mu\text{m}$ on one Al electrode. The probe junction is a N-I-S junction but the N-metal, because of the large volume, is strongly thermalized to the cryostat temperature.

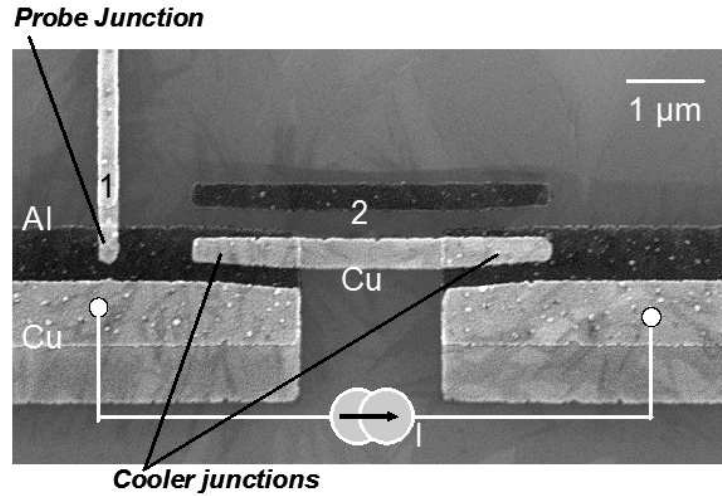


Figure 5.5: *Sample B: Scanning electron micrograph of a cooler with no external thermometer on the central N-island. Cooler junctions are two Al-AlO(x)-Cu junctions in series. The area of a cooler junction is $1.5 \mu\text{m} \times 0.3 \mu\text{m}$. In addition to the cooler there is one of the three Al-AlO(x)-Cu probe junction on one of the superconducting arm of the cooler junction.*

In comparison to the previous design (sample A), a cooler with no external thermometer can be more efficient due to a large cooler junction area/total volume ratio. This is because the Cu island is much shorter while the cooler junctions area is the same.

5.3.3 Experiments

The current-voltage characteristic is measured across either the cooler or a probe junction. The differential conductance dI/dV for every junction is numerically obtained.

Fig. 5.6 shows the differential conductance obtained from the cooler junction and one of the probe junction in a logarithmic scale at a 278 mK cryostat temperature. The probe junction characteristic is fitted (dotted line) by an isotherm at $T_N = 300$ mK obtained from Eq. 5.1. In an isotherm, we assume that the electron distribution is at thermal equilibrium, given by a Fermi distribution function. This implies that the electrons in the probe are at thermal equilibrium to the cryostat temperature, due to the large volume of N metal in comparison to the cooler junction. The fit temperature on the probe is only slightly higher than the cryostat temperature.

On the other side, the isotherm does not fit the characteristic obtained from the cooler junctions. The experiment on the cooler junction and the simulated isotherm coincide only at zero bias for sub gap bias. At zero bias, there is no heat current out of the N metal, so the electrons are thermalized to the cryostat temperature. In the sub-gap region, the differential conductance of the cooler is smaller than the isotherm prediction. This behavior exemplifies the cooling of the electronic population in the central normal metal.

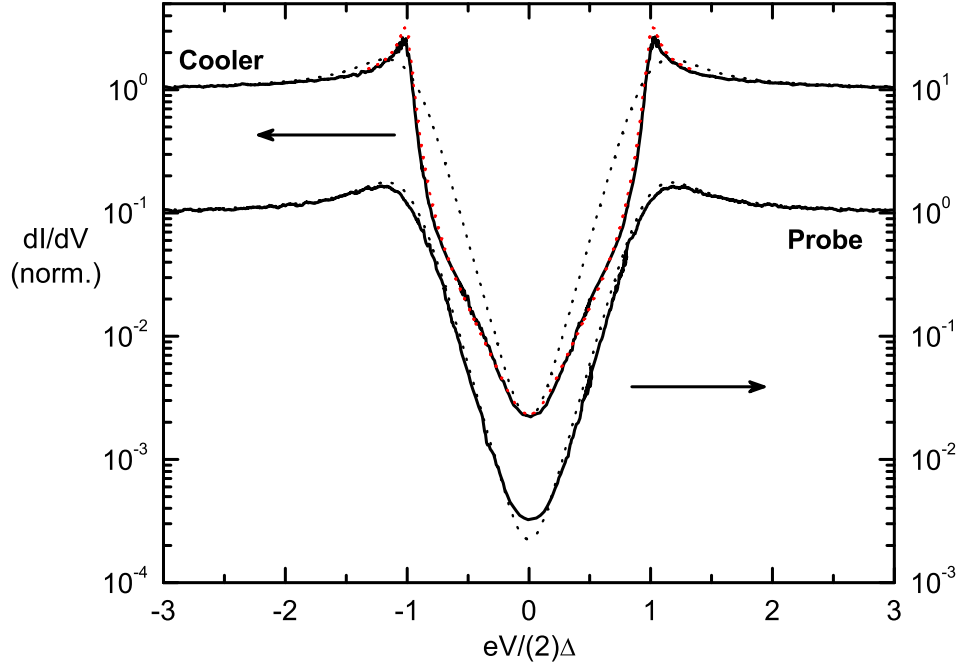


Figure 5.6: *Sample B: Differential conductance data obtained from the cooler junction and probe junction at the bath temperature of 278 mK. Top curve: cooler junction data (full black line) compared with the calculated isotherm at $T_e = 300$ mK with $R_n = 2.8$ k Ω ; $2\Delta = 0.42$ meV. Red dotted line on the cooler characteristic is the fit with the thermal model in the device [43]. Bottom curve: complete line shows the characteristic curve obtained from the probe junction and the dotted line is the calculated isotherm with $R_n = 5.7$ k Ω ; $\Delta = 0.22$ meV. The voltage is normalized to 2Δ (top curve) and Δ (bottom curve).*

Fig. 5.7 shows the differential conductance obtained from the cooler at different bath temperatures [34]. Again all the plots are in logarithmic scale. As expected, the differential conductance at zero voltage bias decreases as the bath temperature of the cryostat decreases. However at very low temperature ($T = 90$ mK), the differential conductance at zero bias does not decrease further. On the contrary, the differential conductance increases at zero bias when the temperature is decreased.

There are two clear signature differences in the cooling junction data in comparison to the theoretical isotherm conductance curve (Fig. 3.13). First, the differential conductance has a curvature in the sub-gap bias in comparison to the linear behavior. Secondly, at very low temperature the differential conductance has a zero bias anomaly, which cannot be explained by any linear leakage.

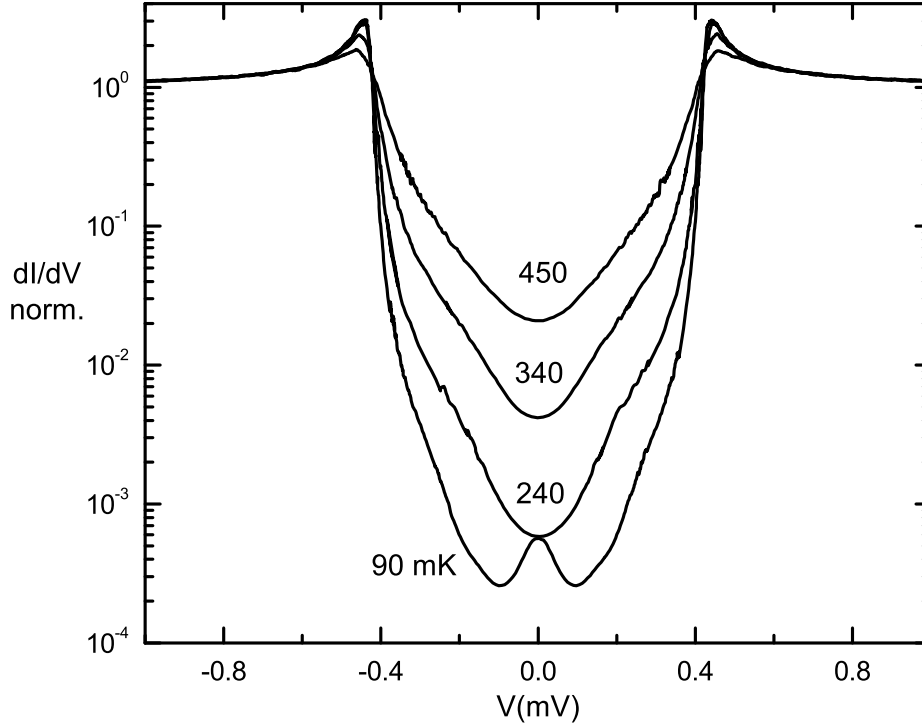


Figure 5.7: *Sample C: Normalized differential conductance of the cooler junctions as a function of voltage bias at different cryostat temperatures. Dimension of the N island : 4 μm long, 0.3 μm wide and 50 nm thick. Normal state resistance $R_N = 1.9 \text{ k}\Omega$ and $2\Delta = 0.43 \text{ meV}$*

5.3.4 Quasi-equilibrium in the S-I-N-I-S cooling junction

A normal metal cooled by electron tunneling is in principle in out-of-equilibrium situation. The normal metal states are populated due to the electrons coming from the left superconducting electrode and depopulated by the right electrode. The electron-electron inelastic scattering equilibrates the energy distribution towards a Fermi distribution. The electron-phonon coupling thermalizes the electron population to the phonon temperature of the metal. As a result, depending on the relative magnitudes of the injection, electron-electron scattering and the electron-phonon scattering rates, different situations can be met.

If the electron-electron and electron-phonon scattering rates are small compared to the injection rates, then electrons occupy a non-equilibrium $f_N(E)$ which can be very much different from the Fermi distribution. If the electron-electron scattering rate is large compared to the injection rate, the normal metal electrons follows a Fermi distribution $f_0(E, T_e)$ at

an electronic temperature T_e . In the later case, two different regime can be defined. If the electron-phonon relaxation time is short enough, the temperature of electrons in the normal metal T_e is equal to the phonon temperature. This is the standard equilibrium situation. In the opposite case, electrons in the normal metal attain a temperature T_e different from the phonon temperature. This is a quasi-equilibrium situation.

If heat is injected in the electron population, the electron temperature T_e will be higher than the phonon temperature. A hot electron regime is then achieved [44, 45]. In superconducting micro-coolers, heat is extracted from the normal metal electron population and a cold electron regime is achieved. In every case, the temperature difference between electrons and phonons is of the order of $P/\Sigma UT^4$ where P is the power, Σ is the electron-phonon constant and U is the metal volume.

In the following, we will solve a kinetic balance equation in the central N - island to determine the electron distribution. Here we will follow Ref. [46], to describe a electron distribution in central N island of S-I-N-I-S junction. We assume identical tunnel barriers and superconductors on either side of the normal metal. It is also assumed that the superconducting electrodes remain at equilibrium and the energy distribution there is given by the Fermi-Dirac distribution f_0 at the temperature of the cryostat (T_0).

The tunnel current from the superconductor to the normal metal (in S-I-N-I-S junction) can be written as:

$$I(V) = \frac{2}{eR_N} \int_{-\infty}^{\infty} dE N_S(E - \frac{eV}{2}) [f_0(E - \frac{eV}{2}) - f_N(E)], \quad (5.4)$$

R_N is the normal state conductance of the double barrier, f_N is the electron distribution function in the normal metal and $V/2$ is the voltage across each N-I-S junction in series. $N_S(E)$ is the normalized density of states in the superconductor

$$N_S(E) = \frac{E}{\sqrt{E^2 - \Delta^2}}. \quad (5.5)$$

The rate of population of a certain energy level due to injection from superconductor to the normal metal is given by:

$$\frac{2}{R_N} N_S(E - eV/2) [f_0(E - eV/2) - f_N(E)], \quad (5.6)$$

and the rate of depopulation of the energy level due to the extraction is given by:

$$\frac{2}{R_N} N_S(E + eV/2) [f_N(E) - f_0(E + eV/2)]. \quad (5.7)$$

Within the relaxation time approximation, the inelastic relaxation of the injected quasi-particles with a certain energy level E in the normal metal is given by:

$$ALN_N(E) e^2 \frac{f_N(E) - f_0(T_e, E)}{\tau_E} \quad (5.8)$$

A , L are the cross-section area and the length of the normal metal, $N_N(E)$ the non-normalized density of states in the normal metal and τ_E the relaxation time. Here T_e is the electronic temperature that the normal metal electrons would reach if the electron-electron scattering is strong enough to ensure the quasi-equilibrium. In the non equilibrium, it is thus an effective temperature.

At steady state Eq. 5.6 = Eq. 5.7 + Eq. 5.8. Thus we get,

$$f_N(E) = \frac{N_S(E - eV/2)f_S(E - eV/2) + N_S(E + eV/2)f_S(E + eV/2) + f_0(E)/(\tau_E\Gamma)}{N_S(E - eV/2) + N_S(E + eV/2) + 1/(\tau_E\Gamma)}, \quad (5.9)$$

Γ^{-1} being the mean residency time which is given by :

$$\Gamma = \frac{2}{N_N(E_F)R_N A L e^2} \quad (5.10)$$

It is worth noticing that Eq. 5.9 is identical as obtained by Pekola et al. in Ref. [11] for completely non-equilibrium distribution in N-metal. It describes a crossover from completely non-equilibrium to equilibrium distribution depending on the thermalization of the injected N electron in the central N island.

The ratio of the relaxation rate and rate of injection the electron in the normal metal is mainly accountable for the distribution of the electrons in the central N island. For $\tau_E\Gamma \gg 1$ the distribution function in the normal metal is different from the equilibrium Fermi distribution function and if $\tau_E\Gamma \ll 1$, the normal metal follows a Fermi distribution function. In every case, the current through N-I-S junction is obtained by substituting Eq. 5.9 in Eq. 5.4.

Fig 5.8 displays the complete non-equilibrium ($\tau_E\Gamma \rightarrow \infty$) distribution function for different bias at very low cryostat temperature. This plot shows the broadening of the distribution function up to $eV/2\Delta = 1$ and later sharpening for higher bias.

Fig. 5.9 displays the differential conductance as a function of voltage bias for both complete equilibrium ($\tau_E\Gamma \rightarrow 0$) and non-equilibrium ($\tau_E\Gamma \rightarrow \infty$) distribution in the normal metal at different bath temperatures. It is worth noticing that for the two opposite distribution in the N metal, the differential conductance at the zero bias is the same.

As seen for $T = 320$ mK, there is clear dip in the non-equilibrium differential conductance near zero bias in comparison its equilibrium isotherm. As argued in Ref. [11], the smaller differential conductance for sub-gap bias voltage could be interpreted in terms of cooling in the central N island and similarly above gap it is argued as heating. It was further argued that the cooling - heating cycle gets reversed at very low temperature ($T = 100$ mK) since the differential conductance increases at low bias. In the following section, we will argue and present evidence, which shows that our experiments are not in this regime and the electrons in the cooling N island are at quasi-equilibrium.

Fig. 5.10 shows the differential conductance isotherm for different values of $\tau_E\Gamma^{-1}$ from 0 to ∞ at $T_0 = 320$ mK. It shows a cross-over from the complete non-equilibrium to equilibrium distribution. As the relaxation time for an electron decreases, the isotherm

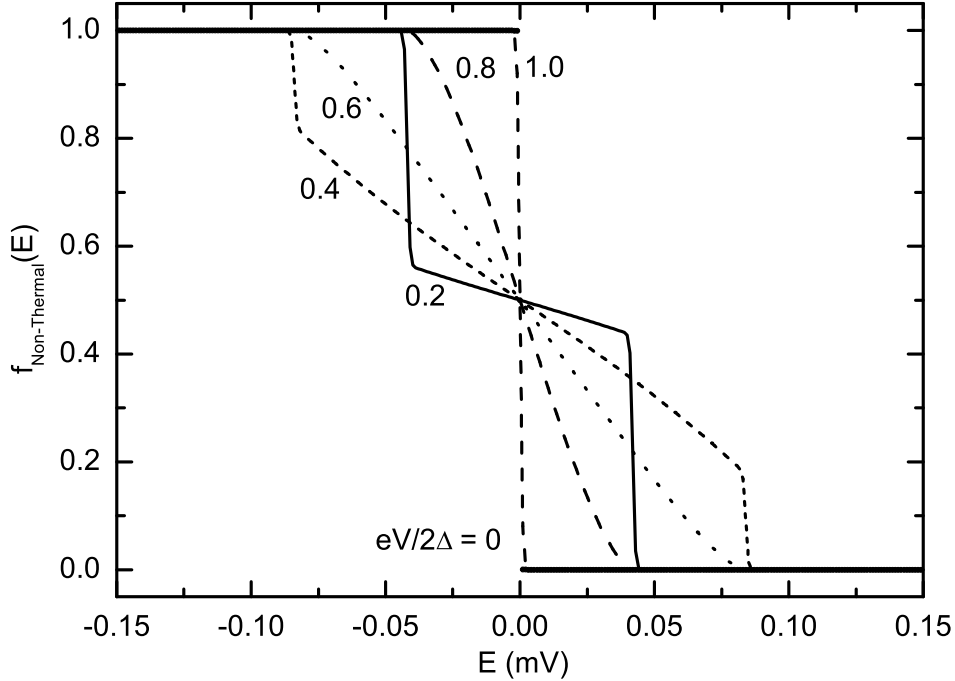


Figure 5.8: Complete non-equilibrium ($\tau_E \Gamma \rightarrow \infty$) distribution function in the normal metal for different bias voltages. Parameters for plot: $\Delta = 0.21$ meV and $T_0 = 5$ mK.

goes from completely non equilibrium to quasi equilibrium distribution in central N island. For $\tau_E \Gamma^{-1} \gg 20$, the quasi-equilibrium characteristic cannot be distinguished from the isotherm.

5.3.5 Comparison with experiments

The normalized density of states is given by (Ashcroft and Mermin [47]):

$$N_N(E_F) = \frac{2mk_F}{2h^2\pi^2} \quad (5.11)$$

In our sample for Cu, we have $R_N = 1.4$ k Ω ; $k_F = 1.75 \times 10^{10}$ m $^{-1}$; $A.L = 5$ μ m \times 0.3 μ m \times 50 nm. We thus find the mean residency rate of the electron in the central Cu island Γ^{-1} is of the order of 10^7 s $^{-1}$.

The inelastic time of scattering in the normal metal is obtained separately by weak localization correction to the resistance. Magnetoresistance experiment is done on Cu line made with the same source as for cooling N island. The Cu is of purity 6N (99.9999 %).

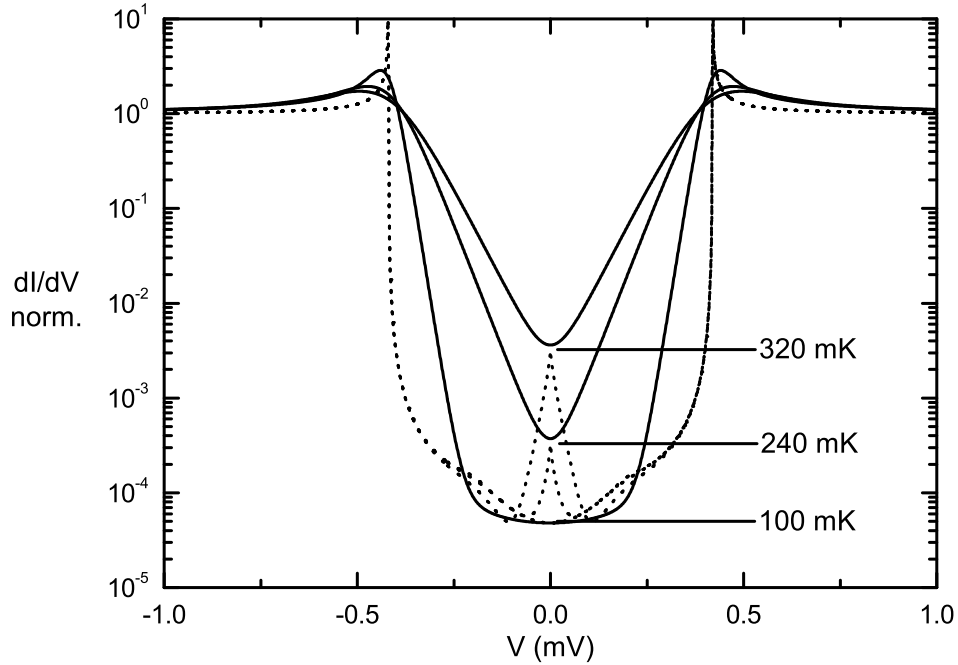


Figure 5.9: *Differential conductance vs voltage bias plot for complete non-equilibrium ($\tau_E\Gamma \rightarrow \infty$) and complete equilibrium ($\tau_E\Gamma \rightarrow 0$) distribution function in the normal metal for different temperatures. Full and dashed line correspond to the equilibrium and the non equilibrium distribution for 320mK, 240 mK and 100 mK. Parameter for plot: $\Delta = 0.21$ meV.*

The dephasing time τ_ϕ is obtained by fit using the weak localisation theory [48]. Dephasing time τ_ϕ is found to be 150 ps at 275 mK [49, 50]. This correspond to $(\tau_E\Gamma)^{-1}$ of the order of 600. As compared to Fig 5.10, the electrons in the normal metal are at thermal equilibrium.

Although the experimentally obtained dephasing time gives a measure of cut-off to the electron-electron scattering time, we compare the experiment to the calculations with $\tau_E\Gamma$ as a free parameter. Fig. 5.11 shows the comparison of the differential conductance of the cooler with different quasi equilibrium distribution in the central N island. The symbol-line shows the experiment at $T = 330$ mK along with the simulated curve obtained using Eq. 5.9. Dotted line, dashed dotted line and dashed dot are simulated curve for $\tau_E\Gamma^{-1} = 10, 50$ and 90 respectively at low bias voltage. The full complete line is an isotherm for complete thermal distribution in the N island. The inset shows the complete comparison in the sub-gap region. This clearly shows that in the intermediate temperature regime ($T = 330$ mK), the cooler can neither be fitted with a out of equilibrium model nor by the thermal equilibrium distribution in the central N island.

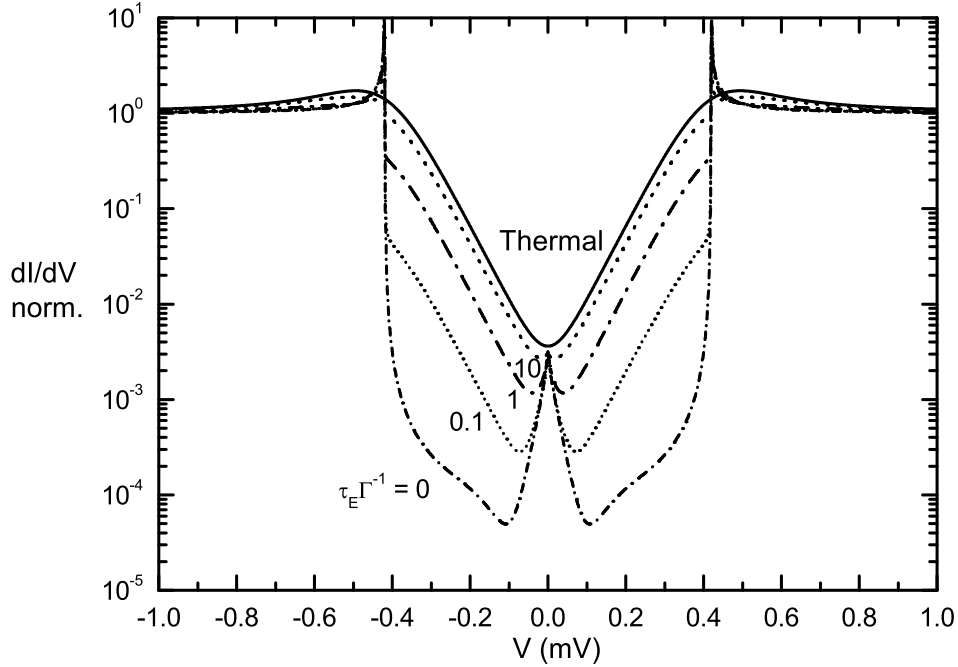


Figure 5.10: *Differential conductance vs voltage bias plot for different ratio of the relaxation rate to the rate of injection in the normal metal. Parameters for plot: $\Delta = 0.21$ meV and $T_0 = 320$ mK.*

Fig. 5.12 shows the zero bias anomaly obtained from cooler junction at $T = 90$ mK along with the simulated curve for different $\tau_E \Gamma^{-1}$. It clearly shows that the enhancement of zero bias conductance cannot be fitted with a non thermal or a quasi thermal distribution in central N island. The zero bias anomaly is due to the presence of phase-coherent Andreev current. This will be discussed in chapter 7 of this thesis. We also conclude that, in our case, the electrons in the central N island can be considered as being at thermal equilibrium

5.4 Assumption to extract electronic temperature

In order to simplify the extraction of the electronic temperature, we have to make the following assumptions:

(1) the two refrigerating N-I-S junctions are identical so that there is an equal voltage drop across each junction. For slight asymmetry between the two N-I-S junction, the total current across the cooler is little affected. This is due to the singularity of the differential

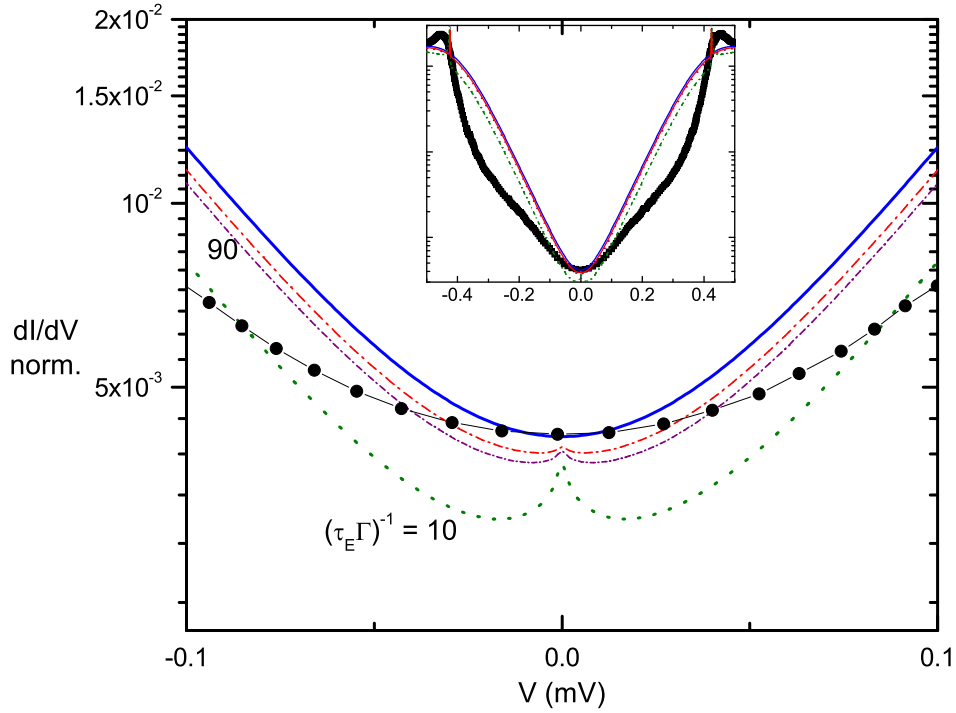


Figure 5.11: *Differential conductance plot (Sample B) at $T = 330$ mK of cooler junction along with the simulated curve at different relaxation time $\tau_E \Gamma^{-1} = 10, 50$ and 90 at low bias. Inset shows the complete curve.*

conductance at a gap which regularizes the voltage. The error in the current is maximum at the gap voltage, where the error is proportional to the asymmetry [51]. For our junction, the difference between the two junctions is less than 5 %. Therefore, for simplicity we consider the two junctions to be identical.;

(2) leakage channels through the junction are assumed to be absent and also there are no energy states within the super-conducting gap;

(3) higher order tunneling process is neglected.

In the following, we shall discuss in detail the above assumptions.

5.4.1 Energy states in superconductor energy gap

A non - ideal superconductor can have single electron states within the energy gap (Δ), given by the Dynes parameter. The Dynes parameter (η) in the density of states of super-

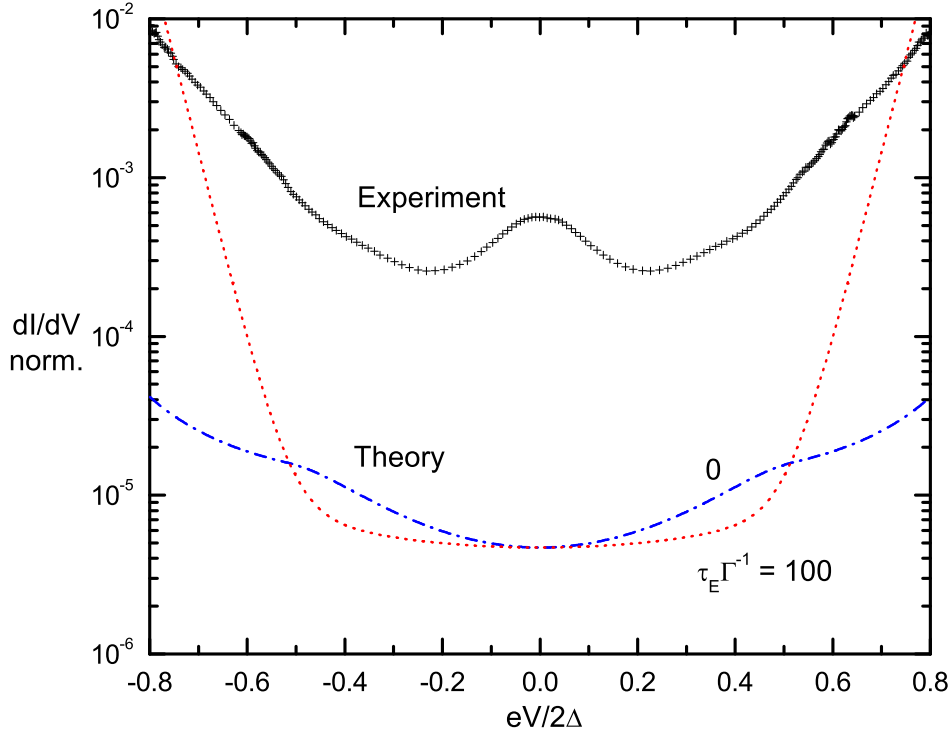


Figure 5.12: *Differential conductance plot ($T = 90$ mK) (Sample C) of the cooler junction along with the simulated curve at different relaxation times in the central N island.*

conductors is given by [52]:

$$N_S(E) = \left| \text{Re} \frac{E + i\eta}{\sqrt{(E + i\eta)^2 + \Delta^2}} \right|. \quad (5.12)$$

η depends on the phonon induced quasiparticle recombination rate and leads to broadening of energy gap (Δ). It is expected to be dominant for strongly coupled superconductor like Pd and negligible for Al. However, we always include a very small $\eta = 10^{-6}$ meV so as to ensure a good convergence of the numerical calculations.

Fig. 5.13 shows the experiment at the cryostat temperature of 90 mK along with the simulated non equilibrium curve ($\tau_E \Gamma^{-1}$) = 0 with different Dynes parameter (η). The complete line shows the experiment with zero bias anomaly. The dotted line shows the simulated curve with $\eta = 10^{-6}$, 5×10^{-5} and 10^{-4} meV at complete non equilibrium electron distribution in the N island. It shows that the zero bias anomaly cannot be fitted with the different η parameter even with a complete non-Fermi distribution in N island.

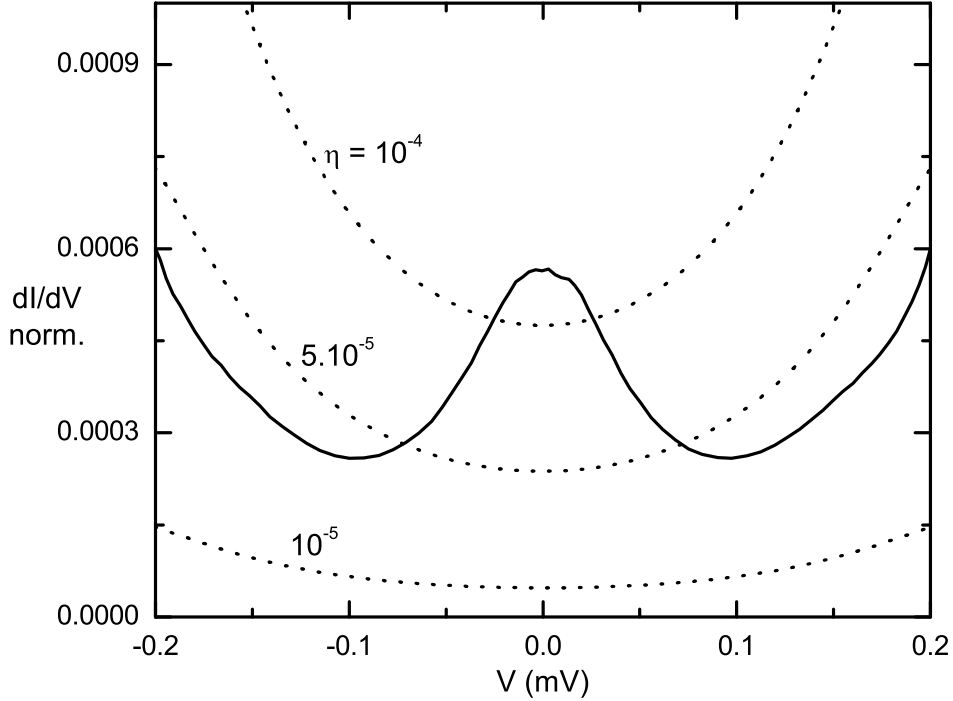


Figure 5.13: Zero bias anomaly in differential conductance from the cooler at $T = 90$ mK (Sample C) along with the calculated non-Fermi distribution in N island at different η .

5.4.2 Tunnel current due to second order processes

As discussed in the chapter 3 for a tunnel barrier, the amplitude of transfer of electron pairs due to Andreev reflection vanishes with the transparency of the junction [14]. However the disorder in the electrode leads to coherent addition of many individual transmission probability amplitudes for the transfer of electron pairs across the junction. This leads to an enhancement of the sub gap conductivity [17, 16].

Fig. 5.14 shows the calculated current voltage characteristic across N-I-S junction at relatively higher temperature (above 300 mK) and with a transparency (10^{-5}) similar to our junction. Full and dotted line shows the contribution due to the quasiparticle current and the phase-coherent Andreev current respectively. The contribution due to Andreev current is negligible in comparison to the single quasiparticle tunnel current. Therefore, for simplicity in high temperature regime, we will ignore the Andreev current contribution to the total current.

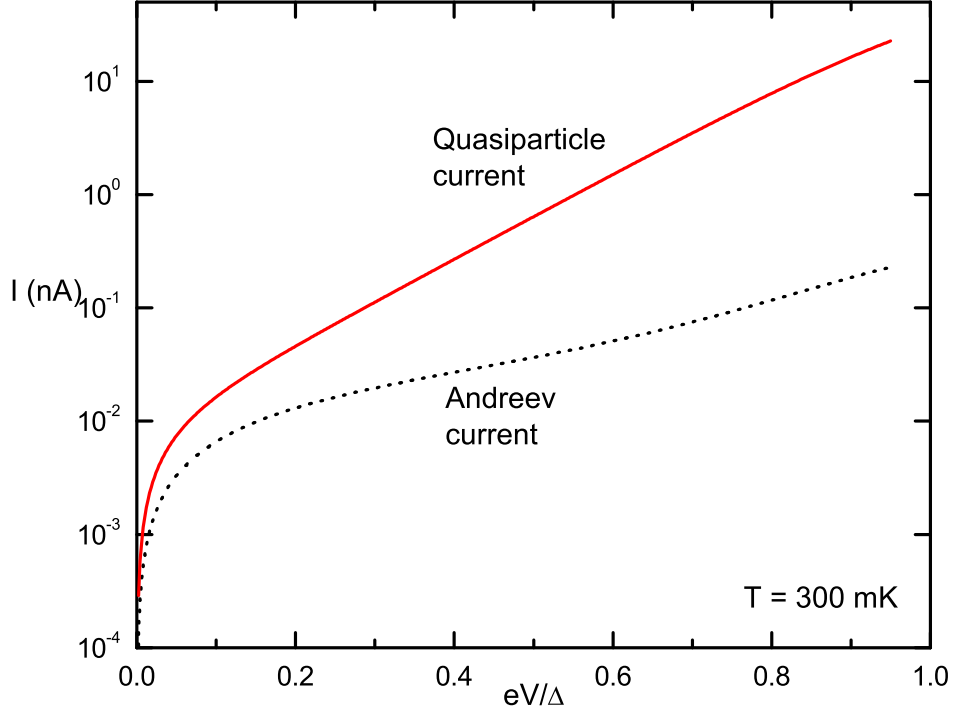


Figure 5.14: *Calculated current-voltage characteristic of the N-I-S junction at $T_e = 300$ mK. Full line shows the contribution due to quasiparticle current and dotted line shows the Andreev current.*

5.5 Extraction of electron temperature

With the above assumptions, we extract the temperature $T_e(V)$ in the sub-gap region by superimposing the experimental current-voltage characteristic from the cooling S-I-N-I-S junction on a series of theoretical isotherm curves obtained from Eq. 5.1. Every crossover point between the experiment and the isotherm gives the electronic temperature in the central N island at a particular bias.

Fig. 5.15 shows the current voltage characteristic of the cooler junction at the cryostat temperature of 300 mK along with the calculated isotherms. At zero bias, there is crossover between the experiment (black complete line) and the isotherm corresponding a 292 mK electron temperature. As the cooler bias increases, the dashed red isotherm no longer satisfies the experiment, and there is a crossover with the blue isotherm and the electrons correspond to the temperature of the blue isotherm. For a bias near the gap, the electrons in the central N island have cooled from the bath temperature of 292 mK down to 98 mK. For calculating the isotherms, the normal state resistance and the superconducting gap are obtained from the differential conductance plot. Here the normal state conductance for

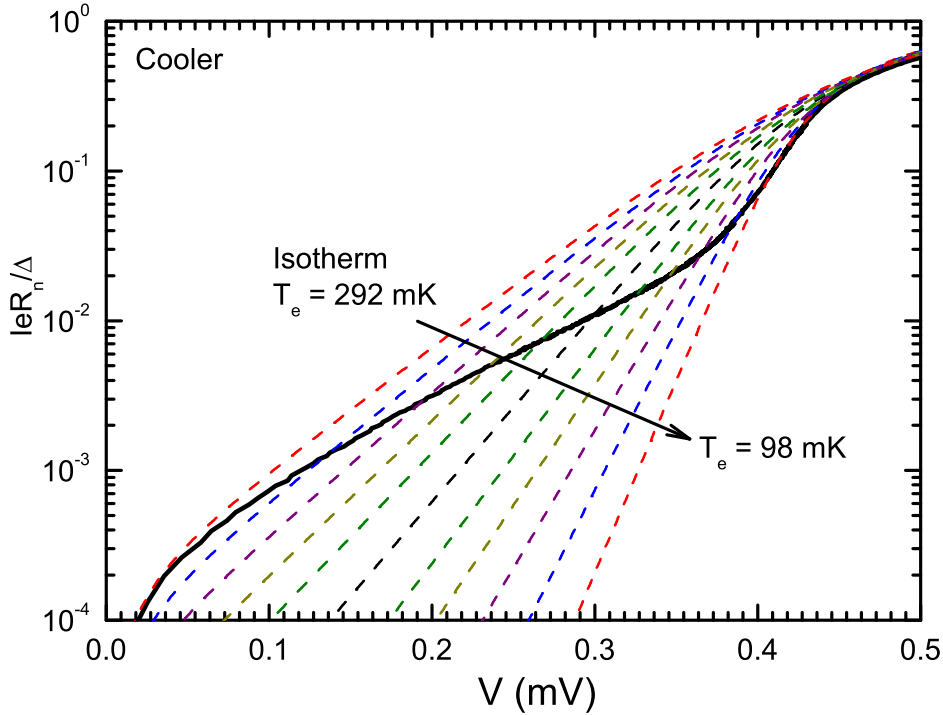


Figure 5.15: *Sample B: Experimental current-voltage characteristic at a 275 mK cryostat temperature (full line, black) superposed on a series of calculated isotherm characteristic following Eq. 5.1 from $T = 292$ mK (top) to $T = 98$ mK (bottom). Every crossing point gives the electronic temperature T_e in the central N metal at a particular bias. Parameters for calculated isotherms: $R_N = 2.8$ k Ω and the $2\Delta = 0.428$ meV.*

the S-I-N-I-S cooler is 2.8 k Ω and the $2\Delta = 0.428$ meV.

It is interesting to note that such extraction of the electron temperature in the central N island from the direct current-voltage characteristic cannot be done on the differential conductance-bias plot, for instance on Fig. 5.6. This is due to the error in the isotherm, as shown below. The tunneling current (I_T) is a function of bias and temperature. In our case, both are changing, so that we can write,

$$\frac{dI_T}{dV} = \frac{dI(V, T)}{dV} + \frac{dI}{dT} \frac{dT}{dV}$$

The second part on right side of above equation contributes to an error in determining the electron temperature from the differential conductance curve.

Fig. 5.16 shows the electronic temperature (Sample B) in the central N island as a function of cooler bias voltage for three different cryostat temperatures. The temperature

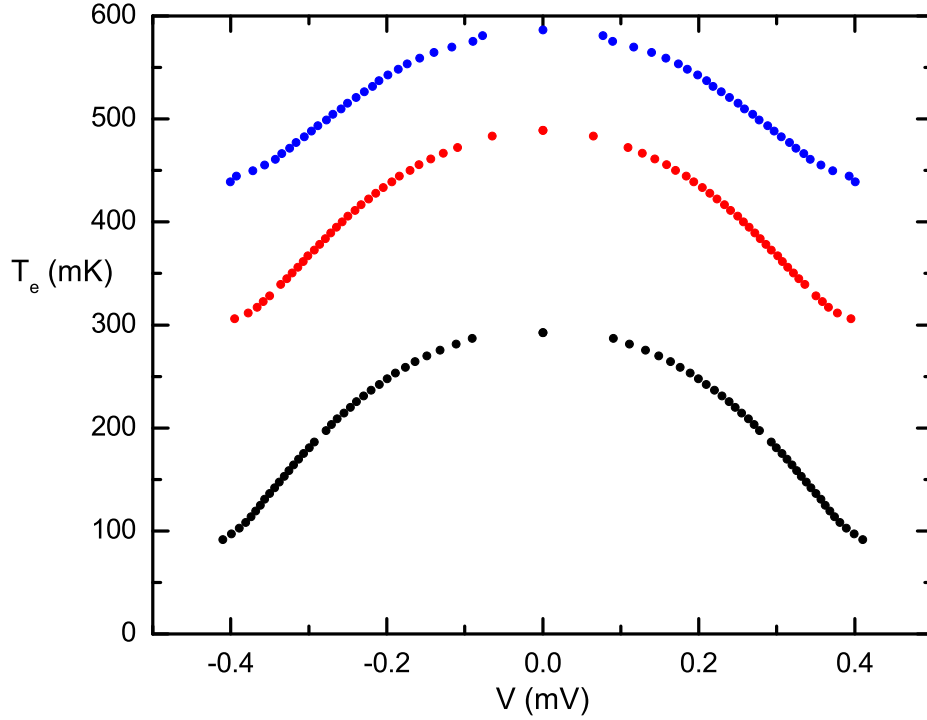


Figure 5.16: *Sample B: Electronic temperature of the central N metal as a function of cooler bias at three different cryostat temperatures.*

is obtained directly from the current voltage characteristic of the cooler junction as shown in Fig 5.15. The black, red and blue symbols correspond to the cryostat temperatures of 275, 470 and 570 mK. The bath temperature extracted from the data is, respectively, 292, 489 and 586 mK. The electronic temperature at zero bias is only slightly higher than the cryostat temperature.

Fig. 5.17 shows the extracted electronic temperature (Sample C) for each data point in the sub-gap region. It is to note that the technique could be in principle exploited for voltages above the gap voltage. However it is not preferred due to two reasons: for $eV > \Delta$ all the isotherm curve (for instance in Fig. 5.15) merges together, which makes it difficult to extract temperature. Also Eq. 5.1 will no more be accurate since the superconductor will be in strong out of equilibrium state.

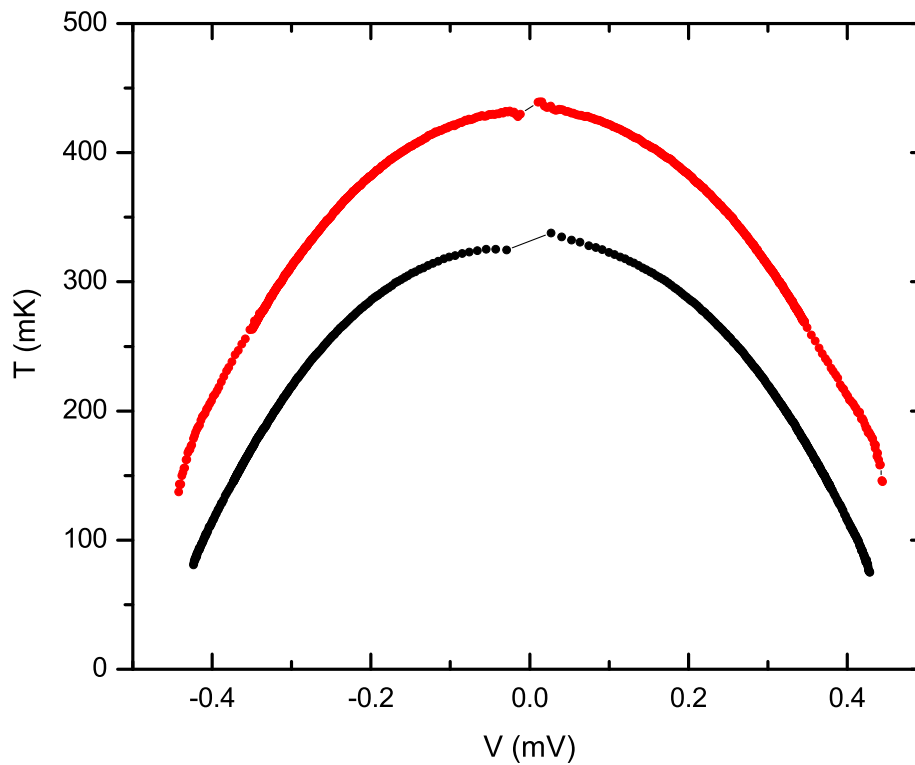


Figure 5.17: *Sample C* : Electronic temperature of central *N* metal as a function of cooler bias at a cryostat temperature of 330 and 440 mK.

5.6 Conclusion

We investigated the cooling of the central *N*-island in the S-I-N-I-S junction with **no external thermometer**. We have proposed a new technique to obtain the electron temperature in the central *N* island by comparing the device current - voltage characteristics to the theoretical prediction. The electrons in the *N*-metal cool down from 300 mK to below 100 mK.

Chapter 6

Electron and phonon cooling in micro-coolers

6.1 Introduction

This chapter is concerned with the thermal distribution of the heat in superconductor based micro-coolers. In the chapter 5, we discussed the precise investigation on the electronic temperature in the Superconductor - Normal metal - Superconductor tunnel junctions with a design with no external thermometer. This design optimizes the cooling due to two main reasons. Firstly, the contact surface area ratio between the central normal metal and the substrate to its volume is much smaller than in samples with an external thermometer. Secondly, our samples have a higher tunnel junction area to the volume of normal metal ratio which leads to a better optimization of the coolers.

The normal metal electron temperature is extracted by comparing the experiment with the theoretical isotherm. Now, we will consider a simple thermal model in the coolers and quantitatively compare the experimental electronic temperature with the result of thermal model. The thermal model includes the electron - phonon coupling in the Normal metal and the Kapitza resistance between the substrate and the normal metal phonons. Here, we will discuss the experiments done at intermediate temperature regime ($T > 300$ mK)

In this chapter, we shall start by discussing the thermal model based on hot electron experiments. Hot electron experiments were done at very low temperature ($T < 100$ mK) and gave an independent measurement of the electron-phonon coupling in the normal metal (like Cu). Then, we will ascribe the micro-coolers to a thermal model by taking into account the electron-phonon coupling and the Kapitza resistance. Here we will discuss the different simplifications considered in our heat model and discuss the non-equilibrium phonon distribution of population in more detail. At the end, we will present an evidence showing the cooling of the normal metal phonons in addition to its electrons.

In this chapter, I will discuss the experiments done on one of the five similar samples cooled in the He3 refrigerator or the dilution refrigerator. The detailed description of the sample has been done in the first article which is reproduced at the end of the thesis.

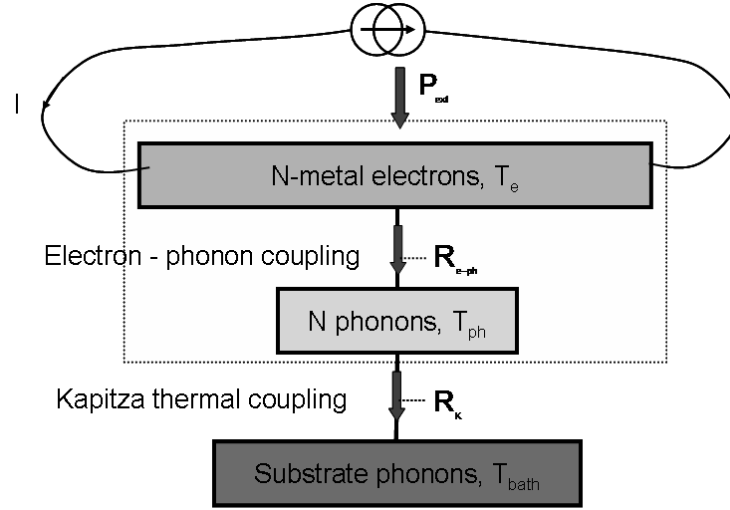


Figure 6.1: Heat flow paths between the different constituents in hot electron devices. An external power P_{ext} heats the electron in the N metal, which further heats the N-metal phonons via thermal resistance R_{e-ph} . The heat flows into the insulating substrate via the Kapitza resistance R_K .

6.2 The thermal model

The simplest constituents to the thermodynamics of any N-metal nano-device are the electrons and the phonons. These are coupled interacting systems with a thermal resistance [53]. If the device is on an insulating substrate then the phonons can be subdivided as the phonons in the substrate and the phonons in the N-metal. The thermal resistance between the two phonon baths is due to the lattice mismatch between the two interfaces, it leads to Kapitza resistance [54, 55]. This phenomenological model has been popularly used in the context of hot electron effects in a N metal [45].

In the case of hot electron effects, an external power P_{ext} is supplied to the electrons, leading to the increase in the electronic temperature in the N-metal. The final electron temperature is given by the steady state situation where the power P_{ext} is transferred to the N-metal phonons. Consequently, the temperature of phonon increases until the it is compensated by the heat transfer from the substrate. Therefore, depending on the strength of interaction between the electron-phonon and phonon-phonon, the electrons and the phonons in the N-metal attain well defined but different steady state temperatures.

Hot electron effects have been experimentally studied [56, 44, 57, 45] for the semiconductor at room temperature and for a normal metal at low temperatures. Different regimes are reached due to the difference in the carrier density of the two systems. The larger carrier density in the normal metal makes their hot-electron effects small at room temperature.

In thin films, the hot electron effect is more pronounced due to the larger ratio of power dissipation per unit volume to contact surface area to the substrate. Also, the

phonon distribution in the normal metal can in some cases no longer be differentiated to that of the substrate. Therefore, the hot phonon effect is more difficult to observe. For a thin film of thickness d to have a distinct population of the phonons, the temperature has to be $T \geq \hbar v_s / 2kd$, where v_s is the sound velocity [45]. For example: For $d = 50$ nm, the temperature should be $T \geq 350$ mK in order to construct a wave packet of phonon. The thickness also plays a critical role in optimizing the ratio of the power dissipated per unit area to the power dissipated per unit volume to heat the N metal phonons.

From the above discussion, it is clear that the hot electron and phonon effects can be manipulated or optimized depending on the geometry of the sample. In our samples, we have taken extra care to optimize the ratio of two powers for the cooling of phonons in the N-metal film at intermediate temperature. Sample without external thermometer [43] helps us to attain a smaller film - substrate contact surface area to volume ratio in comparison to the geometry with an external thermometer [5]. In this chapter, we will use the thermal model discussed above for our cooling device with a difference that P_{ext} leads to electron cooling.

6.2.1 Thermal model taken for cooling device

We have made the following assumptions in order to simplify the thermal model [45]:

(i) The cooling power P_{cool} is well defined for tunnel junctions. The cooling power out of the normal metal from the individual N-I-S junction (complete S-I-N-I-S junction) has been calculated in chapter 2 in this thesis:

$$P_{cool} = \frac{1}{e^2 R_N} \int_{-\infty}^{\infty} dE (E - eV/2) N_S(E) [f_N(E - eV/2) - f_S(E)]. \quad (6.1)$$

where $f_{S,N}$ is the electron distribution function in the superconductor and the normal metal respectively.

(ii) The two N-I-S junctions of the S-I-N-I-S cooler junction are assumed to be identical such that net cooling power is $2P_{cool}$ [51].

(iii) The electron-electron interaction in the normal metal island is strong enough for the electrons to attain a thermal equilibrium. It means that the electrons follow a Fermi distribution at an electronic temperature T_e that is lower than the cryostat temperature. It has been checked and discussed in detail in chapter 5 of this thesis.

(iv) The phonons are also at a well defined temperature (T_{ph}) which is much smaller than the Debye temperature (θ_D). In our experiment $T_{ph}/\theta_D \leq 10^{-3}$. At such temperature we can neglect the optical phonons. Only acoustic phonons, which at low energy have a linear dispersion relation $\varepsilon_q = \hbar v_s q$, where q is the phonon wavevector, are considered. It is also assumed that the phonon distribution is spatially uniform [47].

(v) The allowed phonon state spectrum is assumed to be the 3D continuum.

(vi) The electron-phonon interaction is given by a scalar deformation potential. It means that only the longitudinal phonons couple to the electrons and the transverse phonons are neglected [58].

The first three assumptions have been discussed in Chapter 5 in the context of quasi-equilibrium distribution in the central N metal. Here we will discuss the assumption (iv) in detail.

6.2.2 Non equilibrium phonon distribution

Let us consider the phonon distribution N_q in the N-metal. The simple phenomenological description of the energy exchange between the N-metal phonons with the substrate and with the electronic system is given by:

$$\frac{dN_q}{dt} = \frac{dN_q}{dt} |_{ph-sub} + \frac{dN_q}{dt} |_{el-ph}. \quad (6.2)$$

The first term in right side of Eq. 6.2 is the rate of phonon exchange with the substrate. It can be written as a relaxation of the N metal phonons to the substrate phonons with a characteristic time $\tau_{ph-sub} = \eta d/v_s$, where v_s is the velocity of sound; d the thickness of the N-metal and η is a numerical factor (< 1) which accounts for the lattice mismatch between the substrate and the N-metal phonons [54]. Thus we have,

$$\frac{dN_q}{dt} |_{ph-sub} = \frac{N_q(T_0) - N_q}{\tau_{ph-sub}}. \quad (6.3)$$

Here $N_q(T_0)$ is the equilibrium phonon distribution given by a Bose distribution $N_q(T_0) = 1/[1 - \exp(\frac{\hbar\omega}{kT_0})]$ at the substrate temperature $T = T_0$.

The relaxation of N metal phonons is accompanied by an energy transfer with the substrate phonons. The energy transfer is obtained by multiplying Eq. 6.3 by the phonon energy and summing over the phonon density of states. For $T \ll \theta_D$, the corresponding power is given by:

$$P_{ph-sub} = \int_0^\infty \hbar\omega \frac{Ad\omega^2 d\omega}{2\pi^2 v_s^3} \frac{v_s}{\eta d} [N_q(T_0) - N_q]. \quad (6.4)$$

For a phonon distribution N_q at equilibrium temperature T_{ph} , Eq. 6.4 gives a heat transfer proportional to $(T_0^4 - T_{ph}^4)$ through the area A . It is worthnoticing that P_{ph-sub} is independent of the thickness (d) of the N metal film.

The second term in Eq. 6.2 shows the rate of change of the phonon distribution in the N-metal due to the interaction with the electron gas of temperature $T = T_e$. Similarly, it contributes for the relaxation of the N metal phonon to the electron temperature with a characteristic time τ_{el-ph} , which describes the phonon absorption and emission by the electron gas:

$$\frac{dN_q}{dt} |_{el-ph} = \frac{N_q(T_e) - N_q}{\tau_{el-ph}}. \quad (6.5)$$

The characteristic time τ_{el-ph} can be obtained from the free electron approximation. τ_{el-ph} depends on the phonon wavevector and on the deformation potential $C = 2E_F/3$, where E_F is the Fermi energy, m being the electron mass and ρ the density of the film.

$$\frac{1}{\tau_{el-ph}} = \frac{m^2 C^2 q}{2\pi \hbar^3 \rho}. \quad (6.6)$$

It is worth noticing that the coupling of phonons to the electron gas increases with the phonon wave-vector. Therefore, the phonon cooling is more efficient for the high frequency part of the phonon distribution.

The energy exchange between electrons and phonons can be written in the same way as above, except that now we use 6.6. Thus the energy transfer between the electrons and phonons can be written as:

$$P_{el-ph} = \int_0^\infty \hbar\omega \frac{A d \omega^2 d\omega}{2\pi^2 v_s^3} \frac{m^2 C^2 q}{2\pi \hbar^3 \rho} [N_q(T_e) - N_q(T_{ph})]. \quad (6.7)$$

Thus we get,

$$P_{el-ph} = \Sigma \cdot A \cdot d (T_{el}^5 - T_{ph}^5), \quad (6.8)$$

where Σ is the electron-phonon coupling parameter given by:

$$\Sigma = \frac{m^2 C^2 k^2 \zeta(5)}{4\pi^3 \hbar^7 \rho v_s^4}. \quad (6.9)$$

From above, the predicted Σ for Cu is $10^8 \text{ W}\cdot\text{m}^{-3}\cdot\text{K}^{-5}$ is much smaller than most of the experimental results obtained by hot electron experiments [44, 45]. It may be due to assumption of free electron model and impurity free material [59]. For instance, the density of states obtained from heat capacity experiments is 1.38 times larger than the free electron model [60].

The difference in power is due to the energy dependence of the electron-phonon characteristic time. The presence of the thickness d in Eq. 6.8 is also worth noticing in comparison to the phonon interaction.

Now we consider the steady state distribution of the N-metal phonons, i.e. $\frac{dN_q}{dt} = 0$. The solution of Eq. 6.2 gives the phonon distribution, which is a combination of the distributions at T_0 and T_e respectively weighted by their respective relaxation times:

$$N_q = \frac{N_q(T_0) + (\tau_{ph-subst}/\tau_{el-ph})N_q(T_e)}{1 + (\tau_{ph-subst}/\tau_{el-ph})} = \frac{N_q(T_0) + \eta \cdot \alpha \cdot d \cdot q N_q(T_e)}{1 + \eta \cdot \alpha \cdot d \cdot q}, \quad (6.10)$$

where $\alpha = m^2 C^2 / 2\pi \hbar^3 v_s$ and η is the acoustic mismatch coefficient lying between 0 and 1. Eq. 6.10 illustrates that N_q is close to the (hot) bath temperature T_0 at small wavevector and approaches the cold distribution (T_e) at high wavevector. This is due to the better electron-phonon coupling at high energy. Increasing the thickness d of the N-metal also improves the cooling of the phonon distribution.

Fig. 6.2 shows the Planck spectrum for thickness $d = 50 \text{ nm}$ same as our sample and $v_s = 4400 \text{ m/s}$. In our experiment, the temperature of electrons in the central N-island decreases from the bath temperature of 300 mK to around 100 mK at the optimum bias. The olive and blue line correspond to the equilibrium spectrum at $T_{bath} = 300 \text{ mK}$ and $T_e =$

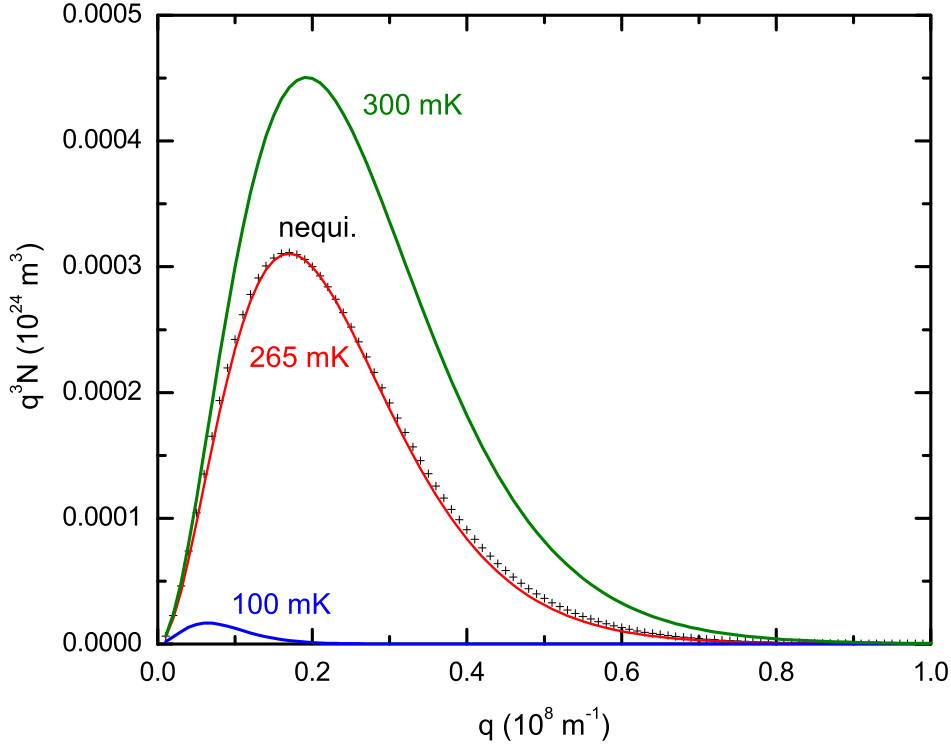


Figure 6.2: The plot of energy spectra $q^3 N_q$. The olive and blue lines correspond to equilibrium energy spectra at the bath temperature $T_{bath} = 300$ mK and at the cold point $T_e = 100$ mK respectively. The black crosses are the non equilibrium phonon energy spectra obtained from Eq. 6.10 with $\eta = 0.03$; $d = 50$ nm and $v_s = 4400$ m/s. The red line is the equilibrium energy spectra with the effective phonon temperature $T_{ph} = 265$ mK.

100 mK. The black crosses are the non-equilibrium distribution of phonons in the N-metal obtained from Eq. 6.10 with $\eta = 0.03$. It is interesting to note that the non-equilibrium distribution of N metal phonons can be approximated with an equilibrium one (red line) with an effective phonon temperature $T_{ph} = 265$ mK in between the bath temperature of the cryostat and the cold electronic temperature [61].

Finally, it is worth noticing that the energy transfer between electrons and the bath can be obtained without assuming an effective phonon temperature in the metal film. Inserting the distribution Eq. 6.10 in Eq. 6.4, we get

$$P_{el-subst} = \int_0^\infty \hbar\omega \frac{A d \omega^2 d\omega}{2\pi^2 v_s^3} \frac{[N_q(T_e) - N_q(T_{bath})]}{\tau_b + \tau_{el-ph}}. \quad (6.11)$$

Interestingly, although the electron gas is coupled to the substrate through the phonons

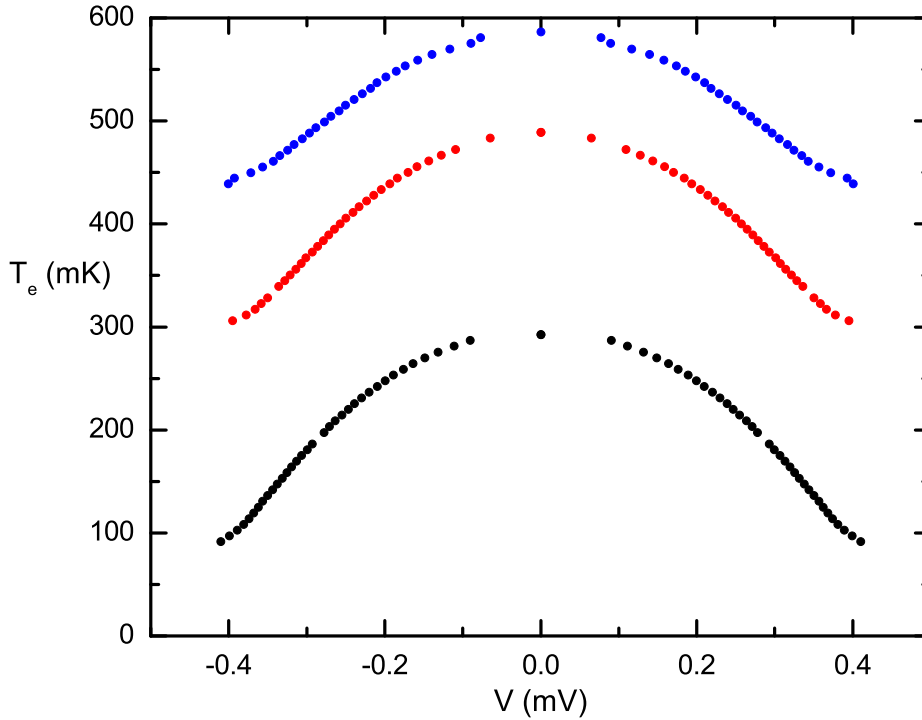


Figure 6.3: *Sample B: Electronic temperature of the central N metal as a function of cooler bias at three different bath temperatures. Parameters same as in Fig. 5.16: $R_n = 2.8 \text{ k}\Omega$ and $2\Delta = 0.428 \text{ meV}$.*

of the metal film, the details of their non-equilibrium distribution does not appear in the integral. There is no simple form for T_{el} and T_{ph} since the denominator has ω dependence.

6.3 Experiments on a S-I-N-I-S cooler

Here, we discuss the same sample as discussed in the previous chapter. Fig 6.3 shows the electronic temperature in the central N-island as a function of cooler voltage bias across the cooler junction at three different bath temperatures.

The temperature at zero bias corresponds to the bath temperature of the central N island. As the cooler bias voltage increases, the electrons in the N metal cool down till it reaches the gap voltage. For instance, the black dots correspond to $T_{bath} = 292 \text{ mK}$ at $V = 0 \text{ mV}$. As bias voltage increases, the electrons cool down to below 100 mK at the optimum bias. Similarly, the red and blue dots correspond to $T_{bath} = 489$ and 586 mK respectively.

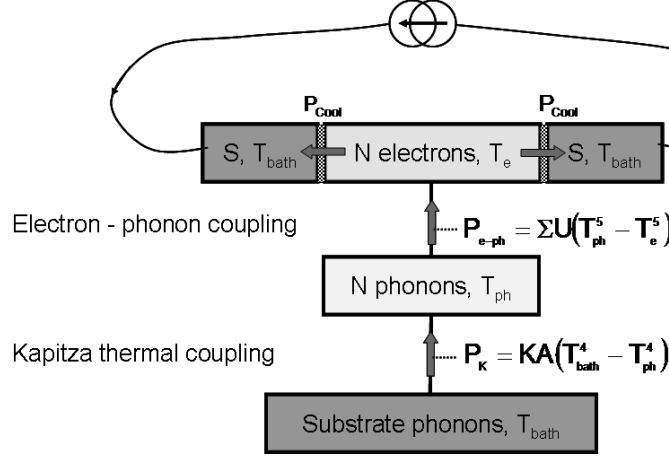


Figure 6.4: Heat flow paths between the different constituents in the cooler.

6.4 Thermal model in a S-I-N-I-S cooler

Here, we will extend the previously considered thermal model for our S-I-N-I-S cooling device. Fig. 6.4 shows the schematic of the considered thermal model, which is similar to the one discussed in the framework of hot electrons in metal. The electrons in the central normal metal are at quasi thermal equilibrium at the temperature T_e . The electrons cool down due to the extraction of the high-energy quasiparticles from the normal metal to superconductor. The two superconducting reservoirs are assumed to be thermalized to the bath temperature T_{bath} of the cryostat. We will re-consider the latter assumption in more detail in chapter 8.

For sub-gap bias at S-I-N-I-S junction, the quasiparticles tunnel from N to S. This uni-directional flow of hot quasiparticle leads to a heat current out of the normal metal. The corresponding cooling power P_{cool} can be written as:

$$P_{cool} = \frac{1}{e^2 R_n} \int_{-\infty}^{\infty} dE (E - \frac{eV}{2}) n_s(E) [f_n(E - \frac{eV}{2}) - f_s(E)], \quad (6.12)$$

Furthermore, the electrons in the normal metal are coupled to its phonons via electron-phonon coupling. The N-metal phonons are assumed to have an effective temperature T_{ph} . The electron-phonon scattering is the dominant energy exchange driving heat into the electronic system given by Eq. 6.8: $P_{el-ph} = \Sigma \cdot U \cdot (T_e^5 - T_{ph}^5)$, where Σ is the material dependent prefactor and U is the volume of the central island. At steady state, the heat balance equation for the N-metal electrons is given by:

$$2P_{cool}(T_e, T_{bath}, V) + P_{el-ph}(T_e, T_{ph}) = 0 \quad (6.13)$$

where the factor 2 accounts for the presence of two symmetric N-I-S junctions in series.

The normal metal phonons are coupled to the substrate phonons which is at temperature T_{bath} via Kapitza coupling. The heat transfer due to coupling between the two phonon

baths is given by, $P_{ph-sub} = K.A.(T_{bath}^4 - T_{ph}^4)$, where A is the interface area and K depends on the interface in contact. At steady state, the heat balance equation for the N metal phonons is given by:

$$P_{el-ph}(T_e, T_{ph}) + P_{ph-sub}(T_{ph}, T_{bath}) = 0. \quad (6.14)$$

For the phonons thermalized to the bath temperature correspond to $T_{ph} = T_{bath}$. This corresponds to an infinite Kapitza coefficient (K) in the thermal model. It implies that the heat balance for N-metal electron is given by: $2P_{cool}(V, T_e, T_{bath}) + P_{el-ph}(T_e, T_{bath}) = 0$, where $P_{el-ph} = \Sigma.U.(T_e^5 - T_{bath}^5)$. It can be reformulated as:

$$\left(\frac{T_e}{T_{bath}}\right)^5 = 1 - \frac{1}{\Sigma.U} \frac{2P_{cool}}{T_{bath}^5}$$

This means that the quantity $(T_e/T_{bath})^5$ depends linearly on $2P_{cool}/T_{bath}^5$ with a slope given by the constant $1/\Sigma U$. Here, we will check the validity of this approach, in particular at a higher cryostat temperature ($T > 300$ mK) regime. Fig. 6.5 shows a plot for $(T_e/T_{bath})^5$ as a function for $2P_{cool}/T_{bath}^5$ for different bath temperature. The cooling power P_{cool} is calculated from Eq. 6.12. It indeed shows that the low bias data at a given bath temperature has a linear dependence. The related Σ is obtained from the slope of the fit. Σ depends significantly on the bath temperature of the cryostat. For instance, at $T_{bath} = 292$ and 586 mK, the fit gives $\Sigma = 1.22$ and 0.78 nW. $\mu\text{m}^{-3}.\text{K}^{-5}$ respectively. Moreover, the fitted Σ are well below the expected experimental value of 2 nW. $\mu\text{m}^{-3}.\text{K}^{-5}$ [44, 45, 40, 62]. It means that the coupling between the electrons and the substrate is weaker than expected.

In this discussion, we neglected a leakage in the sub-gap current. It is demonstrated by the fact that the differential conductance at $V = 0$ of the coolers coincides with the isotherm prediction at the cryostat bath temperature. It is due to the relatively high bath temperature ($T > 300$ mK) in the experiment. Considering a leakage resistance of 5 MOhm would lead to an additional current at the bias edge below 0.1 nA, which about 0.1 % of the measured current at this point. This change would modify the electron temperature by less than 1 mK at the gap edge, which is much smaller than the discrepancy between the data and the fixed phonon temperature. At zero bias, this gives a change of 10 mK for the electron temperature extracted from the data that would be actually difficult to justify from the fit.

We conclude that the experiments on our cooling S-I-N-I-S device without an external thermometer cannot be understood within the thermalized phonon hypothesis. It is also worth noticing that $2P_{cool}/T_{bath}^5$ cannot be linearly fitted at the gap edge. This will be discussed in chapter 8.

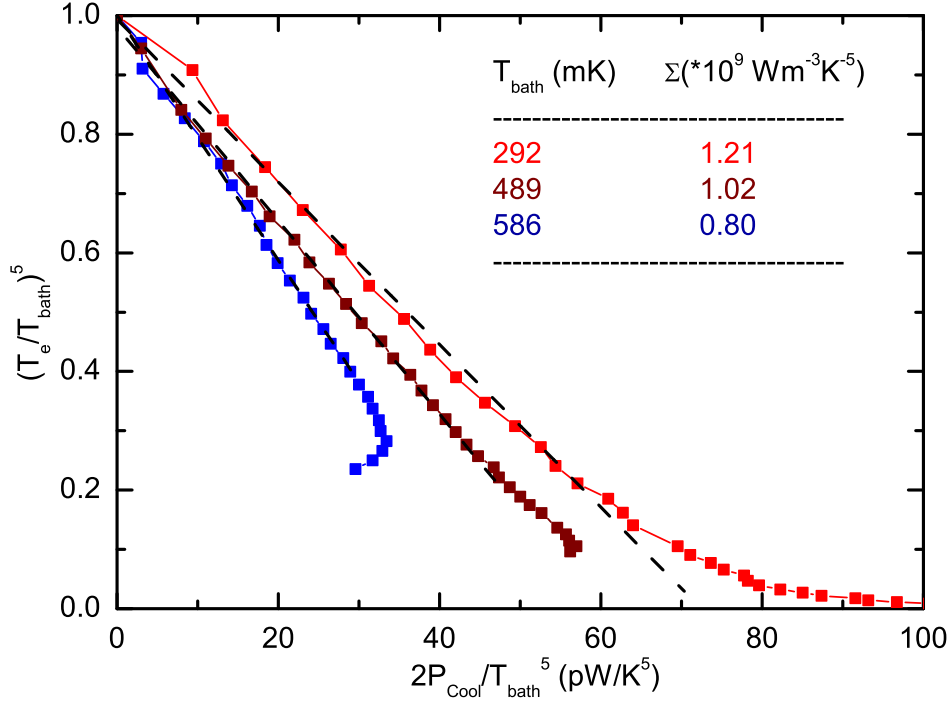


Figure 6.5: *Sample B: Measured bias dependence of the quantity $(T_e/T_{\text{bath}})^5$ for three different bath temperatures T_{bath} of 292, 489 and 586 mK as a function of $2P_{\text{cool}}/T_{\text{bath}}^5$. Dotted line shows the linear fit to the experiment which gives the values of Σ parameter equal to 1.22, 1.02 and 0.78 respectively.*

6.5 Electron and Phonon cooling in the S-I-N-I-S junction

In order to understand the data, we consider the full thermal model as shown in Fig. 6.1. It means that we self consistently solve the two heat balance equations for the electrons and the phonons given in Eq. 6.13 and Eq. 6.14 in order to calculate the electron and phonon temperatures as a function of bias voltage. Here we have taken the electron - phonon coupling constant Σ to be equal to $2 \text{ nW} \cdot \mu\text{m}^{-3} \cdot \text{K}^{-5}$ [44, 45, 40, 62] and used the quantity $K.A$ to fit the experiment.

Fig. 6.6 shows the fit of the experiment with the thermal model. Black, red and blue dots are the extracted electron temperature of the central N island for the bath temperature of 292, 489 and 586 mK respectively. The full and dotted lines shows the calculated electron and phonon temperature obtained from the thermal model at the respective bath

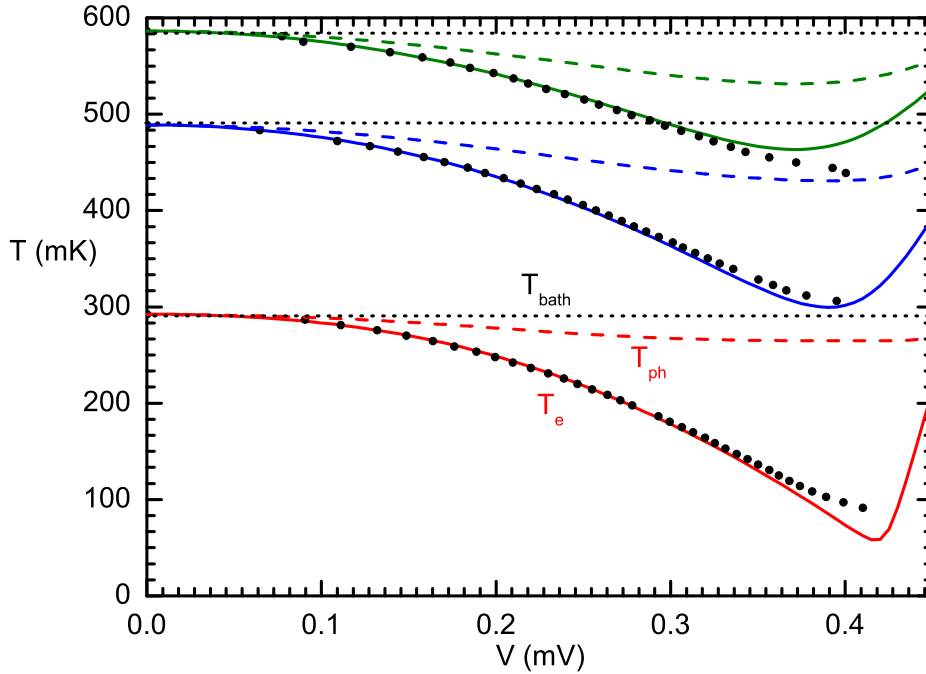


Figure 6.6: *Electron and phonon temperature as a function of cooler bias voltage for a cryostat temperature of 275 mK, 470 mK and 570 mK. The bath temperature extracted from the cooler data ($V = 0$ mV) is respectively 292 mK, 489 mK and 586 mK respectively. The dots are the experimental points. The full and dotted lines shows the calculated electron and phonon temperatures respectively obtained from the thermal model for $\Sigma = 2$ nW. $\mu\text{m}^{-3} \cdot \text{K}^{-5}$ and $K.A = 66$ pW. K^{-4} .*

temperature. We have obtained the best fit for $K.A = 66$ pW. K^{-4} . We have taken the measured values of superconducting gap Δ and the normal state conductance R_n .

The model shows an acceptable fit between the experiment and the calculated electrons temperature. This demonstrates the cooling of normal metal phonons in addition to the standard electron cooling [63] in the S-I-N-I-S tunnel junction. The phonons cooling is more efficient at higher temperature. For instance, at $T_{bath} = 489$ mK the phonons reach at the optimum bias a temperature about 50 mK below to the bath temperature. The dependence of cooling of N-metal phonons on the bath temperature of the cryostat can be understood simply by comparing the temperature dependence of the electron-phonon and the phonon-phonon couplings. At low temperature, the ratio between the phonon cooling and the electron cooling decreases because the electron - phonon decoupling ($\propto T^{-5}$) dominates the Kapitza resistance ($\propto T^{-4}$).

For a consistency check between the model and experiment, we compare the differ-

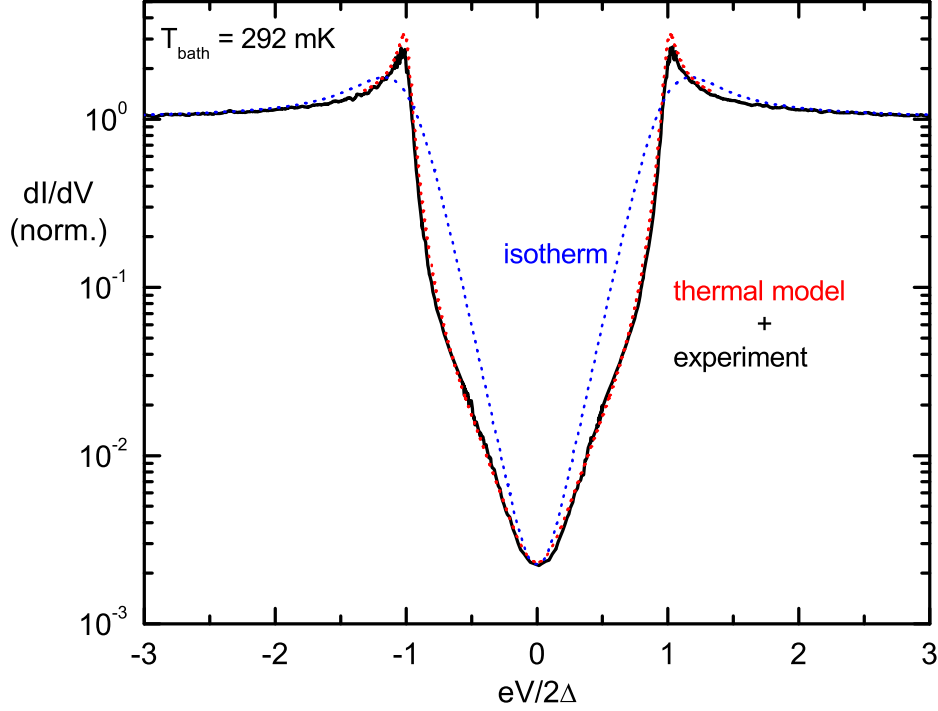


Figure 6.7: Cooler junction data (full black line) along with the calculated curve. The blue dotted line shows the calculated isotherm at $T_e = 292$ mK with $R_n = 2.25$ k Ω ; $2\Delta = 0.42$ meV. The red dotted line on the cooler characteristic is the fit with the thermal model of the device. The thermal model is solved for $\Sigma = 2$ nW. $\mu\text{m}^{-3}.\text{K}^{-5}$ and $K.A = 66$ pW. K^{-4} .

ential conductance calculated from the electronic temperature evolution in the thermal model with the experiment. Fig. 6.7 shows the comparison of the experiment (black line) differential conductance with the thermal model (red line) for the cryostat temperature of 292 mK. The two curves show a very good agreement (note the logarithmic scale) for a sub-gap bias voltages. The blue line is the isotherm which does not fit either of the two other curves.

The parameter $K.A$ accounts for the total Kapitza coupling of the Cu island to the SiO_2 substrate that includes the contributions of both a direct Cu/SiO_2 contact and a contact through the oxidized Al film with a presumably weaker efficiency. Dividing the fit-derived KA parameter by the full area of the Cu island provides an effective mean value $\langle K \rangle$. We found that $\langle K \rangle$ varies from sample to sample in the range 40 - 120 pW. $\text{m}^{-2}.\text{K}^{-4}$ (see Table 1 at the end of thesis). $\langle K \rangle = 40$ pW. $\text{m}^{-2}.\text{K}^{-4}$ is about a factor 3 below the values calculated for bulk Si/Cu interface [54] and only a factor 2 below

the experimental value in Ref. [44]. It could be due to the fact that our samples are made on Si/SiO₂ substrate and the oxide is expected to reduce the $\langle K \rangle$.

6.6 Conclusion

In conclusion, we followed a precise investigation of the S-I-N-I-S cooler characteristics, in the frame-work of a model mainly used for the hot electron effects with a very low bath temperature.

We demonstrated the cooling of N-metal phonons in addition to its electrons [43]. For instance, at $T_{bath} = 489$ mK, the electrons in the N-metal cools down to 300 mK and the phonons reach at the optimum bias a temperature about 50 mK below the bath temperature. We showed the relevance of the phonon cooling, which can be demonstrated by the dimensionless parameter $\Sigma dT/K$ here of the order of unity.

The thermal model gave an acceptable fit and understanding of the electron cooling in the normal metal. However the model shows a poor fit at the gap edge, due to mechanisms that are not included. For instance, the assumption of superconductor remaining at the bath temperature will not be correct at the gap edge, where the maximum injection of hot quasiparticle in S takes place. It can lead to some back-flow of hot quasiparticles accumulated close to the junctions. We will consider this situation in greater detail in chapter 8, where the diffusion of hot quasiparticles in the superconductor shall be discussed.

Let us consider the thermal model in different temperature regime. Fig. 6.8 shows the calculated electron temperature (full line) and phonon temperature (dashed line) in the central normal metal as a function of the cooler bias voltage at different cryostat temperatures. Here we have considered only the single quasiparticle tunneling across the N-I-S junction. At very low bath temperature ($T < 250$ mK), the phonon cooling has a minimal effect in comparison to the high bath temperature. Only the heat contribution due to quasiparticles is considered and other processes like Andreev current are neglected.

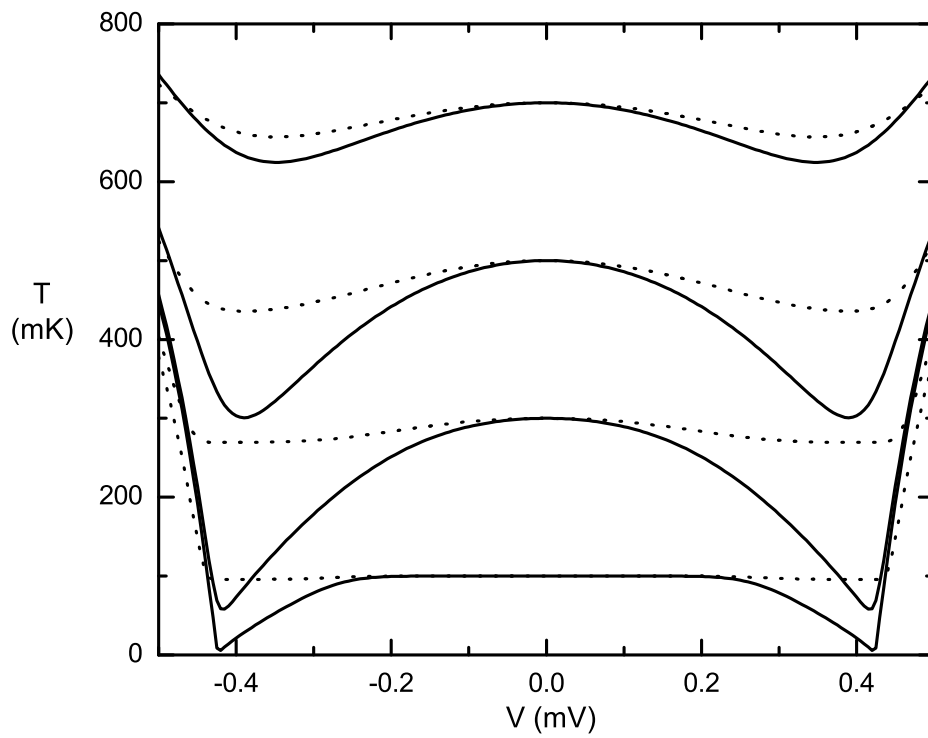


Figure 6.8: Full and dashed line represent the calculated electron and phonon temperatures as a function of the cooler bias voltage for different cryostat temperatures. Calculation parameters: $\Sigma = 2 \text{ nW} \cdot \mu\text{m}^{-3} \cdot \text{K}^{-5}$; $K.A = 60 \text{ pW} \cdot \text{K}^{-4}$; $d = 50 \text{ nm}$; $2\Delta = 0.424 \text{ meV}$; $R_n = 1 \text{ k}\Omega$.

Chapter 7

Andreev current-induced dissipation

7.1 Introduction

This chapter is mainly concerned with experiments done at very low temperature. As discussed in Chapter 2 and 3, the charge transfer across the N-I-S junctions is mainly governed by two processes. For an electron with energy $E > \Delta$, tunnel from N to S leading to both charge and heat current. At intermediate temperature ($T > 300$ mK), the electrons in the central N island cool down significantly, for example from 300 mK to below 100 mK [63]. For energy below the gap ($E < \Delta$), the higher order process Andreev reflection is responsible for electron pairs transfer across the junction [12, 13]. The Andreev reflection provides a conversion of dissipative electrical current in the normal current into a dissipationless supercurrent [35].

Here, we discuss the experiments, done on the S-I-N-I-S cooler junctions and the probe junction at a very low temperature. There is an explicit crossover between the quasiparticle current and the phase-coherent Andreev current in the total current across the probe junction. We use the Hekking and Nazarov model discussed in chapter 3 to fit the phase-coherent contribution due to Andreev current. Then we discuss the experiments done on the cooler junction. Here we will extend the thermal model discussed in the chapter 6 for our cooling device, by considering the thermal contribution due to the phase-coherent Andreev current. The thermal model shows the need of an extra non-linear dissipation. It is being identified as a dissipation due to phase-coherent Andreev current. Later, the consequence of dissipative Andreev current as a increase of the electron temperature shall be discussed. Lastly, the influence of several external parameters, like the phase-coherence length, shall be discussed.

7.2 Experimental observation of phase-coherent Andreev current

7.2.1 Introduction

As discussed in Chapter 3, at a N-S interface a specularly reflected electron undergoes elastic scattering from the impurities which leads to trajectories re-directed towards the barrier. These trajectories add constructively and are immune to the phase-randomization induced by the disorder [18]. At zero temperature, the relevant length scale for the constructive coherent addition of probability amplitude is given by the phase-coherence length (L_ϕ) or by the actual length of the wire [28, 64]. For a finite temperature or bias, the two-electrons originating from the superconductor have a difference in energy E and the energy-dependent length scale is $L_E = \sqrt{\hbar D/E}$. If we consider the whole thermal population, the resulting phase-coherence length given by:

$$L_N = \sqrt{\frac{\hbar D}{\max[eV, kT]}}, \quad (7.1)$$

is much larger than the mean free path. This leads electron pairs tunneling to add coherently over a large distance. Thus the phase-coherent Andreev current enhances the probability for transfer of electron pairs across the junction.

In the following, we fit the experimental data acquired on the probe junction where the normal metal thermalized to the bath temperature, taking into account the quasi-particle current and the phase-coherent Andreev current.

7.2.2 Experiment on Probe junction

In all our samples, we have 3 Al-AlO_x-Cu junctions called probe junctions on the Al electrode in addition to the cooler junctions. As discussed previously, the N-metal on the probe junction is strongly thermalized to the cryostat temperature.

Fig. 7.1 shows the differential conductance of one probe junction (1.55 μm from the cooler junction) as a function of voltage bias at the cryostat temperature of 90 mK. Clearly in comparison to the Fig. 5.6 of chapter 5, the probe junction at low temperature has a different characteristic at low bias. Instead of a monotonous exponential decay of the differential conductance in the subgap bias, the differential conductance has a peak at zero bias. Similar differential conductance characteristics are also obtained on the other two probes.

The dotted red line is the fit to the experiment by considering only the single quasi-particle tunnel current given by Eq. 5.1 with a electronic temperature of 105 mK. The enhancement of differential conductance at zero bias clearly cannot be fitted by the single quasiparticle tunnel equation. The electronic temperature T_e extracted from the fit is slightly higher than the cryostat temperature.

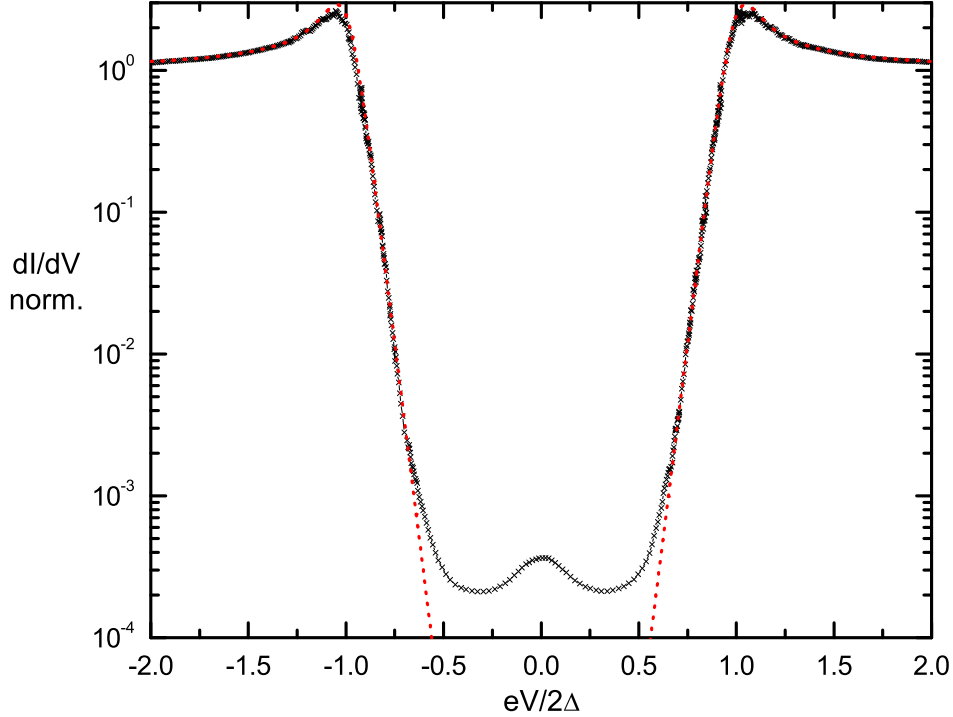


Figure 7.1: *Sample C: Normalized differential conductance as a function of voltage at a cryostat temperature of 90 mK. The black cross symbol line shows the experiment on the probe junction. The dotted red line shows the quasiparticle fit to the experiment with $R_N = 2.76 \text{ k}\Omega$, $\Delta = 0.228 \text{ meV}$ and $T_e = 105 \text{ mK}$.*

The zero bias conductance increases when the cryostat temperature is lowered below about 200 mK, which suggests that it is a phase-coherent effect (see Fig. 7.2). The zero bias anomaly is similar to the one obtained by Kastalsky et. al. [17].

7.2.3 Phase-coherent Andreev current in Probe junction

The zero bias peak in the differential conductance cannot be accounted by a linear leakage as it would lead to a saturation of the conductance near zero bias. As discussed in chapter 5, the zero bias anomaly cannot be fitted by considering a non-equilibrium distribution in N-metal or by considering a smeared density of states [24, 11].

As discussed in chapter 3, in the normal metal - superconductor tunnel junction the phase-coherent Andreev current leads to the enhancement of the differential conductance at low temperature. Thus we will ascribe the zero bias enhancement of the differential

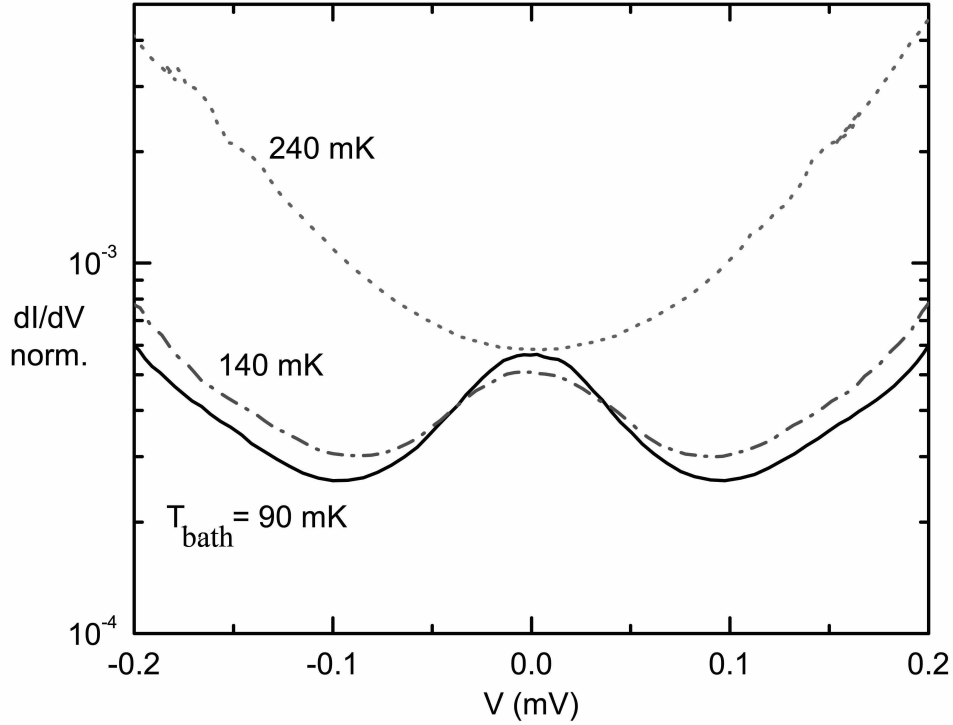


Figure 7.2: *Sample C: Normalized differential conductance of the cooler junction as a function of voltage at a different cryostat temperatures.*

conductance to a phase-coherent Andreev current. We will follow the theory and equations (Eq. 3.13 and Eq. 3.14) for the phase-coherent Andreev current obtained in Chapter 3.

The coherence length L_N of an Andreev pair at $T = 90$ mK is $0.8 \mu\text{m}$, which is much greater than the width dimension ($= 0.12 \mu\text{m}$) of the central Cu wire. Therefore we consider the 1D diffusion of the Cooperon, where the coherence length of an Andreev pair in the normal metal L_N is much larger than the cross-section area of the electrode.

We have obtained the phase-coherent Andreev current (I_A) by taking into account the disorder both in the normal metal and the superconductor electrode. The calculation takes into account the finite gap of superconductor and is valid for $eV, kT < \Delta$. The propagation of the Cooperon in the electrode is cut by the phase-coherence length (L_ϕ).

Fig 7.3 shows the tunnel current as a function of the voltage bias for the probe junction (black dots) at a cryostat temperature of 90 mK. The complete line shows the fit of the phase-coherent Andreev current and the dotted line shows the single quasiparticle current.

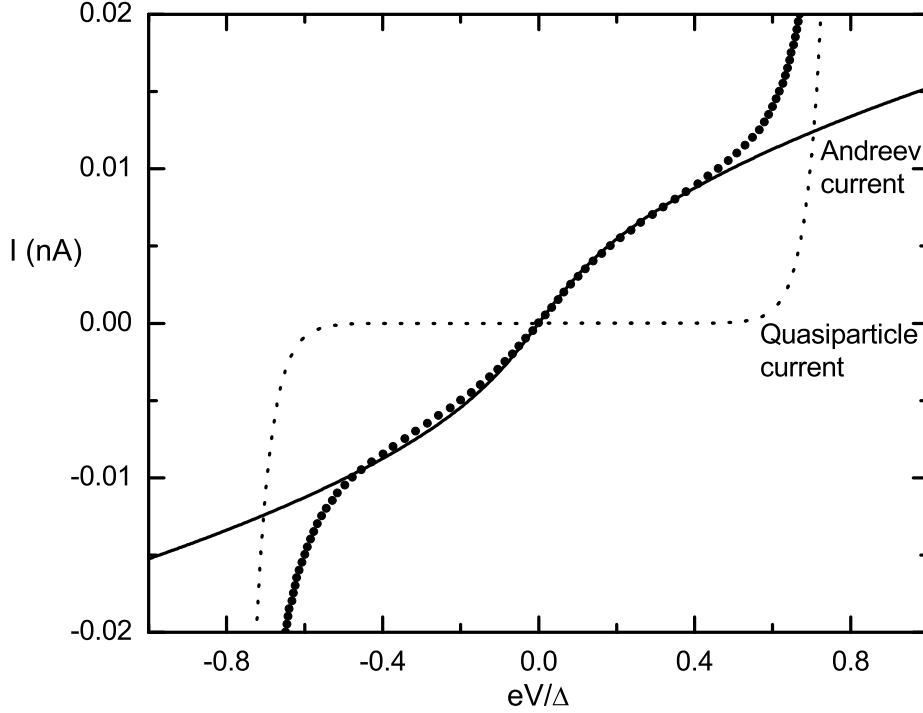


Figure 7.3: *Sample C: Current - voltage characteristic of the probe junction at the cryostat temperature of 90 mK. The dots show the experiment, the continuous line is the fit with the phase-coherent Andreev current given by Eq. 3.13 and 3.14 and the dotted line shows the fit with single quasiparticle current. The fit parameters are : $D = 80 \text{ cm}^2/\text{s}$, $L_\Phi = 1.5 \text{ }\mu\text{m}$, $R_N = 2.76 \text{ k}\Omega$, $\Delta = 0.228 \text{ meV}$, $T_e = 105 \text{ mK}$ and $M = 1.37$ to fit the experiment.*

7.2.4 The Fit parameters for the phase-coherent Andreev current

The phase-coherent Andreev current has been computed for the sample geometry and dimensions. The fit parameters are : $L_\Phi = 1.5 \text{ }\mu\text{m}$, $R_N = 2.76 \text{ k}\Omega$, $\Delta = 0.228 \text{ meV}$. We took the measured diffusion coefficient as $D = 80 \text{ cm}^2/\text{sec}$. Here, the electron temperature of 105 mK is obtained from single quasiparticle fit (Fig. 7.1), which is slightly higher than the cryostat temperature. L_Φ is close to the the phase-coherence of $2.1 \text{ }\mu\text{m}$ found at $T = 275 \text{ mK}$ from a weak localization experiment on a wire fabricated with the same material (see chapter 5) and also agrees well with the expected value for a pure metal at very low temperature [49, 50].

We have used the same parameters to fit the experiments on the other two probe junctions and also on other samples. For different samples, the fit phase-coherence length

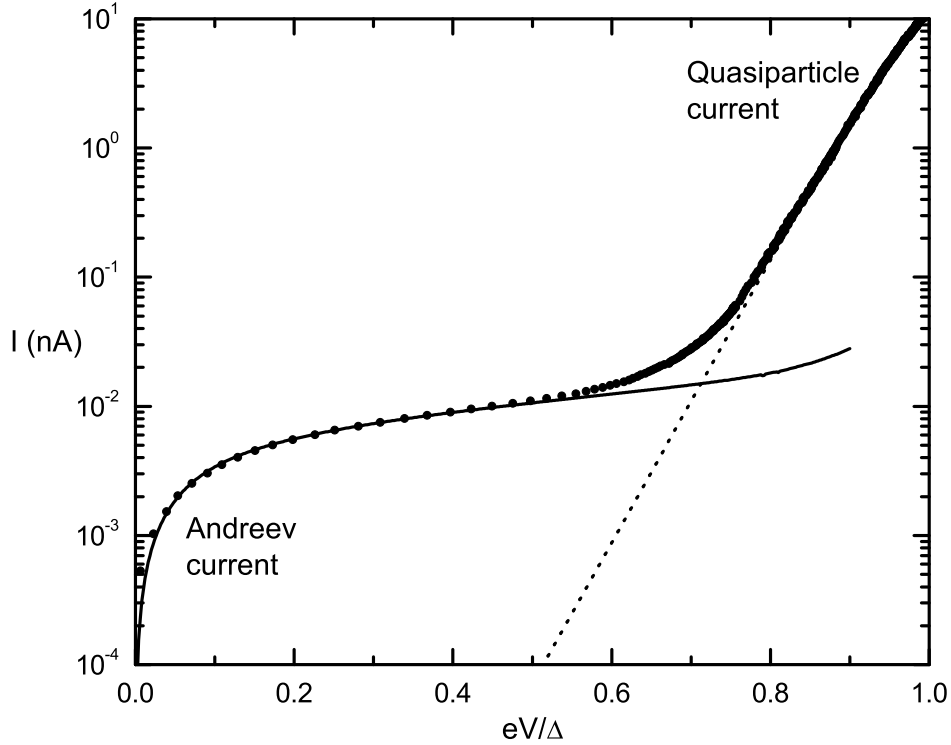


Figure 7.4: *Sample C: Current - voltage characteristic of the probe junction at a cryostat temperature of 90 mK. The dots show the experiment, the complete line is the fit with phase-coherent Andreev current and the dotted line with single quasiparticle current.*

is found to be slightly different. The difference in dephasing time could be due to a number of reasons like the different evaporation conditions during different samples fabrication or the contamination of the Copper between the evaporation and mounting the sample in the dilution refrigerator. In the fit, we had to scale the phase-coherent Andreev current by a multiplying factor $M = 1.37$, which is done in the same way as done previously by Pothier et al. [18].

Fig. 7.4 shows an excellent fit of the experiment with the phase-coherent Andreev current and the single quasiparticle current. Thus we conclude that the sub-gap current in the N-I-S junction is the superposition of the single quasiparticle tunnel current and the two particle Andreev current. The factor M could be possible contribution of pinholes or inhomogeneities in the tunnel barrier (see chapter 3), which are not considered here in obtaining the Andreev current.

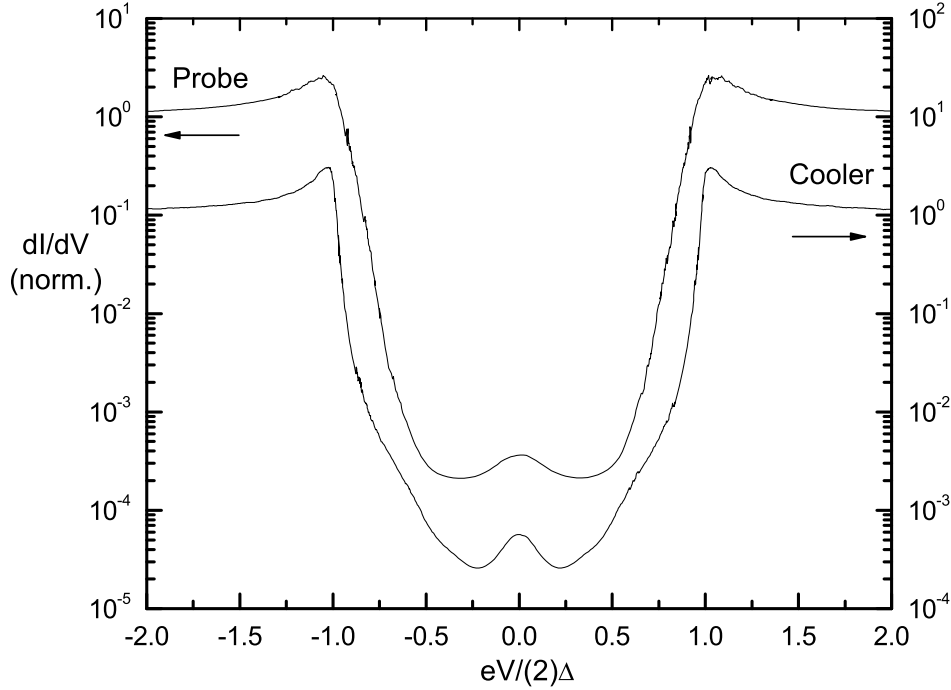
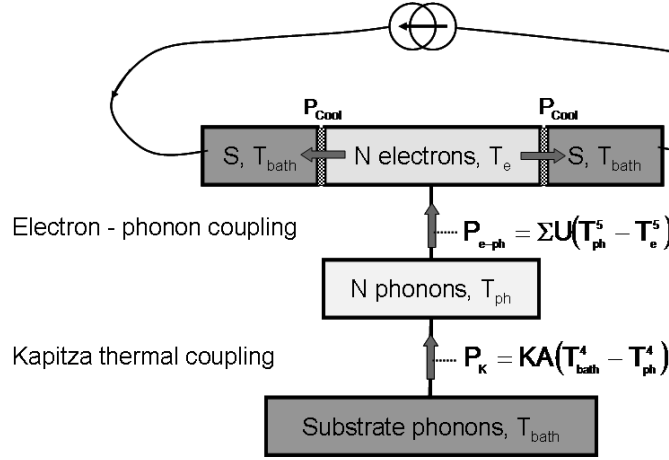


Figure 7.5: *Sample C: Differential conductance at a cryostat temperature of 90 mK. Top curve - the dI/dV of one probe junction $1.55 \mu\text{m}$ from the cooler junction which has been fitted in the previous section with the phase-coherent Andreev current and the single quasiparticle current (see left y-axis). The normal state resistance of the probe junction, $R_N = 2.76 \text{ k}\Omega$. Bottom curve: cooler junction data (see right y-axis) with normal state resistance, $R_N = 1.9 \text{ k}\Omega$.*

7.3 Cooler junction at low temperature

Fig. 7.5 shows the differential conductance of the cooler and one of the probe junctions at the cryostat temperature of 90 mK. As discussed in the previous section, the enhancement of the differential conductance near zero bias is associated to the phase-coherent Andreev current.

The differential conductance obtained from the probe junction has a linear slope below the gap voltage, which corresponds to the isotherm nature of the probe. This is not the case in the cooler junction experimental data. The differential conductance peak at gap bias from the cooler junction is larger than in the case of the probe junction, which exemplifies the cooling of the N island electrons at the optimum bias.

Figure 7.6: *Schematic of the thermal model.*

7.3.1 The behavior of the cooler junction in the presence of an Andreev current

In order to understand the behavior of the S-I-N-I-S cooler junction, we need to consider the heat balance in the central normal metal. Here we assume the quasi-equilibrium situation similar to the previous chapter: the electrons and the phonons in the central N island follow a thermal distribution function at a respective temperature T_e and T_{ph} , which are in general different from the bath temperature T_{bath} of the cryostat.

In the schematic above, the single quasiparticle current is responsible for the cooling power out of the central N-island. The cooling power is compensated by the electron-phonon coupling power such that:

$$2P_{cool}(V, T_e, T_s) + P_{el-ph}(T_e, T_{ph}) = 0, \quad (7.2)$$

where the factor 2 is due to the double N-I-S junction in series. We consider that the heat given to the phonons in the normal metal is compensated by the Kapitza coupling with the phonons of the substrate, such that

$$P_{el-ph}(T_e, T_{ph}) + P_K(T_{ph}, T_{bath}) = 0. \quad (7.3)$$

The Kapitza thermal resistance is significant only for higher temperature ($T > 300$ mK), which leads to the cooling of the normal metal phonons [43]. As seen in Chapter 6, at low temperature ($T < 250$ mK) the assumption of perfect thermalization N phonons to the bath temperature would change the total current by only 2%. Therefore the cooling of phonons has a negligible role at very low temperature.

The total current through the N-I-S junction is the sum of the single quasiparticle current I_T and the phase-coherent Andreev current I_A so that:

$$I_{cooler} = I_T(V, T_e) + I_A(V, T_e). \quad (7.4)$$

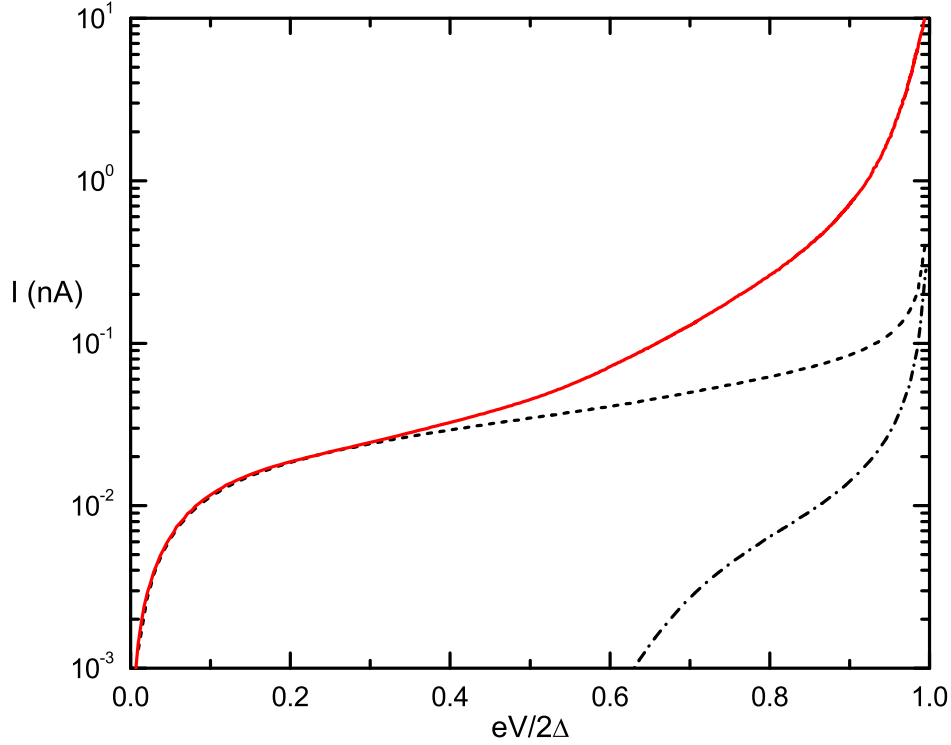


Figure 7.7: *Current - voltage characteristic of the S-I-N-I-S cooler junction along with the simulated curve at bath temperature of 90 mK. The full red line shows the experiment. The dashed curve and dotted dash line shows calculated curve. The dotted dash curve includes only the single quasiparticle contribution to the thermal model with the parameters: $2\Delta = 0.43$ meV, $KA = 144$ W.K⁻⁴ and the dashed line includes the Andreev current contribution with the parameters: $D = 80$ cm²/s; $L_{\Phi} = 1.5$ μ m and $M = 0.49$*

To fit the experiment, we first numerically solve the thermal model for relatively high temperature ($T > 300$ mK), where the contribution due to the phase-coherent Andreev current is negligible. We take the electron-phonon coupling coefficient $\Sigma = 2$ nW. μ m⁻³.K⁻⁵ and obtain the electron phonon coupling parameter $KA = 144$ W.K⁻⁴. The Kapitza coefficient $\langle K \rangle$ is comparable to the one discussed in chapter 6.

We turn afterwards to the very low temperature regime of interest here. Fig. 7.7 shows the direct current-voltage characteristic obtained from the cooler junction (full red line) along with calculated curves (dashed and dotted-dash lines). The dotted-dash line is the calculated current-voltage characteristic at a 90 mK cryostat temperature including the charge and heat currents of the single quasi-particle tunneling only. The agreement is poor,

which confirms the need to include the Andreev current contribution to the junction. The dashed line shows the result of the calculation based on the thermal model with the charge current given by the sum of the single quasi-particle current and the Andreev current. The fit parameters are the same than for the probe except for the scaling factor $M = 0.49$. The difference with the probe junction factor is not understood, although it could be due to the difference in geometry between the two junctions. The addition of the phase-coherent current provides an acceptable fit at low bias but shows a clear discrepancy at intermediate voltage. The experimental curve shows a larger current than what is obtained from the thermal model. This demonstrates that an excess dissipation term or an extra current contribution is missing in the thermal model.

Assumption: Contribution due to the linear leakage current

Fig. 7.8 shows the comparison between the experiment and calculated curve from the thermal model, which consider an excess dissipation due to a linear resistance. Here the leakage contributes both as a heat in the thermal model and to the total current across the junction.

The minimum leakage resistance can be estimated from the differential conductance plot of the cooler junction, which corresponds to a minimum leakage as $20 \text{ M}\Omega$. Fig. 7.8 shows that adding an extra dissipation term in the thermal model due to a linear leakage does not provide a good description of the experiment.

Thus a significant thermal contribution is missing in the heat balance equations of the described thermal model.

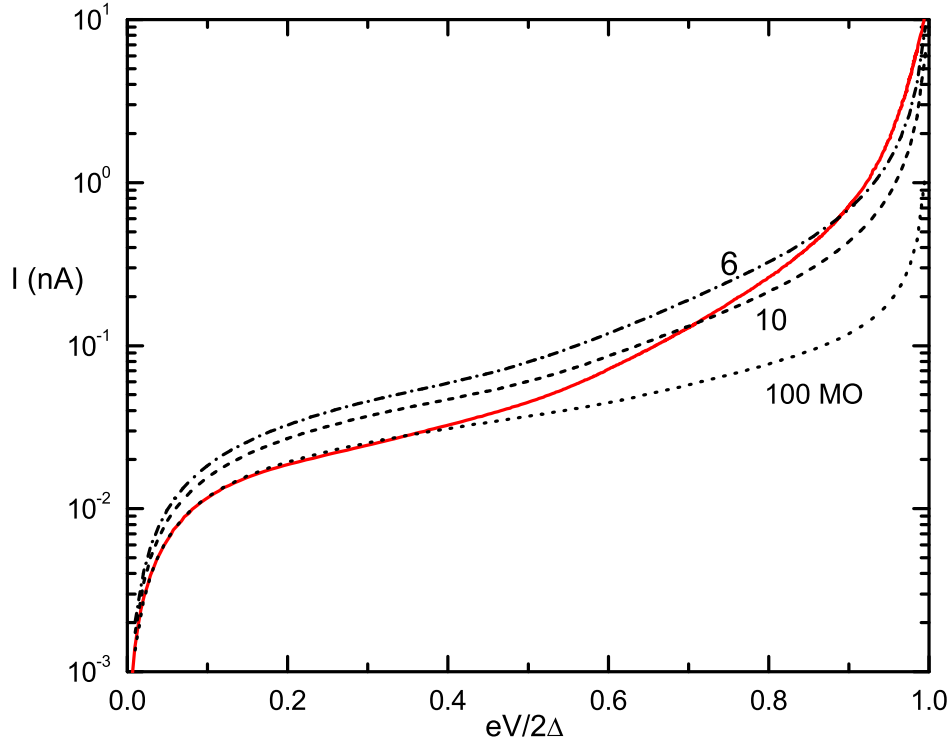


Figure 7.8: *Current -voltage characteristic of the cooler junction along with the calculated thermal model curve, which considers an excess leakage due to a linear resistance.*

7.4 The Andreev current induced dissipation

In chapter 3 we discussed the heat transfer due to the Andreev current in a N-I-S tunnel barrier. We found that the work performed by the current source feeding the circuit with an extra current due to Andreev reflection (I_A) generates a Joule heat $P_A = I_A \cdot V$ [25]. This induced dissipation due to the Andreev current is deposited entirely in the N metal and does not perturb the superconductor. Hence, the net cooling power of the S-I-N junction due to the tunneling of hot single quasiparticle out of the N metal will be reduced by the Joule heat deposited into N by the Andreev current. The net cooling power of the device is re-defined as, $P_{net} = P_{cool} - P_A$.

The Andreev current induced dissipation depends strongly on the temperature and transparency of the junction. For low transparency and at intermediate temperature ($T > 300$ mK) the phase-coherent Andreev current contribution is negligible in comparison to the single quasiparticle current. Thus the Joule heat dissipation in N-island is small. At very low temperature and low bias, the cooling power is negligible in comparison to

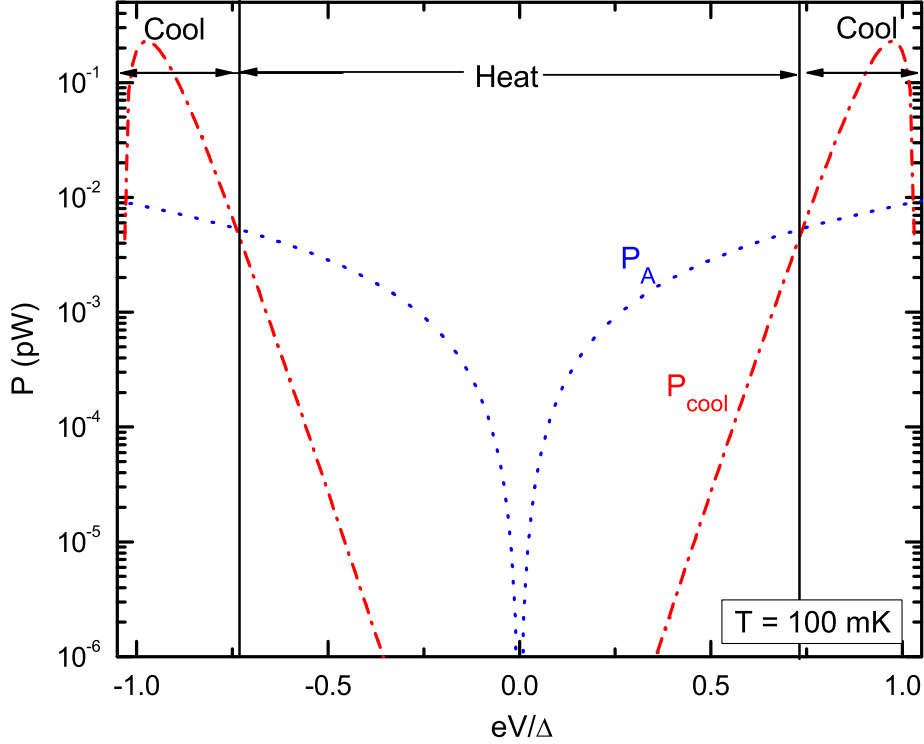


Figure 7.9: Calculated power due to quasiparticle cooling (P_{cool}) and the heat dissipation due to Andreev current (P_A) as a function of voltage bias at $T_{bath} = 100$ mK. Parameters used in the calculation are the same as in Fig. 7.7.

the induced Andreev power. The induced dissipation will then subjugate the quasiparticle cooling and lead to heating of the electrons in N-island.

Fig. 7.9 shows the quantitative comparison of the cooling power (P_{cool}) due to single quasiparticle tunneling (red dotted dash line) and the Andreev current (blue dotted line) induced dissipation (P_A) at very low temperature. Due to the absence of quasiparticles, P_{cool} is almost zero near zero bias and attains its maximum near the gap. However the phase-coherent Andreev current induces the dissipation as a Joule heat ($I_A V$) in the N metal, which increases sharply near the zero bias. At a bias close to the gap voltage, the cooling power out-does the dissipation due to the Andreev current.

As Andreev current induced dissipation depends on the transparency of the junction, it surpasses the single quasiparticle cooling at a varying temperature. For our cooling device with a low transparent tunnel barrier (10^{-5}), the Andreev current dissipation becomes relevant only at low temperature ($T < 200$ mK).

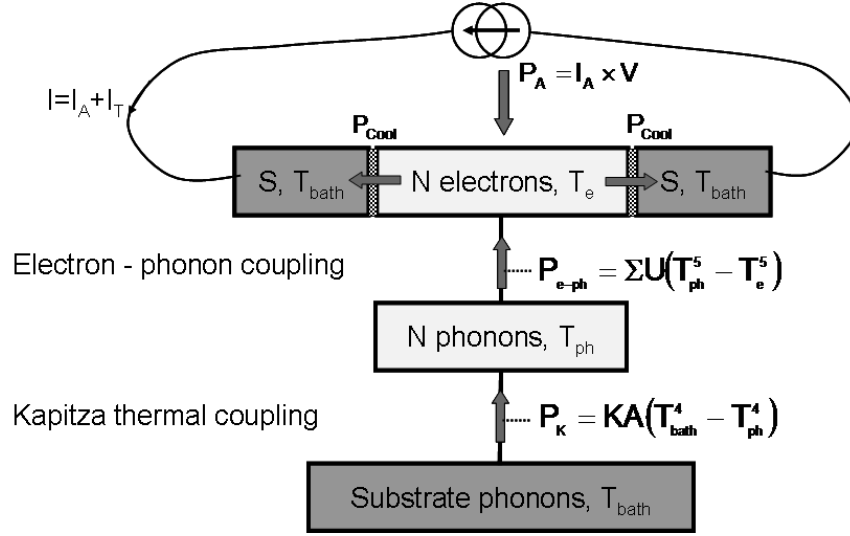


Figure 7.10: *Schematic of complete thermal model of the device.*

7.5 Thermal model with Andreev dissipation

Fig. 7.10 shows the complete schematic of the thermal model of the device. Here we have included the work done on the central N island by the current source with a current I_A as a Joule heating. At steady state, the heat balance for the electrons in N island can be rewritten as:

$$2P_{cool}(V, T_e, T_s) - P_{el-ph}(T_e, T_{ph}) - I_A V = 0. \quad (7.5)$$

With this complete heat balance equation taken into account, we solve the thermal model and calculate the total contribution to the current in the cooler junction. Fig. 7.11 shows the comparison of the experiment (complete lines) and the thermal model (dotted lines). The agreement is excellent between the experiment and theory for 4 order of magnitude of current in the sub-gap bias and at every accessible cryostat temperature. The fit parameters for the Andreev current are the same as obtained from the probe junction except the global scale factor on the Andreev current, $M = 0.49$.

The above conclusion on the Andreev heat is independent of the phonon cooling. Assuming the perfect thermalization of the phonons to the substrate temperature would change the total calculated current by less than 2 % at 90 mK, which means that phonon cooling has a negligible role in data analysis at very low temperature. This is due to the negligible amplitude of the phonon cooling at very low temperature (see chapter 6).

The above fit with the thermal model also provides us with the electron temperature for every bias. Fig. 7.12 shows the calculated electron temperature in the central N island as a function of voltage bias across the cooler junction for different cryostat temperatures $T_{bath} = 90, 140$ and 230 mK. At very low temperature, the electron temperature first increases with the bias as Andreev current-induced heat is dominant, till voltage bias reaches the

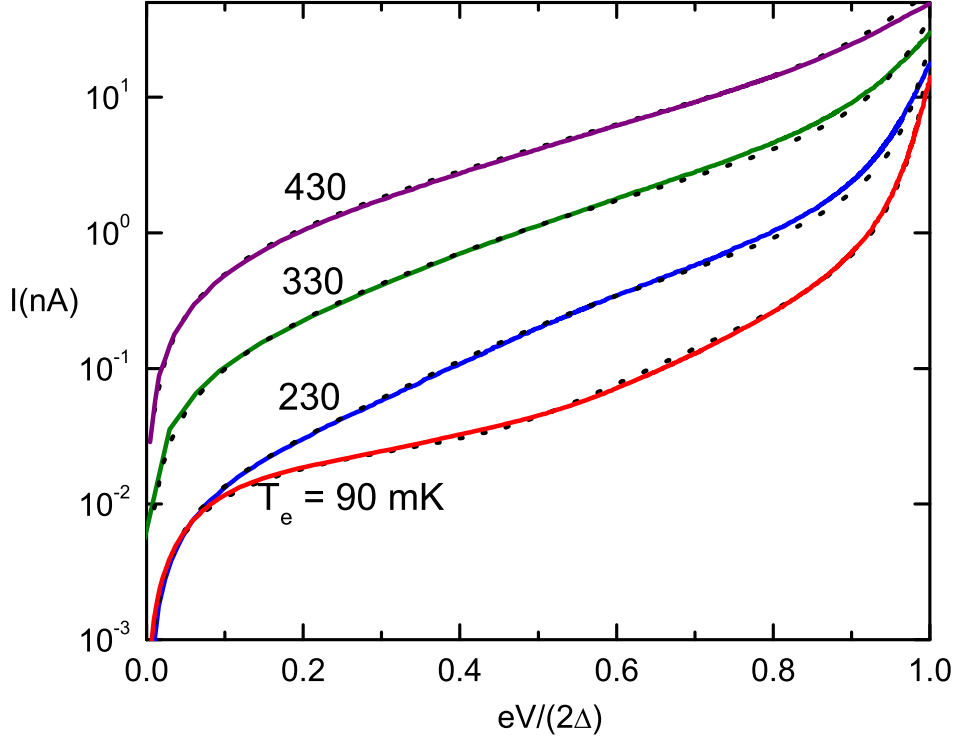


Figure 7.11: *Current voltage characteristic of the cooler junction at different cryostat temperatures together with the calculated best fit from the full thermal model, including the charge and heat contributions due to the Andreev current.*

gap where single quasiparticle based cooling dominates. As the bath temperature increases the Andreev current induced-dissipation become less effective and for $T_{bath} = 230$ mK the cooling always prevails over induced heat.

The above analysis clearly demonstrates the dissipation due to the phase-coherent Andreev current [34]. Although the Andreev reflection is a higher order tunneling process, its heat contribution is dominant at very low temperature and low bias. A naive explanation for this is the following: The efficiency of the electronic cooling is of the order of T_e/Δ , which is about 5% at a 100 mK electron temperature. In comparison to the Joule effect of the Andreev current is fully efficient (100%). This explains why although the Andreev charge current is small to the quasiparticle current at the optimum bias its heat contribution still has a significant effect. It shows that to achieve a minimum temperature of below 10 mK, the transparency of the cooler junction has to be further decreased.

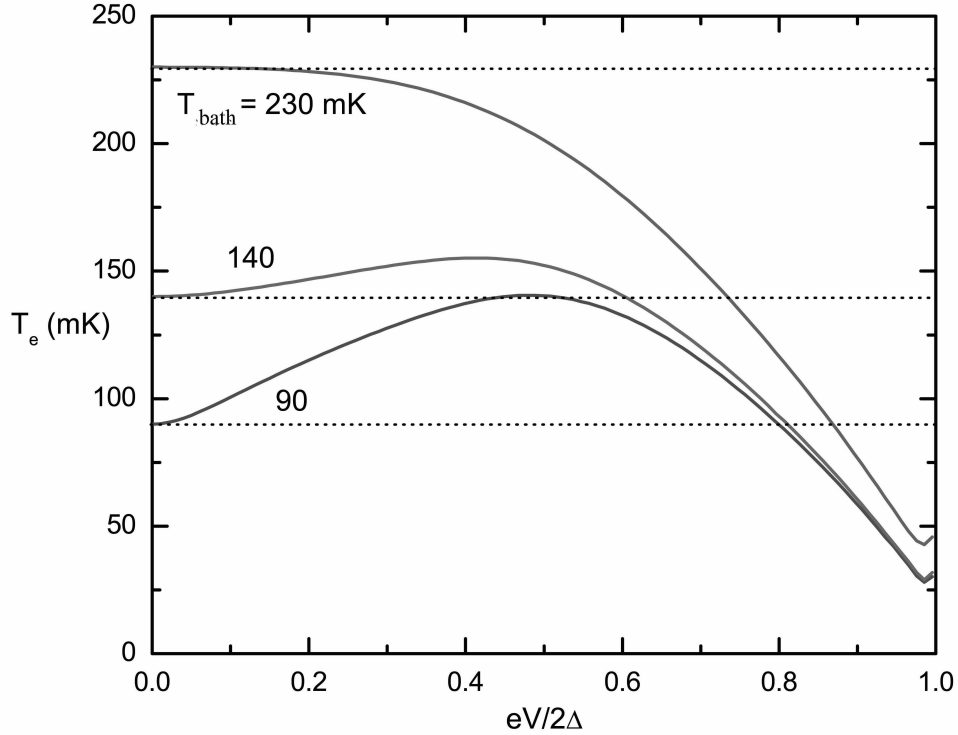


Figure 7.12: *Dependence of the calculated electronic temperature with the voltage for a series of cryostat temperatures: 90, 140 and 230 mK. The parameters are obtained from the fit to experiment.*

7.6 Conclusion

We observed a peak in the differential conductance at low bias in the probe junction and the cooler junctions. The precise investigation on the current-voltage characteristic of the probe junction led us to the conclusion that this enhancement is due to the phase-coherent Andreev current.

We have also devised a quantitative analysis on the current-voltage characteristic of the cooler junction. The thermal model includes the heat contribution of the Andreev current. We demonstrated the importance of the induced dissipation due to the phase-coherent Andreev current. The phase-coherent Andreev current induced dissipation is universal to the S-I-N-I-S junction and dominates the cooling power at very low temperature.

The above conclusion poses a challenge to diminish extra non-linear induced dissipation by the phase-coherent Andreev current in the central N island.

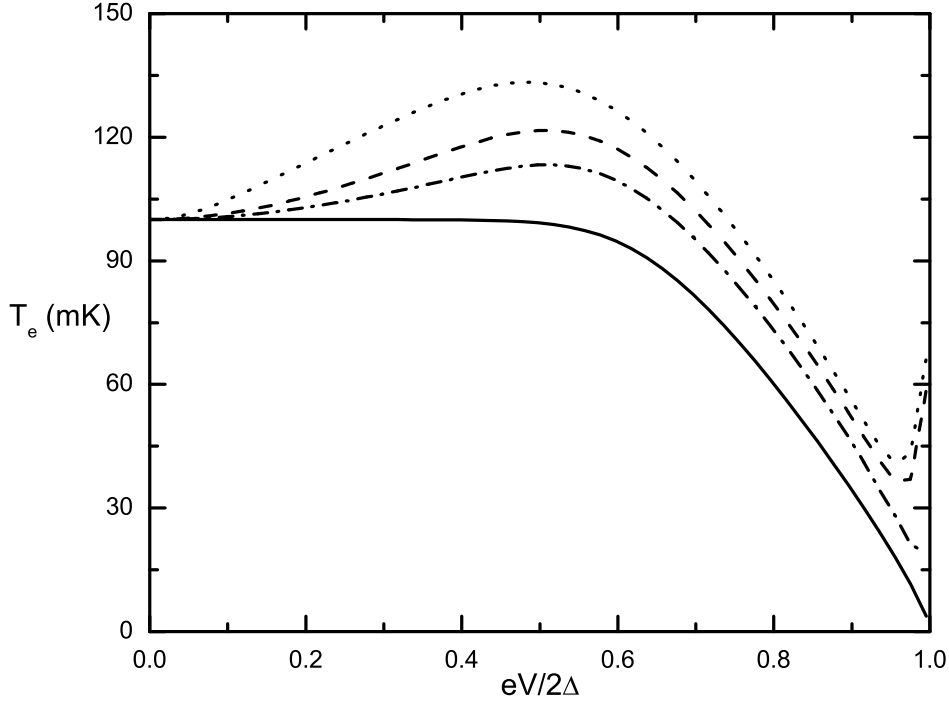


Figure 7.13: *Calculated electronic temperature as a function of bias at a 100 mK bath temperature for different dephasing length. Complete, dotted dash, dash and dotted line correspond to $L_\Phi = 0, 0.01, 0.1$ and $1 \mu\text{m}$ respectively. Parameters same as in Fig. 7.7.*

7.6.1 Taper coherence

The phase-coherent Andreev current induces a non linear dissipation in the device. As discussed in chapter 3, the subgap Andreev current is strongly enhanced due to coherent scattering of electrons by impurity. The coherent propagation of two-electrons in the electrode is limited by decoherence effect. The electron-electron interactions naturally induce decoherence and the cooperon propagation is cut by the phase-coherence length (L_Φ).

Fig. 7.13 shows the simulated electronic temperature as a function of bias for different dephasing length at 100 mK bath temperature. The complete line shows the solution for an ideal N-metal with no coherence ($L_\Phi = 0$), as seen there in no Andreev current dissipation. With increasing L_Φ , the phase-coherent Andreev current contribution to the charge current as well as to the thermal dissipation increases. For instance, the AuPd is a better choice as a N metal in coolers as it has a much shorter phase-coherence length than Copper [65].

7.6.2 The ultimate cooling device

For a fixed L_Φ , what are the right parameters needed to optimize the cooling power of the S-I-N-I-S based coolers?

The induced dissipation due to the Andreev current depends strongly on the transparency. It scales as the square of the normal state conductance (G_N). In comparison, the quasiparticle cooling P_{cool} is linear with conductance. The net power out of the N-metal is given by: $P_{net} = P_{cool} - P_A$. The cooling power P_{cool} across the N-I-S is given by :

$$P_{cool} = \frac{1}{e^2 R_N} \int_{-\infty}^{\infty} dE (E - eV) N_S(E) [f_N(E - eV) - f_S(E)] = \frac{1}{R_N} F_{cool}. \quad (7.6)$$

with F_{cool} being the integrant of the cooling power.

The Andreev current induced dissipation in the N island is given by:

$$P_A = I_A \cdot V = \frac{1}{R_N^2} F_A \quad (7.7)$$

with F_A being the integrant of the Andreev heat.

Therefore, the optimum normal-state resistance for which net cooling of electron is maximum ($\frac{dP_{net}}{dR} = 0$) is given by:

$$R_{N,optimum} = 2 \frac{F_A}{F_{cool}}. \quad (7.8)$$

As T increases, the sub-gap transfer of the quasiparticle increases, thus $R_{N,optimum}$ decreases. At the optimum bias, the Andreev current is insignificant in comparison to the single quasiparticle tunneling. Fig. 7.14 shows the normal state resistance at the optimum bias, $V_{optimum} \approx 2\Delta - 0.26T$, as a function of the bath temperature.

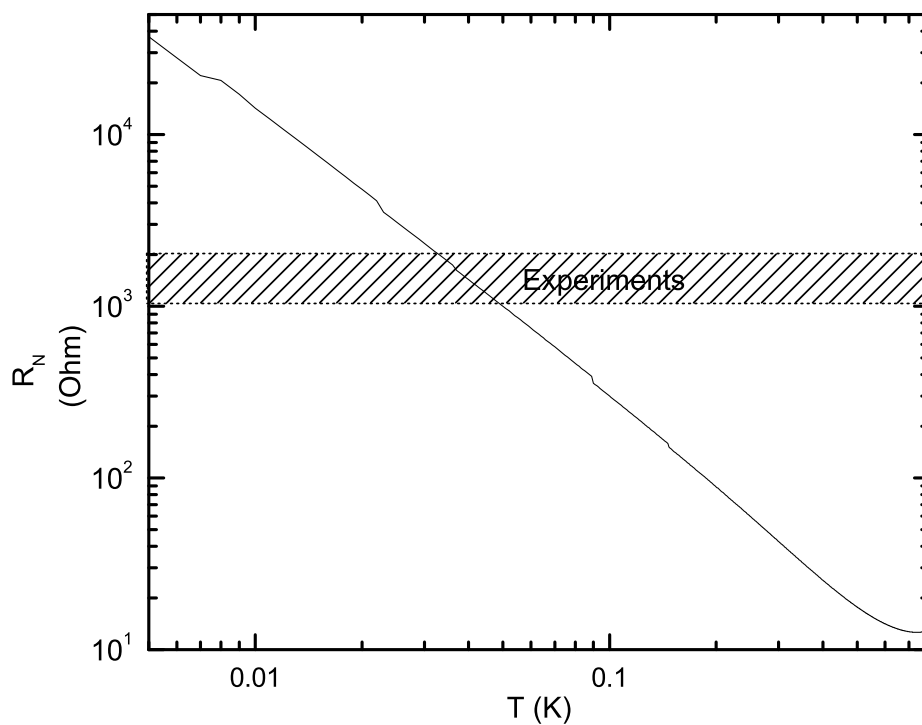


Figure 7.14: *Optimum normal state resistance at optimum bias voltage $V \approx \Delta/e$ as a function of bath temperature of the cryostat.*

Chapter 8

Quasiparticle diffusion based heating in S-I-N-I-S coolers

8.1 Introduction

In a S-I-N-I-S cooler, the extraction of hot quasiparticles from the central normal metal (N) to the two superconductors (S) leads to the cooling of N - metal electrons. It is widely assumed that for a sub-gap bias injection the superconductor remains at the bath temperature [43, 63]. This assumption is further strengthened due to the presence of N - metal trap junctions on the side of the superconductor electrode. The N-metal traps help the injected quasiparticles in the superconductor to relax faster, thus maintaining the bath temperature in the superconductor [66, 67].

For a sub-gap bias, the hot quasiparticles are injected in the superconductor at the gap edge (Δ) and thus have a zero group velocity ($dE/dk \sim 0$). It leads to an accumulation of hot quasiparticles close to the junction area of the cooler. The accumulated quasiparticles in the superconductor at the junction edge inhibit the optimum performance of the cooling device due to two main mechanisms: quasiparticle backscattering due to increase in the population of hot quasiparticle near the junction edge and re-absorption of the 2Δ phonons in the normal metal strips.

In this chapter, we shall attempt to understand the phenomenon involving the hot quasiparticles diffusion near the junction area along the superconducting Al strip. A phenomenological model based on the recombination and pair breaking mechanism in the superconductor is discussed. The transfer of 2Δ phonons to the substrate is included in the formalism. The model also includes the escape of the quasiparticles in the normal metal strip acting as a trap. Eventually, a quantitative comparison between the experiments and the model is done along with its implication on the coolers behavior.

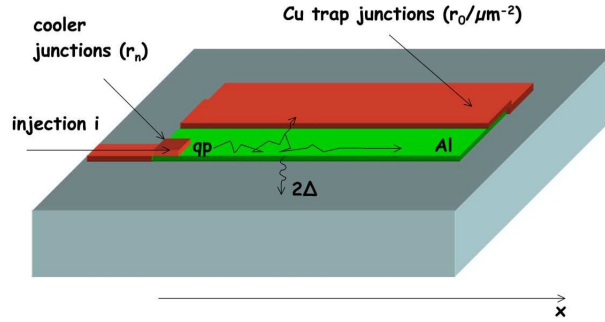


Figure 8.1: Cooler sample and the schematic of the system considered.

8.2 Quasiparticle diffusion along the superconducting strip

8.2.1 Introduction

As discussed in chapter 6, the understanding of the electron cooling from our thermal model is little (see Fig. 6.6) at the gap bias voltage [43]. Electrons cool down to around 100 mK at an optimum bias, which is significantly greater than the expected 70 mK electronic temperature. In our simplified thermal model, we assumed that the superconducting electrode is always at thermal-equilibrium to the bath temperature of the cryostat. However, the current driven in the device creates an injection of non-equilibrium quasiparticles near the gap energy [68]. The insufficient relaxation of non-equilibrium quasiparticles perturbs the cooling of the central N island.

Fig. 8.1 shows the schematic which is at par with our sample on the S-I-N-I-S cooler. For simplicity we consider only one side of the cooler. The superconductor is Al and the normal metal is Cu. We take into account the following physical processes:

- Diffusion of quasiparticles along the Al strip;
- Recombination and pair breaking processes;
- 2Δ phonons transfer to the substrate;
- Escape of the quasiparticles to the normal metal traps

The excess quasiparticles injected by the cooler junction into the superconducting electrode will diffuse out of the injection region. We shall consider the 1D diffusion of the quasiparticles in the Al electrode of infinite length along with the trap N metal. The trap junction is assumed to remain at the bath temperature of the cryostat and overlap completely the superconducting electrode.

8.2.2 Phenomenological model

Recombination of non-equilibrium quasiparticles in the superconducting electrode has been studied both theoretically [69, 70, 71] and experimentally [72, 66, 73]. Rothwarf and

Taylor [69] gave a phenomenological model involving both the recombination of the hot quasiparticles and emission of the 2Δ phonons in the superconductor.

Based on Rothwarf and Taylor model, we have added two extra contributions: the diffusion of the quasiparticle along the superconducting strip and quasiparticle absorption by the trap junction. We obtain:

$$\begin{aligned} \left(\frac{d}{dt} - D_{qp}\frac{d^2}{dx^2}\right)N_{qp} &= -RN_{qp}^2 + bN_{2\Delta} + I_e - \frac{N_{qp} - N_{qp0}}{\tau_0} \\ \frac{d}{dt}N_{2\Delta} &= \frac{R}{2}N_{qp}^2 - \frac{b}{2}N_{2\Delta} - \frac{N_{2\Delta} - N_{2\Delta0}}{\tau_\gamma}, \end{aligned} \quad (8.1)$$

where D_{qp} is the quasiparticle diffusion coefficient, R is the recombination coefficient, b is the absorption rate of 2Δ phonons and I_e is the injection current. The diffusion coefficient constant for quasiparticles (D_{qp}) differs from that of normal metal since quasiparticles in superconductor have zero group velocity at the gap energy [74]. The injection term I_e is a $\delta(x)$ function localized at $x = 0$, proportional to the cooler electrical current.

The two relaxation terms on the right of each equation describe respectively the rate of quasiparticles escaping to the N-metal trap τ_0^{-1} and the rate τ_γ^{-1} of 2Δ phonon escape to the substrate. Both the substrate and the trap N metal are assumed to remain at the temperature of the cryostat.

N_{qp} is the density of quasiparticles and $N_{2\Delta}$ is the density of the phonons with energy greater than 2Δ . We assume that excess quasiparticles have energy about Δ and recombination phonons have an energy close to 2Δ . The low energy phonons ($\leq \Delta$) are ignored since a BCS superconductor is transparent for those phonons [75, 76]. There is no gradient term for the phonon equation since the 2Δ phonon absorption rate (term b , which will be replaced by $2/\tau_B$) is very high. We ignore the charge imbalance effects since both electron-like and hole-like branches contribute additively to the current and energy. Charge imbalance is noticeable only at bias voltage larger than the gap [68, 77], which is irrelevant for the cooler operation.

The equilibrium quasiparticle (N_{qp0}) density at low temperature $T = T_0$ is given by :

$$N_{qpT} = N(E_F)\Delta \sqrt{\frac{\pi kT}{2\Delta}} \exp\left[-\frac{\Delta}{kT}\right]. \quad (8.2)$$

where Δ is the superconducting energy gap and $N_N(E_F)$ is the electron density of states at the Fermi energy. The number of quasiparticles decreases exponentially with the temperature. For instance in Al, there are only 10 quasiparticles per cubic micron at $T = 300$ mK.

The coefficient b is the absorption rate of 2Δ phonons. The time scale of the phonon breaking process (τ_B) does not vary much with the temperature. Theoretical predictions for various materials can be found in Ref. [71]. For Al the (τ_B) is predicted to be around 1.8×10^{-10} s.

The coefficient R is the recombination coefficient. For a pair of quasiparticles at the gap edge, the expression for the recombination constant is [73]:

$$R = \left(\frac{2\Delta}{k_B T_c} \right)^3 \frac{1}{2\Delta N_N(E_F) \tau_{el-ph}}. \quad (8.3)$$

where Δ and T_c are the superconducting energy gap and the critical temperature respectively and τ_{el-ph} is the time scale of the electron-phonon interaction. The value of τ_{el-ph} is material-dependent and the predicted value is in Ref. [71]. Various experiments have given the value of τ_{el-ph} for Al to be around 100 ns [78].

Eq. 8.1 is a system of coupled non-linear equations for the diffusion of quasiparticle (N_{qp}) and the density of 2Δ phonons N_Δ in the superconducting strip.

Here we do a comparison with our S-I-N-I-S cooler experiment. The injection current density at an optimum bias is typically 10^3 A/m², corresponding to the injection rate of 10^{19} /s.m². For the typical Al strip thickness of 40 nm, the density of the injected carrier is about 10^{28} /m³.s. For Al, the theoretically calculated lifetime is of the order of 10^{-7} s [71]. Therefore, the steady state density of the injected quasiparticles is of the order of 10^{21} /m³ which is much larger than the equilibrium number of exponential decaying quasiparticles (N_T) at low temperature. For $T \ll T_c$, the steady state density of the injected quasiparticles in the superconductor can be much larger than the thermally generated quasiparticles density.

If one eliminates the phonon density and assumes steady state conditions, Eq. 8.1 reduces to a damped diffusion equation for the quasiparticle density. As shown below, the differential equation can be solved analytically in the general non-linear case.

8.2.3 Connection to experimental parameters

We first discuss how the phenomenological parameters introduced in Eq. 8.1 can be related to the experiments. For no injection, all temperatures are equal to the bath temperature T_0 .

The intrinsic recombination time is $\tau_R^{-1} = 2RN_{qp0}$ where R is the recombination coefficient. τ_R diverges as $\exp \Delta/kT_0$ at low temperature. It is discussed in detail and tabulated in Ref. [71]. If the escape time exceeds the pair breaking time, then the effective quasiparticle recombination time (τ_{eff}) is renormalized and is given by:

$$\tau_{eff} = \tau_R \left(1 + \frac{\tau_\gamma}{\tau_B} \right). \quad (8.4)$$

The phonon breaking time $\tau_B = 2/b$ is weakly dependent on the temperature and again has been discussed in detail Ref. [71].

The decay rate of the quasiparticle density in the S - strip involves both τ_{eff} and τ_0 . We now introduce the relevant diffusion length λ and the corresponding time ratio α as:

$$\lambda^{-2} = \left(\frac{1}{D_{qp}\tau_{eff}} + \frac{1}{D_{qp}\tau_0} \right).$$

$$\alpha = 1 + \frac{\tau_{eff}}{\tau_0}. \quad (8.5)$$

We also introduce a zero-dimensional injection parameter I_{inj} defined as the density of the quasiparticles injected in the diffusion volume λA (A being the cross-section of the superconducting strip) during the diffusion time λ^2/D_{qp} :

$$I_{inj} = \frac{i\lambda}{D_{qp}N_{qp0}eA}, \quad (8.6)$$

with i being the electrical current in the cooler junction. It is worth-noticing that we do not need the cooler junction area since it is included in electrical current i through the junction conductance.

An explicit expression for the rate τ_0^{-1} can be written as a function of the characteristic conductance of the trap junction. Considering that τ_0^{-1} is a volume decay rate, it involves the thickness d_{Al} of the S strip and is proportional to the specific resistance R_{NN} (for unit area) and also to the density of states at Fermi level. The expression of τ_0 can be written as:

$$\tau_0 = eR_{NN}N(E_F)d_{Al}, \quad (8.7)$$

where R_{NN} is the specific resistance of the junction in between the trap and the superconductor and d_{Al} is the thickness of S strip.

The phonon escape time for the 2Δ phonon to the substrate can be written as [61]:

$$\tau_\gamma \approx \frac{2d_{Al}}{\eta c_{ph}}. \quad (8.8)$$

For our typical cooler sample with $R_{NN} = 5.62 \times \mu \Omega/\text{cm}^2$ and $d_{Al} = 40 \text{ nm}$, this gives $\tau_0 = 0.19 \mu\text{s}$. The diffusion constant of our Al films is $D = 30 \text{ cm}^2/\text{s}$. This corresponds to the trapping length of $\lambda_0 = \sqrt{D\tau_0} \approx 20 \mu\text{m}$. The phonon escape time, $\tau_\gamma \approx \frac{2d_{Al}}{\eta c_{ph}} \approx 8.10^{-11} \text{ s}$. The effective recombination time for the quasiparticle as defined in Eq. 8.4 is $\tau_{eff} \approx 1.5\tau_R$.

8.2.4 Exact solution

The diffusion non-linear equation (Eq. 8.1) has a complete analytic solution, which depends on the experimentally obtained parameters. The general solution of the quasiparticle density profile has a simple form:

$$\boxed{\begin{aligned} N_{qp}(x) &= N_{qp0}[1 + z(x)] \\ z(x) &= 1 + \frac{6[1 + \frac{\tau_{eff}}{\tau_0}]}{\cosh[\frac{x+x_0}{\lambda}] - 1} \\ I_{inj} &= z(0)\sqrt{1 + \frac{z(0)}{3\alpha}} \end{aligned}} \quad (8.9)$$

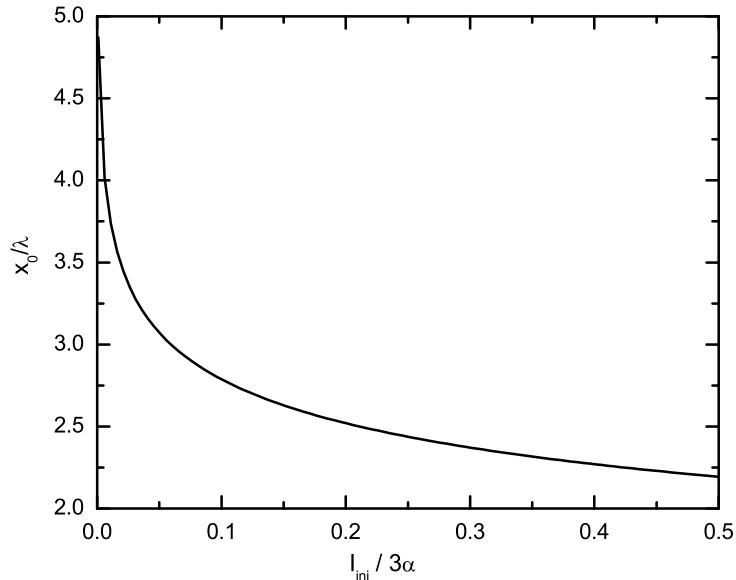


Figure 8.2: x_0 as a function of injection current.

The injection term appears in the last line of Eq. 8.9. It fixes the integration constant x_0 . This constant goes to 0 at high injection and diverges at low injection. The constant $z(x)$ at $x = 0$ is important since it provides the steady state local increase of the density of quasiparticles in the S strip of the S-I-N-I-S cooler junction. It depends linearly on the injection current at low injection ($I_{inj} \ll \alpha$) as $z(0) \approx I_{inj}$ and as a power law at strong injection $z(0) \approx 3\alpha I_{inj}^{1/3}$. The diffusion coefficient of the quasiparticle (Eq. 8.1) combines the two mechanisms of absorption/recombination and trapping of quasiparticles.

In the following, we will plot the result obtained in this section and will use the parameters obtained from the experiment.

8.3 Parasitic power in the cooler

As discussed in Ref. [79], one can identify two mechanisms which re-inject the undesirable power back to the central cooling metal in the S-I-N-I-S junction.

8.3.1 Quasiparticle back-tunneling

Due to the increase in the temperature of the superconductor [70], some heat is sent back to the central Cu electrode across the tunnel junction.

We know that the particle heat current through the tunnel barrier from the normal

metal to the superconductor is controlled by twice the Fermi function at the superconductor temperature T_s . We find it preferable to use the combination of the distribution functions $2f_s(E) - f_n(E - eV) - f_n(E + eV)$ at $V = 0$ to ensure the zero power injection at $T_s = T_n$. By integrating over the energy, one can obtain the parasitic power due to backtunneling of quasiparticles from S to N:

$$P_{bt} = \frac{2\Delta}{e^2 R_N} \frac{N_{qp}(0) - N_{qpn}}{N(E_F)}, \quad (8.10)$$

where N_{qp0} is the injected quasiparticle density at junction edge $x = 0$ (see Eq. 8.9), N_{qpn} is the equilibrium quasiparticle density in the normal metal at temperature T_N , R_N is the normal state conductance of the single junction in the cooler junction. It is worth noticing that the above equation is equivalent to the cooling power (P_{cool}) of the N-I-S junction for $T_S (\neq T_N)$ at zero bias. As already discussed, Eq. 8.2 can be inverted to obtain the effective superconductor temperature (T_S) at $x = 0$. Since the trap and cooler junction have the same thickness of the barrier, we can use Eq. 8.7 in the above expression Eq. 8.10. Thus we get:

$$P_{bt} = 2\Delta Ad_{Al} \frac{N_{qp}(0) - N_{qpn}}{\tau_0}. \quad (8.11)$$

8.3.2 Reabsorption of 2Δ phonons

The second mechanism is the reabsorption of 2Δ phonons in the Cu electrode. The 2Δ phonon density can be obtained from the steady state phonon density in the Al electrode. The transfer of 2Δ phonon depends on absorption coefficient between the Cu electrode and the Al electrode. In our cooler sample, the Al electrode at the cooler junction is in between the substrate (bottom) and the Cu electrode (top). Therefore one has to compare the corresponding phonon transfer rate τ_{CuAl} (for the Cu-Al interface) and the τ_Γ (for the Al-interface). Since the interface area in between the Cu-Al (cooler junction area) is smaller in comparison to the Al-substrate contact, we can assume that the junction does not disturb the phonon density in the Al electrode. The steady state phonon density at $x = 0$ can be obtained from Eq. 8.1 as:

$$N_{2\Delta} - N_{2\Delta 0} = \left(\frac{1}{\tau_B} + \frac{1}{\tau_\gamma} \right) \frac{R(N_{qp}^2 - N_{qp0}^2)}{2}. \quad (8.12)$$

The 2Δ phonon density in the Cu is given by:

$$N_{Cu} = \frac{N_{2\Delta} \tau_N}{\tau_N + \tau_{CuAl}} \quad (8.13)$$

where τ_N is the phonon lifetime due to the electron-phonon interaction on the Cu. Therefore, the power dissipated by the phonons in the Cu is:

$$P_{2\Delta} = 2\Delta \cdot A \cdot d_{Cu} \frac{N_{Cu}}{\tau_N}. \quad (8.14)$$

Since $\tau_N \gg \tau_{CuAl}$ and for Al $\tau_B > \tau_\gamma$. Thus we get:

$$P_{2\Delta} \approx 2\Delta \cdot A \cdot d_{Cu} \frac{\tau_\gamma}{\tau_N} \frac{R(N_{qp}^2 - N_{qp0}^2)}{2}. \quad (8.15)$$

8.3.3 Comparison of parasitic back-tunneling and phonon reabsorption power

At high bath temperature and low injection current, $P_{2\Delta}$ can be expanded near N_{qp0} . The ratio between the 2Δ reabsorption power to the backtunneling power can be written as:

$$\frac{P_{2\Delta}}{P_{bt}} \approx \frac{d_{Cu}\tau_0}{\tau_R} \cdot \frac{\tau_N}{2d_{Al}\tau_\gamma}. \quad (8.16)$$

Eq. 8.16 involves the film thickness of the two films (N and S) and the ratio of the two rates: τ_0/τ_R compares the quasiparticle escape rate to the trap junction with the recombination time in Al. For our sample, this ratio vanishes at very low temperature and reaches unity at 0.3 K. The second, τ_γ/τ_N compares the time escape for the phonon to the substrate and the phonon reabsorption to the Cu island in the cooler junction. The estimated 2Δ phonon mean free path in Cu [80] gives $\tau_N \approx 0.5$ ns compared to the time escape of phonon to the substrate for our sample $\tau_\gamma = \eta \cdot d_{Al}/c \approx 60$ ps. Thus we find that $P_{2\Delta}$ is 1/5 of P_{bt} at 0.3 K and becomes much smaller at low temperatures.

At lower temperature the thermal population vanishes. The 2Δ phonons are produced only by the recombination of the injected quasiparticles. The $P_{2\Delta}$ is quadratic in current (I) and is independent of the bath temperature of system. For our typical cooler sample it goes as: $P_{2\Delta}/I^2 \approx 8.5$ fW/ μA^2 .

In conclusion, our experiments at low temperature the main parasitic power is the heat carried by back tunneling of quasiparticles (P_{bt}) from superconductor to normal metal.

8.4 Preliminary experimental connection with theory

In this section, we will compare the previous experiment (chapter 6) on cooling of electrons in the S-I-N-I-S junction and in particular at the gap edge. We will re-examine the considered thermal model and take into account the quasiparticle induced heating in the superconductor.

In the considered thermal model (chapter 6), we assumed that the superconductor is well thermalized to the bath temperature. However this assumption is countered in the previous section. It is argued that quasiparticle injection in the S strip leads to two additional parasitic heat sources: back-tunneling of hot quasiparticles in the normal metal (P_{bt}) and the reabsorption of 2Δ phonon power ($P_{2\Delta}$) into the normal metal. Since the

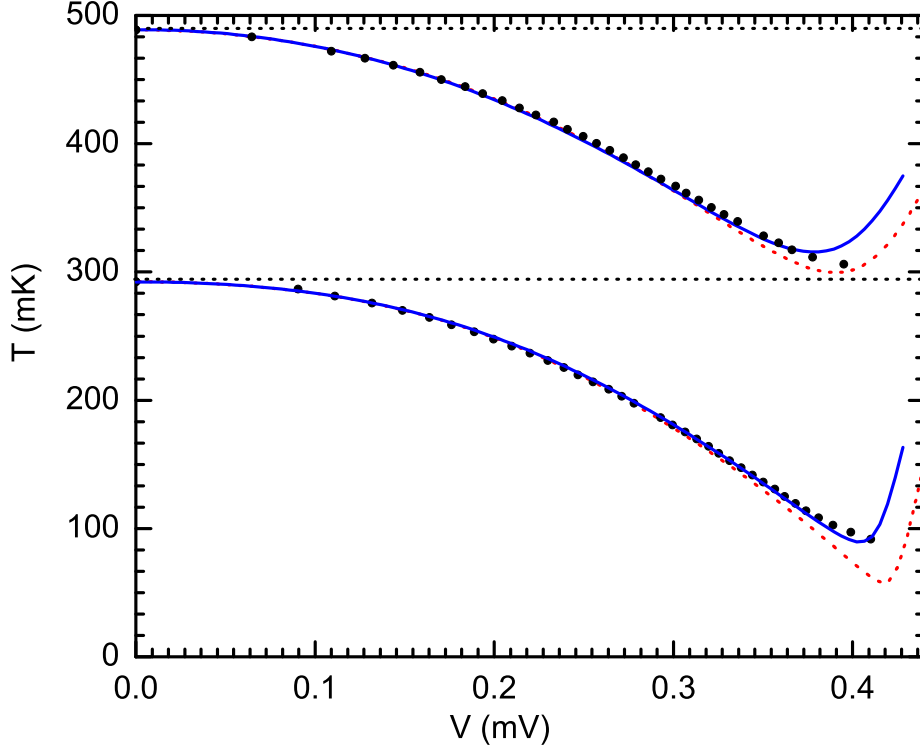


Figure 8.3: *Sample B experiment. Electronic temperature as a function of bias. Fit parameters: For complete blue line $\Sigma = 2 \text{ nW} \cdot \mu\text{m}^{-3} \cdot \text{K}^{-5}$, $K \cdot A = 54 \text{ pW} \cdot \text{K}^{-4}$ and $f_{\text{expt}} = 0.01 \text{ pW/nA}$ and for red dotted line same as in Fig. 6.6.*

coolers are operated mostly in the sub-Kelvin temperature, we have $P_{2\Delta} \ll P_{bt}$. The quasiparticle density at the cooler junction edge ($x = 0$) can be obtained from Eq. 8.9. For our sample parameters (sample B), the injected current given by Eq. 8.6 reads as $I_{inj} \approx i(\mu\text{A})$ and is independent of temperature. The back-tunneling power given by Eq. 8.11 for the cooler device reads as:

$$P_{bt} = 2 \frac{2\Delta \lambda d_{Al}}{eD_{qp}\tau_0} \cdot i = f_{theory} \cdot i. \quad (8.17)$$

$$f_{theory} = 2 \frac{2\Delta \lambda d_{Al}}{eD_{qp}\tau_0}. \quad (8.18)$$

where a factor 2 is due a pair of a N-I-S junction in series in the cooler. It is worth noticing that the parasitic power due to backtunneling of quasiparticles (Eq. 8.17) is proportional to the current in the device.

In the following, we will include the parasitic power given by Eq. 8.17 in the thermal model described previously. In addition we will do the quantitative comparison with sample B, whose results has been discussed in Fig. 6.6 of chapter 6. Fig. 8.3 shows the comparison of the experiment (black dots) with the calculated curve (red and blue lines). The red line is obtained from the thermal model with no parasitic backtunneling power and blue line considers the P_{bt} into the thermal model. Clearly the red line has a poor agreement with the experiment at the gap edge and the blue one fits well. The only additional fit parameter used in the blue curve is $f_{expt} = 0.01$ pW/nA.

For our sample: $d_{Al} = 40$ nm, $D = 30$ cm²/s and $\Delta = 0.214$ meV. The calculation of τ_0 given by Eq. 8.7 assumes the complete coverage of Al by the trap (Cu) junction. However as seen in SEM picture of sample Fig. 5.5, the Cu on trap overlaps the superconductor only around one-half of its width which correspond to $\tau_0 = 0.19 \times 2 \mu s = 0.38 \mu s$ and $\lambda = \sqrt{D\tau_0} = 34 \mu m$. It corresponds to a prefactor in P_{bt} given by Eq. 8.18 as: $f_{theory} = 0.001$ pW/nA.

The theoretical pre-factor f_{theory} is less only by a factor ten in comparison to f_{expt} . This could be due to underestimation of f_{theory} where we used the diffusion coefficient in Al which is measured at 4 K (normal state) using the free electron approximation. On the contrary, the injected quasiparticle at the gap edge has a small or zero group velocity i.e. $dE/dk \rightarrow 0$, which leads to the suppression of the D_{qp} in comparison to the one obtained from the free electron model [74]. Narayanamurti et. al. found that D_{qp} decreases by a factor of 2.5 at 0.5 K and more at lower temperature.

The qualitative agreement at gap bias voltage demonstrates that the parasitic power due to the back-tunneling of quasiparticles brings heat into the N metal. The parasitic heat deposition due to back-tunneling is maximum at the gap edge.

Chapter 9

Conclusions and perspectives

In this thesis, we have realized the solid - state cooling of electrons in a Copper strip using superconductor - normal metal - superconductor tunnel junctions. In the following, I will summarize the main conclusions of this work and give a few perspectives.

Inherent thermometer: One of the challenges in this field is to fabricate a nano cooling device with less external perturbations on the central N island and more efficient designs. In our first work (chapter 5), we found a "nouvelle vague" to extract the electrons temperature without any external thermometer. The electronic temperature is extracted directly from the experimental current - voltage characteristic of the cooler (S-I-N-I-S) junction. The cross-over between the experiment and the theoretical isotherms enables us to extract the temperature of electrons in the N metal. This sample design with no external thermometer attains a smaller contact surface area of the N-metal with the substrate, in comparison with the design having external thermometer, which can contribute to a better cooling of the island.

Phonon cooling: To understand the cooling mechanism in the central N island, we devised a quantitative thermal model (chapter 6). It takes into account the electron - phonon coupling in the N metal and the Kapitza coupling between the phonons of the central N metal and the substrate. With this model, we have achieved a thorough description of the charge and the heat currents. We have shown that in an intermediate regime ($T_{bath} > 300$ mK) the effective temperature in the N-metal phonons goes well below the temperature of the cryostat. The model gives an indirect determination of the phonon temperature as a function of cooler bias.

Andreev induced dissipation: The thermal transport in the normal metal - superconductor junctions at very low temperature has always been adventurous. At low temperature and bias, the charge transfer across the normal metal and superconductor is governed by the higher order tunneling process, namely Andreev current. On precise investigation on the thermalized N-I-S (probe junction in our sample) junction, we confirmed the presence of phase-coherent Andreev current in our samples (chapter 7). The charge contribution due to Andreev current subjugates the quasiparticle current of the junction at very low temperature. Similar precise investigation on the cooler junction concluded the induced additional non linear dissipation due to the Andreev current. The Andreev current dissipates

fully its Joule heat in the N metal (chapter 3). This new induced heating regime is quantitatively analyzed in our thermal model, which provides a full description of the electronic temperature evolution with the cooler bias voltage. At low temperature, the quasiparticle based cooling is little efficient while the induced heat dissipation due to Andreev current is fully efficient. It leads to a significant increase of the electronic temperature over a large bias range. Only for the bias close to the optimum bias the quasiparticle based cooling becomes predominant.

Superconductor heating: In a S-I-N-I-S cooler, the driving current injects hot quasiparticle in the superconductor electrodes. The heat contribution of the quasiparticles is generally ignored. However, we presented a model which describes precisely the non-equilibrium processes occurring in the S electrode. It shows that the injection in the superconductor degrades the cooler performance via two main mechanisms: quasiparticle back-tunneling (i.e. increase in the superconductor temperature) and re-absorption of the 2Δ phonons in the normal metal strip. In our model, we have considered the diffusion of quasiparticles in the superconductor and also the trap junction. The solution of the non-linear equation for quasiparticle diffusion is obtained exactly in space as a function of the injection current. The influence of the material and geometric parameters such as diffusion coefficient, tunnel conductance, trapping junction, has been included in the study and will therefore be useful to improve the minimum temperature of the future devices.

Perspectives:

Inherent thermometer method to extract the electronic temperature without any external thermometer can be useful for sand-witched tri-layer geometry. In such designs mounting an external thermometer aggravates the problems in designing the coolers. For instance in Clark et. al. [8] experiment to cool down an external object (NTD sensor), there was no thermometer to measure the temperature of electrons.

Phonons in thin film at low temperature are mostly assumed to thermalize at the cryostat temperature. As discussed in chapter 6, the N-metal phonon distribution depends on film thickness and acoustic mismatch between the N-metal phonons and the substrate. Our experiments on phonon cooling needs more investigation, especially in a high temperature regime ($T > 350$ mK). Now we have devised a phonon thermometer (see 9.1), which is supposed to measure the phonon distribution in the normal metal. The sample consists of two layers of Cu separated by a thick insulator (~ 100 nm Si). Each Cu layer has a S-I-N-I-S thermometer on top of it. Hot electron effects on bottom Cu is measured by the electron thermometer [56, 44, 57, 45]. The thermometer on the 2nd Cu (top) is expected to give a measure of an effective Kapitza resistance between the two Cu layers. This experiment is expected to measure an independent hot electron and phonon effects, which can be manipulated or optimized depending on the geometry of the sample. In S-I-N-I-S junction, cooling of phonons depends on Kapitza resistance between the normal metal and the substrate. The Kapitza resistance can be modified by etching out the N-metal from the substrate.

The induced heat dissipation due to Andreev current is one of the main limitation factor in reaching the very cold electronic temperature. This heat dissipation needs more experimental and theoretical investigation. The basic picture of Andreev current tells us

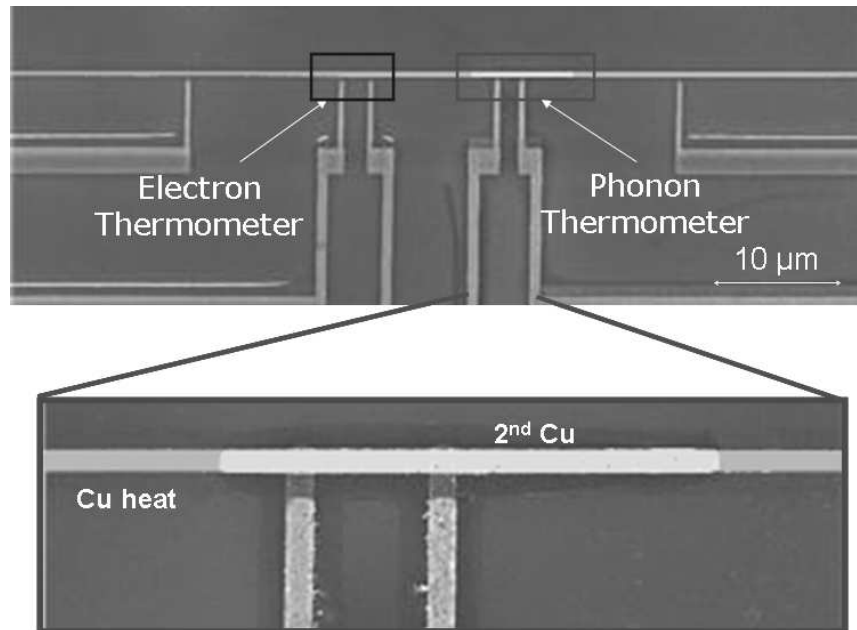


Figure 9.1: *Scanning electron micrograph of a sample having independent electron and phonon thermometer. The top view shows the complete device. The bottom view is the zoom showing the phonon thermometer.*

that it is dominant due to the constructive interference of the probability amplitude of two-electrons tunneling across the barrier. The phase-coherence is mainly cut-off by the natural coherence length (L_Φ). Therefore, an efficient cooler sample should be made from the normal metal with a small L_Φ , for example AuPd. Addition of magnetic impurities like iron could also diminish the coherence and consequently heat dissipation in the normal metal. Also, the transparency of most of the cooler junction made in this thesis were small $\approx 10^{-6}$ which diminished the cooling power of the device. Therefore by choosing a N-metal which has a small L_Φ and also by fabricating more transparent junction can be used for more practical application. More transparent tunnel barrier can be made from on epitaxial aluminium nitride barriers which is better than the aluminium oxide barrier for high critical current densities [81].

The quantitative thermal model for the quasiparticle diffusion in S strip is expected to check the efficiency of the traps. The parasitic power in the cold normal metal is linearly proportional to the injected tunnel current. We have done more experiments on the cooler junction with no traps. They need to be reproduced at lower temperature, lower power and with an optimized choice of geometry. The model shows the requirement of "heat exchangers" in the solid state refrigerators that take the hot quasiparticle out of the superconductor. One way to install heat exchangers in the micro coolers is via cascading.

This thesis could be useful for choosing the right materials to reach a temperature of below 10 mK (illusiv so far!). For instance, half-metallic ferromagnetic materials such as CrO_2 [82] could be an important candidate for the coolers. For practical application, it

is also required to cool from liquid Helium temperature to milli-Kelvin temperature. It can be achieved by cascade arrangement with several stages of coolers. Coolers based on S-I-N-I-S junction can also be useful to cool down a nano-mechanical based devices by cooling down their relevant mechanical modes below the quantum of resonator energy.

Appendix A

Normal state tunnel conductance

The tunnel Hamiltonian for a N1-I-N2 junction can be written as :

$$\widehat{H}_T = \Sigma[t_{k,p}\widehat{a}_{k,\sigma}^\dagger\widehat{b}_{p,\sigma} + t_{k,p}^*\widehat{b}_{p,\sigma}^\dagger\widehat{a}_{k,\sigma}],$$

with $t_{k,p}$ being the phenomenological matrix element associated with the transfer of charge across the barrier; the subscript k and p refers to left and right normal metal electrodes.

The total current across the junction is given by: $I_{N1-I-N2} = I_{N1\rightarrow N2} - I_{N2\rightarrow N1}$. The two currents are given by :

$$\begin{aligned} I_{N1\rightarrow N2} &= e \times \frac{2\pi}{\hbar} \times 2 \sum |t_{k,p}|^2 f(\xi_k)[1 - f(\xi_p)]\delta(\xi_k - \xi_p + 2eV) \\ I_{N2\rightarrow N1} &= e \times \frac{2\pi}{\hbar} \times 2 \sum |t_{k,p}|^2 f(\xi_p)[1 - f(\xi_k)]\delta(\xi_k - \xi_p + 2eV). \end{aligned} \quad (\text{A.1})$$

Real space representation of $t_{k,p}$: We will re-write the tunnel matrix element in the real space coordinates. The tunnel matrix element $t_{k,p}$ can be written in terms of the complete set of wave functions for the disordered electrodes

$$t_{k,p} = \int d^3r d^3r' \phi_p(r) \phi_k^*(r') t(r, r'). \quad (\text{A.2})$$

As a result, the current from N1 to N2 can be obtained by substituting eq. A.2 to eq. A.1. We get

$$\begin{aligned} I_{N1\rightarrow N2} &= \frac{4\pi e}{\hbar} \sum f(\xi_k)[1 - f(\xi_p)]\delta(\xi_k - \xi_p + 2eV) \int d^3r_1 d^3r_2 d^3r_3 d^3r_4 \\ &\quad \phi_p(r_1) \phi_k^*(r_2) \phi_p(r_3) \phi_k^*(r_4) \tilde{t}(r_1, r_2) \tilde{t}^*(r_3, r_4). \end{aligned}$$

We assume that tunneling predominantly occurs between the neighboring points at the barrier, thus $t(r, r') = t(r)\delta(r - r')\delta(z - z_b)$, where z_b is a point on the barrier and also

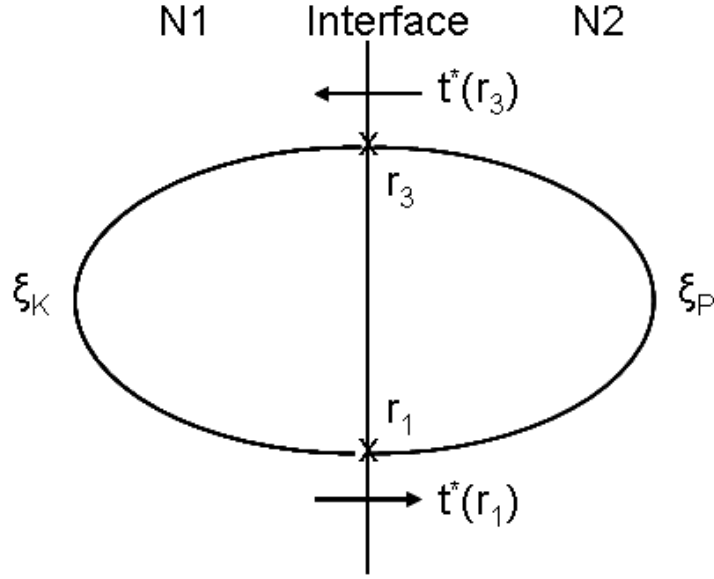


Figure A.1: Diagram corresponding to Eq. A.4. Electrons tunnel at point r_1 and r_3 (marked by crosses) across the N1-I-N2 junction with energy ξ_k and ξ_p . The solid line shows the propagation of the electron in the electrode.

inserting the identity $1 = \int d\xi d\xi' \delta(\xi - \xi_k) \delta(\xi' - \xi_p)$. We get

$$I_{N1 \rightarrow N2} = \frac{4\pi e}{\hbar} \int d\xi d\xi' f(\xi) [1 - f(\xi')] \delta(\xi - \xi' + eV) \int d^3 r_1 d^3 r_3 \tilde{t}(r_1) \tilde{t}^*(r_3) \left[\sum_k \phi_k^*(r_1) \phi_k^*(r_3) \delta(\xi - \xi_k) \right] \left[\sum_p \phi_p(r_1) \phi_p(r_3) \delta(\xi - \xi_k - eV) \right] \quad (\text{A.3})$$

We define a propagator from r_2 to r_1 by $K_\xi(r_1, r_3) = \sum \delta(\xi - \xi_k) \phi_k(r_1) \phi_k(r_3)$. With these definitions we can rewrite the Eq A.3 as:

$$I_{N1 \rightarrow N2} = \frac{4\pi e}{\hbar} \int d\xi d\xi' f(\xi) [1 - f(\xi + eV)] \int d^3 r_1 d^3 r_3 \tilde{t}(r_1) \tilde{t}^*(r_3) K_\xi(r_1, r_3) K_{\xi+eV}(r_3, r_1) \quad (\text{A.4})$$

The physical meaning of Eq. A.4 can be understood easily from Fig. A.1. The cross at r_i for $i = 1, 3$ corresponds to tunneling with amplitude $t(r_i)$. The lines correspond to propagation on the disordered electrodes.

Further progress can be made by including the retarded (G_R) and advanced (G_A) Green's function which can be defined as :

$$G_{A,R}(k, w) = \frac{1}{w - \xi \mp i/2\tau},$$

as well as the propagator function

$$K_\xi(k, w) = (1/2\pi i) [G_A - G_R].$$

Propagator in real space representation can be written as:

$$K_\xi(r, r') = \frac{1}{2\pi i} \sum_k e^{i\vec{k} \cdot (\vec{r} - \vec{r}')} \left[\frac{1}{\xi - \xi_k - i/2\tau} - \frac{1}{\xi - \xi_k + i/2\tau} \right],$$

such that

$$K_\xi(r, r') = \frac{V}{(2\pi)^3} \frac{1}{(r - r')} \int_0^\infty dk [e^{-ik(r-r')} - e^{ik(r-r')}] \left[\frac{1}{\xi - \xi_k - i/2\tau} - \frac{1}{\xi - \xi_k + i/2\tau} \right] \quad (\text{A.5})$$

Since the integration contributes near the Fermi-energy, $k \rightarrow k_F + \kappa$ and we integrate κ from $(-\infty, \infty)$. Also, $\xi_k \approx \frac{\hbar^2}{m} k_F \kappa$ and $k_F + \kappa \approx k_F$, we get

$$K_\xi(r, r') = \nu(0) \exp \frac{-(r-r')}{2i} \frac{\sin[k_F(r - r')]}{k_F(r - r')} \quad (\text{A.6})$$

ν_0 being the density of states per spin.

We can calculate the total impurity-averaged current across N1-I-N2 junction. We use the above definition of propagator Eq. A.6 and substitute in Eq. A.4 to find

$$I_{N1 \rightarrow N2} = \frac{4\pi e \nu_0^2}{\hbar} \int d\xi f(\xi) [1 - f(\xi + eV)] \int d^2 r_1 d^2 r_3 \tilde{t}(r_1) \tilde{t}^*(r_3) \exp \frac{-(r_1 - r_3)}{i} \left[\frac{\sin[k_F(r_1 - r_3)]}{k_F(r_1 - r_3)} \right]^2 \quad (\text{A.7})$$

Now, we assume that the tunneling amplitude is same at all points on the barrier, $t(r_1) = t(r_3) = t(r)$. We use the Jacobian transformation such that $r = r_1 - r_3$; $2R = r_1 + r_3$, then

$$I_{N1 \rightarrow N2} = \frac{4\pi e \nu(0)^2 S}{\hbar k_F^2} F_1(k_F l) \int d^2 R [t(R)]^2 \int d\xi f(\xi) [1 - f(\xi + eV)], \quad (\text{A.8})$$

with $F_1(k_F l)$ being the dimensionless integral given by:

$$F_1(k_F l) = \int d^2 u e^{-\frac{u}{k_F l}} \left[\frac{\sin[u]}{u} \right]^2. \quad (\text{A.9})$$

In accordance with the above, the total impurity-averaged current across the N1-I-N2 junction, $I_{N1-I-N2} = I_{N1 \rightarrow N2} - I_{N2 \rightarrow N1}$ can be written as:

$$I_{N1-I-N2} = \left[\frac{4\pi e^2 \nu(0)^2 S F_1(k_F l)}{\hbar k_F^2} \int d^2 R [t(R)]^2 \right] V = G_{NN} V, \quad (\text{A.10})$$

where G_{NN} is the normal state conductance.

Here the "local barrier tunnel conductance" is given by:

$$g_{NN}(R) = \frac{4\pi e^2 \nu(0)^2 S F_1(k_F l)}{\hbar k_F^2} [t(R)]^2 \quad (\text{A.11})$$

Appendix B

Phase-coherent Andreev current in a N-I-S junction

The tunnel Hamiltonian can be written as:

$$\hat{H}_T = \Sigma[t_{k,p}\hat{a}_{k,\sigma}^\dagger\hat{b}_{p,\sigma} + t_{k,p}^*\hat{b}_{p,\sigma}^\dagger\hat{a}_{k,\sigma}], \quad (\text{B.1})$$

with $t_{k,p}$ being the phenomenological matrix element associated to the transfer of charge across the barrier; the subscript k and p refers to normal metal and superconductor electrode.

An excitation in the superconductor is given by :

$$\hat{b}_{p\uparrow} = u_p\gamma_{p\uparrow} + v_p\gamma_{-p\downarrow}^\dagger, \quad (\text{B.2})$$

$$\hat{b}_{p\downarrow} = u_p\gamma_{p\downarrow} - v_p\gamma_{-p\uparrow}^\dagger, \quad (\text{B.3})$$

u_p and v_p being the BCS coherence factors. The interest of this representation is that it enables us to express the tunnel Hamiltonian in terms of the Bogoliubov quasiparticle operator γ and γ^\dagger . There exists two possibilities for the tunneling of two electrons across the junction. In the first case, the tunnel transfer of two electrons from N to S and vice-versa.

Case 1: From N \rightarrow S:

Let us consider the initial state is given by $|k_1, k_2; \downarrow p\rangle$. Applying second order perturbation theory in \hat{H}_T , we have

$$\hat{H}_T\hat{G}_o\hat{H}_T = [t_{k_1,p_1}^*\hat{b}_{p_1\downarrow}^\dagger\hat{a}_{k_1\downarrow}]\hat{G}_o[t_{k_2,p_2}^*\hat{b}_{p_2\uparrow}^\dagger\hat{a}_{k_2\uparrow}].$$

Using Eq. B.2 and Eq. B.3, we get

$$\hat{H}_T\hat{G}_o\hat{H}_T = t_{k_1,p_1}^*t_{k_2,p_2}^*[(u_{p_1}\gamma_{p_1\downarrow}^\dagger - v_{p_1}\gamma_{-p_1\uparrow})\hat{a}_{k_1\downarrow}]\hat{G}_o[(u_{p_2}\gamma_{p_2\uparrow}^\dagger + v_{p_2}\gamma_{-p_2\downarrow})\hat{a}_{k_2\uparrow}].$$

Clearly in the above equations, there are two allowed processes :

1. As a first possibility, an electron with quantum number k_2 and spin up is annihilated, thereby creating an excitation as a quasiparticle in S. This leads to a virtual state with energy $-E_{p2} - \xi_{k2}$.

2. As a second possibility, an electron with quantum number k_2 and spin up is created, due to annihilation, which leads to no excitation as quasiparticle in S. This leads to a virtual state with energy $E_{p2} - \xi_{k2}$.

We assume that the superconductor is at thermal equilibrium and the temperature is low enough so that there are no excitations as quasiparticles in S. Therefore, only the second possibility contributes to tunneling of two electrons.

$$\widehat{H}_T \widehat{G}_o \widehat{H}_T = -t_{k1,-p}^* t_{k2,p}^* [v_p a_{k1\downarrow}^\dagger \left[\frac{1}{E_p - \xi_{k2}} \right] u_p a_{k2\uparrow}^\dagger]. \quad (\text{B.4})$$

Now we can do the same as above with the initial state in N as $k1 \downarrow$ and the final state as $k2 \uparrow$.

$$\widehat{H}_T \widehat{G}_o \widehat{H}_T = t_{k2,p}^* t_{k1,p}^* [v_p a_{k2\uparrow}^\dagger \left[\frac{1}{E_p - \xi_{k1}} \right] u_p a_{k1\downarrow}^\dagger]. \quad (\text{B.5})$$

The total Hamiltonian is then given by the sum of eq. B.4 and eq. B.5 and sum over all intermediate state 'p'. In eq. B.4 we substitute $p = -p$, thus we get

$$\widehat{H}_T \widehat{G}_o \widehat{H}_T = t_{k2,p}^* t_{k1,p}^* [v_p a_{k2\uparrow}^\dagger \left[\frac{1}{E_p - \xi_{k1}} + \frac{1}{E_p - \xi_{k2}} \right] u_p a_{k1\downarrow}^\dagger].$$

Hence, the total amplitude of the transfer of 2e electron from N to S is given by:

$$A_{N \rightarrow S} = \sum_p t_{k2,p}^* t_{k1,p}^* [v_p a_{k2\uparrow}^\dagger \left[\frac{1}{E_p - \xi_{k1}} + \frac{1}{E_p - \xi_{k2}} \right] u_p a_{k1\downarrow}^\dagger], \quad (\text{B.6})$$

with ξ_k and ς being the electron energies for the normal metal and the superconductor respectively; and quasiparticle energies: $E_p = \sqrt{\Delta^2 + \varsigma^2}$. The denominators in Eq. B.6 reflects the fact that a virtual state is formed when the first electron enters the quasiparticle as a quasiparticle. This is coupled with an another quasiparticle to form a Cooper pair. The total rate of tunneling from N to S is then given by the golden rule :

$$\Gamma_{N \rightarrow S} = 2 \times \frac{2\pi}{\hbar} \times \sum_{k1,k2} [|A_{N \rightarrow S}|^2 f(\xi_{k1}) f(\xi_{k2}) \delta(\xi_{k1} + \xi_{k2} + 2eV)], \quad (\text{B.7})$$

where the factor 2 is due to the other possibility of the spin and the $f(\xi_k)$ is the Fermi functions in the normal metal.

Case 2 : From S \rightarrow N

A similar expression can be written from the transfer of two electrons from S \rightarrow N :

$$\Gamma_{S \rightarrow N} = 2 \times \frac{2\pi}{\hbar} \times \sum_{k1,k2} [|A_{S \rightarrow N}|^2 [1 - f(\xi_{k1})][1 - f(\xi_{k2})] \delta(\xi_{k1} + \xi_{k2} + 2eV)].$$

$A_{S \rightarrow N}$ is the amplitude for the transfer of two electrons from S to N is given by :

$$A_{S \rightarrow N} = \sum_p t_{k_2, p} t_{k_1, p} [v_p a_{k_2 \uparrow}^\dagger [\frac{1}{E_p + \xi_{k_1}} + \frac{1}{E_p + \xi_{k_2}}] u_p a_{k_1 \downarrow}^\dagger].$$

The total 2e charge transfer current across N-I-S junction is given by: $\Gamma_{NIS} = 2e \times [A_{N \rightarrow S} - A_{S \rightarrow N}]$.

Real-space representation of $t_{k, p}$: We will re-write the tunnel matrix element in the real-space coordinates. The tunnel matrix element $t_{k, p}$ can be written in terms of the complete set of wave functions for the disordered electrodes

$$t_{k, p} = \int d^3 r d^3 r' \phi_p(r) \phi_k^*(r') t(r, r') \quad (\text{B.8})$$

As a result the amplitude $A_{N \rightarrow S}$ for the transfer of two electrons from N to S can be written as :

$$A_{N \rightarrow S}(k_1 \downarrow, k_2 \uparrow) = \int d^3 r_1 d^3 r_2 d^3 r_1' d^3 r_2' t^*(r_1, r_1') t^*(r_2, r_2') \phi_{k_1}(r_1) \phi_{k_2}(r_2) F^*(r_1, r_2), \quad (\text{B.9})$$

where we define the quantity

$$F(r_1, r_2) = \sum_p [v_p [\frac{1}{\xi_{k_1} + eV - E_p} + \frac{1}{\xi_{k_2} + eV - E_p}] u_p \phi_p(r_1) \phi_p(r_2)] \quad (\text{B.10})$$

The above equation describes the propagation of an electron between r_1 and r_2 in the superconductor with the tunneling amplitude $t_{r, r'}$ on either side of the barrier. We assume that the tunneling predominantly occurs between the neighboring points at the barrier as given by $t(r, r') = t(r) \delta(r - r') \delta(z - z_b)$, where z_b is a point on the barrier. We obtain

$$A_{N \rightarrow S}(k_1 \downarrow, k_2 \uparrow) = \int_{\text{barrier}} d^2 r_1 d^2 r_2 t^*(r_1) t^*(r_2) \phi_{k_1}(r_1) \phi_{k_2}(r_2) F^*(r_1, r_2)$$

leading to

$$|A_{N \rightarrow S}(k_1 \downarrow, k_2 \uparrow)|^2 = \int_{\text{barrier}} d^2 r_1 d^2 r_2 d^2 r_3 d^2 r_4 t^*(r_1) t^*(r_2) t(r_3) t(r_4) \phi_{k_1}(r_1) \phi_{k_2}(r_2) \phi_{k_1}(r_3) \phi_{k_2}(r_4) F^*(r_1, r_2) F(r_3, r_4). \quad (\text{B.11})$$

Thus Eq. B.7 can be written as:

$$\Gamma_{N \rightarrow S} = \frac{4\pi}{\hbar} \int d\xi d\xi' d\varsigma d\varsigma' f(\xi) f(\xi') \delta(\xi + \xi' + 2eV) [v_\varsigma u_\varsigma v_{\varsigma'} u_{\varsigma'}] [\frac{1}{\xi + eV - E_p} + \frac{1}{\xi' + eV - E_p}] \Xi_{N \rightarrow S}(\varsigma, \varsigma'; \xi, \xi'). \quad (\text{B.12})$$

where we define the quantity

$$\Xi_{N \rightarrow S}(\varsigma, \varsigma'; \xi, \xi') = \int_{\text{barrier}} d^2 r_1 d^2 r_2 d^2 r_3 d^2 r_4 t^*(r_1) t^*(r_2) t(r_3) t(r_4) K_{\xi}(r_2, r_4) K_{\xi'}(r_1, r_3) K_{\varsigma}(r_1, r_2) K_{\varsigma'}(r_3, r_4). \quad (\text{B.13})$$

As discussed in chapter 3, the charge transfer across the N-S junction can be driven by three possibilities.

Possibility(a) depicts the situation when $r_1 \approx r_2$ and $r_3 \approx r_4$, contribution arising due to the interference in the normal metal.

Possibility(b) depicts the contrary situation i.e. $r_1 \approx r_3$ and $r_2 \approx r_4$ where the interference is in the superconducting electrode.

Possibility(c) interference both in normal metal and superconducting electrode is taken into account. The total contribution to the phase coherent Andreev current is the sum of the interference in the normal metal and the superconductor.

Case 1 : *Interference in the normal electrode*

For the interference in the normal metal electrode, we have

$$\Xi_{N \rightarrow S}(\varsigma, \varsigma'; \xi, \xi') = \int_{\text{barrier}} d^2 r_1 d^2 r_2 d^2 r_3 d^2 r_4 t^*(r_1) t^*(r_2) t(r_3) t(r_4) \langle K_{\xi}(r_2, r_4) K_{\xi'}(r_1, r_3) \rangle \langle K_{\varsigma}(r_1, r_2) \rangle \langle K_{\varsigma'}(r_3, r_4) \rangle. \quad (\text{B.14})$$

The average over impurities of the product of the propagator can be written as :

$$\langle K_{\xi}(\vec{r}_1, \vec{r}_2) K_{\xi'}(\vec{r}_2, \vec{r}_1) \rangle = \frac{\nu_0}{2\pi} [P_{\xi-\xi'}(r_1 - r_2) - P_{\xi'-\xi}(\vec{r}_1 - \vec{r}_2)], \quad (\text{B.15})$$

where $P_{\xi'-\xi}(\vec{r}_1 - \vec{r}_2)$ is the Cooperon. The Cooperon is a long-ranged space-dependent quantity with a characteristic length scale $|\vec{r}_1 - \vec{r}_2|$ is given by L_E , which satisfies the equation

$$-\hbar D \Delta P_{\epsilon}(\vec{r}_1 - \vec{r}_2) - i\epsilon P_{\epsilon}(\vec{r}_1 - \vec{r}_2) = \delta(\vec{r}_1 - \vec{r}_2) \quad (\text{B.16})$$

D being the diffusion coefficient.

We assume that the tunnel amplitude obeys $t(r_1) = t(r_2)$ and $t(r_3) = t(r_4)$ and we use the definition of propagator as:

$$K_{\xi}(r, r') = \nu(0) \exp\left[\frac{-(r-r')}{2l}\right] \frac{\sin[k_F(r-r')]}{k_F(r-r')}, \quad (\text{B.17})$$

ν_0 being the density of states per spin. On substituting Eq. B.17 in Eq. B.14, we get

$$\Xi_{N \rightarrow S}(\varsigma, \varsigma'; \xi, \xi') = \frac{\nu_0^3}{2\pi} \int_{\text{barrier}} d^2 r_1 d^2 r_2 d^2 r_3 d^2 r_4 t(r_1)^2 t(r_3)^2 [P_{\xi-\xi'}(r_1 - r_2) - P_{\xi'-\xi}(\vec{r}_1 - \vec{r}_2)] \exp\left[\frac{-(r_1 - r_2)}{2l}\right] \left[\frac{\sin[k_F(r_1 - r_2)]}{k_F(r_1 - r_2)}\right] \exp\left[\frac{-(r_3 - r_4)}{2l}\right] \left[\frac{\sin[k_F(r_3 - r_4)]}{k_F(r_3 - r_4)}\right]$$

We use the Jacobian transformation such that $r = r_1 - r_3$; $2R = r_1 + r_3$ and substituting above

$$\Xi_{N \rightarrow S}(\varsigma, \varsigma'; \xi, \xi') = \frac{\nu_0^3}{2\pi} \int d^2 R [t(R)]^4 \int d^2 r [P_{\xi-\xi'}(0) - P_{\xi'-\xi}(0)] \int d^2 r_2 d^2 r_4 \exp\left[\frac{-(r/2 + R - r_2)}{2l}\right] \left[\frac{\sin[k_F(r/2 + R - r_2)]}{k_F(r/2 + R - r_2)}\right] \exp\left[\frac{-(r/2 + R - r_4)}{2l}\right] \left[\frac{\sin[k_F(r/2 + R - r_4)]}{k_F(r/2 + R - r_4)}\right]$$

The total phase coherent Andreev current is given by $I_{N_{ave},NIS} = 2e(\Gamma_{N \rightarrow S} - \Gamma_{S \rightarrow N})$, due to the transfer of electrons in a N-I-S junction by taking into account the averaging over the disorder in the normal electrode.

$$I_{N_{ave},NIS} = \frac{8\pi e\nu_0^3}{2\pi\hbar} \frac{F_3(k_F l)}{k_F^4} \int d^2 R [t(R)]^4 \int d\xi d\varsigma d\varsigma' (f(\xi) - f(\xi + 2eV)) [v_\varsigma u_\varsigma] [v_{\varsigma'} u_{\varsigma'}] \left[\frac{1}{\xi + eV - E_p} + \frac{1}{\xi' + eV - E_p}\right] \int d^2(r) [P_{2\xi+2eV}(r) + P_{\xi-2eV}(r)] \quad (\text{B.18})$$

$F_3(k_F l)$ being the dimensionless integral defined as :

$$F_3(k_F l) = \int d^2 u d^2 v \frac{\sin[u]}{u} e^{\frac{-u}{2k_F l}} \frac{\sin[v]}{v} e^{\frac{-v}{2k_F l}} \quad (\text{B.19})$$

Case 2 : *Interference in the superconducting electrode*

For the interference in the superconducting electrode, we have

$$\Xi_{N \rightarrow S}(\varsigma, \varsigma'; \xi, \xi') = \int_{\text{barrier}} d^2 r_1 d^2 r_2 d^2 r_3 d^2 r_4 t^*(r_1) t^*(r_2) t(r_3) t(r_4) < K_\xi(r_2, r_4) > < K_{\xi'}(r_1, r_3) > < K_\varsigma(r_1, r_2) K_{\varsigma'}(r_3, r_4) >$$

As in case 1, a similar expression can be obtained for the total current, $I_{S_{ave},NIS}$ due to transfer of 2e electrons in a N-I-S junction by taking into account the averaging over the disorders in the superconducting electrode.

$$I_{S_{ave},NIS} = \frac{8\pi \nu_0^3}{2\pi\hbar} \frac{F_3(k_F l)}{k_F^4} \int d^2 R [t(R)]^4 \int d\xi d\varsigma d\varsigma' (f(\xi) - f(\xi + 2eV)) [v_\varsigma u_\varsigma] [v_{\varsigma'} u_{\varsigma'}] \left[\frac{1}{\xi + eV - E_p} + \frac{1}{\xi' + eV - E_p}\right] \int d^2(r) [P_{\varsigma-\varsigma'}(r) + P_{\varsigma-\varsigma'}(r)] \quad (\text{B.20})$$

The total phase coherent Andreev current through the N-I-S tunnel junction is the sum of Eq. B.18 and Eq. B.20.

Appendix C

Publications

- "Electron and Phonon Cooling in a Superconductor-Normal metal-Superconductor tunnel junction
Sukumar Rajauria, P. S. Luo, T. Fournier, F. W. J. Hekking, H. Courtois, and B. Pannetier,
Physical Review Letters **99**, 047004 (2007).
- "Spin-polarized tunneling with Au impurity layers"
M. S. Gabureac, K. J. Dempsey, N. A. Porter, C. H. Marrows, S. Rajauria, and H. Courtois
Journal of Applied Physics **103**, 07A915 (2008).
- "Andreev Current-Induced Dissipation in a Hybrid Superconducting Tunnel Junction"
Sukumar Rajauria, P. Gandit, T. Fournier, F. W. J. Hekking, B. Pannetier, and H. Courtois,
Physical Review Letters **100**, 207002 (2008).
- "Inherent thermometry in a hybrid superconducting tunnel junction"
H. Courtois, Sukumar Rajauria, P. Gandit, F. W. J. Hekking, and B. Pannetier,
Journal of Low Temperature Physics **153**, 325 (2008).
- "Competition between electronic cooling and Andreev dissipation in a superconducting micro-cooler"
Sukumar Rajauria, P. Gandit, T. Fournier, F. W. J. Hekking, B. Pannetier, and H. Courtois
Journal of Low Temperature Physics **154**, 211 (2009).

- "Quasiparticle diffusion based heating in S-I-N-I-S coolers"
Sukumar Rajauria and Bernard Pannetier,
submitted for publication.
- "Spin-valve effect of the spin accumulation resistance in a double Ferromagnet - Superconductor junction"
P. S. Luo, T. Crozes, B. Gilles, S. Rajauria, B. Pannetier, and H. Courtois
submitted for publication.

Bibliography

- [1] A. A. Penzias and R. W. Wilson. A measurement of excess antenna temperature at 4080 mc/s. *The Astrophysical Journal*, 142:419, Oct 1965.
- [2] Frank Pobell. *Matter and Methods at Low Temperatures*. Springer-Verlag, Germany (1996).
- [3] W. A. Little. Microminiature refrigeration. *Review of Scientific Instruments*, 55(5):661–680, 1984.
- [4] M. Nahum, T. M. Eiles, and John M. Martinis. Electronic microrefrigerator based on a normal-insulator-superconductor tunnel junction. *Applied Physics Letters*, 65(24):3123–3125, 1994.
- [5] M. M. Leivo, J. P. Pekola, and D.V. Averin. Efficient peltier refrigeration by a pair of normal metal/insulator/superconductor junctions. *Applied Physics Letters*, 68(14):1996–1998, 1996.
- [6] A. J. Manninen, M. M. Leivo, and J. P. Pekola. Refrigeration of a dielectric membrane by superconductor/insulator/normal-metal/insulator/superconductor tunneling. *Applied Physics Letters*, 70(14):1885–1887, 1997.
- [7] M. M. Leivo and J. P. Pekola. Thermal characteristics of silicon nitride membranes at sub-kelvin temperatures. *Applied Physics Letters*, 72(11):1305–1307, 1998.
- [8] A. M. Clark, N. A. Miller, A. Williams, S. T. Ruggiero, G. C. Hilton, L. R. Vale, J. A. Beall, K. D. Irwin, and J. N. Ullom. Cooling of bulk material by electron-tunneling refrigerators. *Applied Physics Letters*, 86(17):173508, 2005.
- [9] E. Favre-Nicolin and B. Pannetier. preliminary experiments. 2004.
- [10] P. A. Fisher, J. N. Ullom, and M. Nahum. High-power on-chip microrefrigerator based on a normal- metal/insulator/superconductor tunnel junction. *Applied Physics Letters*, 74(18):2705–2707, 1999.
- [11] J. P. Pekola, T. T. Heikkilä, A. M. Savin, J. T. Flyktman, F. Giazotto, and F. W. J. Hekking. Limitations in cooling electrons using normal-metal-superconductor tunnel junctions. *Phys. Rev. Lett.*, 92(5):056804, Feb 2004.

- [12] A. F. Andreev. *Zh. Eksp. Teor. Fiz.*, 46:1823, 1964.
- [13] D. Saint-James. *J. Phys. France*, 25:899–905, 1964.
- [14] G. E. Blonder, M. Tinkham, and T. M. Klapwijk. Transition from metallic to tunneling regimes in superconducting microconstrictions: Excess current, charge imbalance, and supercurrent conversion. *Phys. Rev. B*, 25(7):4515–4532, Apr 1982.
- [15] B. J. van Wees, P. de Vries, P. Magnée, and T. M. Klapwijk. Excess conductance of superconductor-semiconductor interfaces due to phase conjugation between electrons and holes. *Phys. Rev. Lett.*, 69(3):510–513, Jul 1992.
- [16] F. W. J. Hekking and Yu. V. Nazarov. Subgap conductivity of a superconductor–normal-metal tunnel interface. *Phys. Rev. B*, 49(10):6847–6852, Mar 1994.
- [17] A. Kastalsky, A. W. Kleinsasser, L. H. Greene, R. Bhat, F. P. Milliken, and J. P. Harbison. Observation of pair currents in superconductor-semiconductor contacts. *Phys. Rev. Lett.*, 67(21):3026–3029, Nov 1991.
- [18] H. Pothier, S. Guéron, D. Esteve, and M. H. Devoret. Flux-modulated Andreev current caused by electronic interference. *Phys. Rev. Lett.*, 73(18):2488–2491, Oct 1994.
- [19] Ivar Giaever. Electron tunneling and superconductivity. *Rev. Mod. Phys.*, 46(2):245–250, Apr 1974.
- [20] J. M. Rowell and D. C. Tsui. Hot electron temperature in InAs measured by tunneling. *Phys. Rev. B*, 14(6):2456–2463, Sep 1976.
- [21] M. H. Cohen, L. M. Falicov, and J. C. Phillips. Superconductive tunneling. *Phys. Rev. Lett.*, 8(8):316–318, Apr 1962.
- [22] L. Solymar. *Superconductive Tunneling, and Applications*. Wiley Intersciences, New York, 1972.
- [23] G. E. Blonder and M. Tinkham. Metallic to tunneling transition in Cu-Nb point contacts. *Phys. Rev. B*, 27(1):112–118, Jan 1983.
- [24] D. Quirion, C. Hoffmann, F. Lefloch, and M. Sanquer. Mesoscopic proximity effect in double-barrier superconductor/normal-metal junctions. *Phys. Rev. B*, 65(10):100508, Feb 2002.
- [25] A. Bardas and D. Averin. Peltier effect in normal-metal–superconductor microcontacts. *Phys. Rev. B*, 52(17):12873–12877, Nov 1995.
- [26] C.W.J. Beenakker. *Quantum Mesoscopic Phenomena and Mesoscopic Devices in Microelectronics*. edited by I.O. Kulik and R. Ellialtioglu, NATO Science Series C559 (Kluwer, Dordrecht, 2000): pp. 51–60.

- [27] T. M. Klapwijk. Proximity effect from an Andreev perspective. *Journal of Superconductivity: Incorporating Novel Magnetism*, 17(5):593–611, 2004.
- [28] Ph. Gandit, D. Mailly, H. Courtois, P. Charlat and B. Pannetier. The spectral conductance of a proximity superconductor and the reentrance effect. *Journal of Low temperature Physics*, 116:187–213, 1999.
- [29] Fei Zhou, B. Spivak, and A. Zyuzin. Coherence effects in a normal-metal–insulator–superconductor junction. *Phys. Rev. B*, 52(6):4467–4472, Aug 1995.
- [30] A. F. Volkov and A. V. Zaitsev. Phase-coherent conductance of a superconductor-normal-metal quantum interferometer. *Phys. Rev. B*, 53(14):9267–9276, Apr 1996.
- [31] H. A. Blom, A. Kadigrobov, A. M. Zagoskin, R. I. Shekhter, and M. Jonson. Dissipative electron transport through andreev interferometers. *Phys. Rev. B*, 57(16):9995, Apr 1998.
- [32] P. Charlat, H. Courtois, Ph. Gandit, D. Mailly, A. F. Volkov, and B. Pannetier. Reentrance of the metallic conductance in a mesoscopic proximity superconductor. *Phys. Rev. Lett.*, 77(24):4950–4953, Dec 1996.
- [33] B. L. Altshuler and A. G. Aronov. *Electron-electron interactions in disordered systems*. edited by A. L. Efros and M. Pollak, (North-Holland, Amsterdam), 1985.
- [34] Sukumar Rajauria, P. Gandit, T. Fournier, F. W. J. Hekking, B. Pannetier, and H. Courtois. Andreev current-induced dissipation in a hybrid superconducting tunnel junction. *Physical Review Letters*, 100(20):207002, 2008.
- [35] B. Pannetier and H. Courtois. Andreev reflection and proximity effect. *Journal of Low temperature Physics*, 118(5-6):599–615, 2000.
- [36] H. Courtois, M. Meschke, J. T. Peltonen, and J. P. Pekola. Origin of hysteresis in a proximity josephson junction. *Physical Review Letters*, 101(6):067002, 2008.
- [37] P. Gandit. Phd thesis. *University Joseph Fourier*, (1982).
- [38] D. R. Schmidt, C. S. Yung, and A. N. Cleland. Nanoscale radio-frequency thermometry. *Applied Physics Letters*, 83(5):1002–1004, 2003.
- [39] Z. Jiang, H. Lim, V. Chandrasekhar, and J. Eom. Local thermometry technique based on proximity-coupled superconductor/normal-metal/superconductor devices. *Applied Physics Letters*, 83(11):2190–2192, 2003.
- [40] M. Meschke, J. P. Pekola, F. Gay, R. E. Rapp, and H. Godfrin. Electron thermalization in metallic islands probed by coulomb blockade thermometry. *Journal of Low temperature Physics*, 134(5):1119, 2004.

- [41] D. W. Denlinger, E. N. Abarra, Kimberly Allen, P. W. Rooney, M. T. Messer, S. K. Watson, and F. Hellman. Thin film microcalorimeter for heat capacity measurements from 1.5 to 800 k. *Review of Scientific Instruments*, 65(4):946–959, 1994.
- [42] O. Bourgeois, S. E. Skipetrov, F. Ong, and J. Chaussy. Attojoule calorimetry of mesoscopic superconducting loops. *Physical Review Letters*, 94(5):057007, 2005.
- [43] Sukumar Rajauria, P. S. Luo, T. Fournier, F. W. J. Hekking, H. Courtois, and B. Pannetier. Electron and phonon cooling in a superconductor–normal-metal–superconductor tunnel junction. *Physical Review Letters*, 99(4):047004, 2007.
- [44] M. L. Roukes, M. R. Freeman, R. S. Germain, R. C. Richardson, and M. B. Ketchen. Hot electrons and energy transport in metals at millikelvin temperatures. *Phys. Rev. Lett.*, 55(4):422–425, Jul 1985.
- [45] F. C. Wellstood, C. Urbina, and John Clarke. Hot-electron effects in metals. *Phys. Rev. B*, 49(9):5942–5955, Mar 1994.
- [46] D. R. Heslinga and T. M. Klapwijk. Enhancement of superconductivity far above the critical temperature in double-barrier tunnel junctions. *Phys. Rev. B*, 47(9):5157–5164, Mar 1993.
- [47] N. W. Ashcroft and N. D. Mermin. *Solid State Physics. Saunders College, Philadelphia*, 1976.
- [48] Gerd Bergmann. Weak localization in thin films a time-of-flight experiment with conduction electrons. *Physics Reports*, 107(1), 1983.
- [49] B. Pannetier, J. Chaussy, and R. Rammal. Quantum interferences in superconducting and normal metal arrays. *Physica Scripta*, T13:245–251, 1986.
- [50] F. Pierre, A. B. Gougam, A. Anthore, H. Pothier, D. Esteve, and Norman O. Birge. Dephasing of electrons in mesoscopic metal wires. *Phys. Rev. B*, 68(8):085413, Aug 2003.
- [51] J. P. Pekola, A. J. Manninen, M. M. Leivo, K. Arutyunova, J. K. Suoknuutia, T. I. Suppula, and B. Collaudin. Microrefrigeration by quasiparticle tunnelling in NIS and SIS junctions. *Physica B*, 280:485–490, 2000.
- [52] R. C. Dynes, J. P. Garno, G. B. Hertel, and T. P. Orlando. Tunneling study of superconductivity near the metal-insulator transition. *Phys. Rev. Lett.*, 53(25):2437–2440, Dec 1984.
- [53] J. M. Ziman. *Principles of the Theory of Solids. Cambridge, UK: Cambridge University Press, November 1979.*

- [54] E. T. Swartz and R. O. Pohl. Thermal boundary resistance. *Rev. Mod. Phys.*, 61(3):605–668, Jul 1989.
- [55] A. C. Anderson. *The Kapitza thermal boundary resistance between two solids. in Nonequilibrium Superconductivity, Phonons, and Kapitza Boundaries, edited by K. E. Gray (Plenum, New York), p. 1.*
- [56] Makoto R. Arai. A fundamental noise limit for biased resistors at low temperatures. *Applied Physics Letters*, 42(10):906–908, 1983.
- [57] Frederick C. Wellstood, Cristian Urbina, and John Clarke. Hot-electron limitation to the sensitivity of the dc superconducting quantum interference device. *Applied Physics Letters*, 54(25):2599–2601, 1989.
- [58] F. W. J. Hekking, A.O.Niskanen, and J. P. Pekola. Electron-phonon coupling and longitudinal mechanical-mode cooling in a metallic nanowire. *Physical Review B*, 77(3):033401, 2008.
- [59] S.-X. Qu, A. N. Cleland, and M. R. Geller. Hot electrons in low-dimensional phonon systems. *Physical Review B (Condensed Matter and Materials Physics)*, 72(22):224301, 2005.
- [60] Douglas L. Martin. Specific heat of copper, silver, and gold below 30°k. *Phys. Rev. B*, 8(12):5357–5360, Dec 1973.
- [61] N. Perrin and H. Budd. Photon generation by joule heating in metal films. *Phys. Rev. Lett.*, 28(26):1701–1703, Jun 1972.
- [62] L. J. Taskinen J. T. Karvonen and I. J. Maasilta. Influence of temperature gradients on tunnel junction thermometry below 1 k cooling and electron phonon coupling. *Journal of Low temperature Physics*, 146(1-2):213–226, 2007.
- [63] Francesco Giazotto, Tero T. Heikkilä, Arttu Luukanen, Alexander M. Savin, and Jukka P. Pekola. Opportunities for mesoscopies in thermometry and refrigeration: Physics and applications. *Reviews of Modern Physics*, 78(1):217, 2006.
- [64] F. W. J. Hekking. *Nanophysics : coherence and transport (Les Houches session LXXXI). edited by H. Bouchiat, Y. Gefen, S. Gueron, G. Montambaux and J. Dalibard, (Elsevier, New York, 2004): pp. 381-426.*
- [65] T.C. Lee J.J. Lin and S.W. Wang. Low-temperature electron dephasing time in aupd revisited. *Physica E: Low-dimensional Systems and Nanostructures*, 40(1):25–31, Oct 2007.
- [66] N. E. Booth. Quasiparticle trapping and the quasiparticle multiplier. *Applied Physics Letters*, 50(5):293–295, 1987.

- [67] J. P. Pekola, D. V. Anghel, T. I. Suppala, J. K. Suoknuuti, A. J. Manninen, and M. Manninen. Trapping of quasiparticles of a nonequilibrium superconductor. *Applied Physics Letters*, 76(19):2782–2784, 2000.
- [68] M. Tinkham. Tunneling generation, relaxation, and tunneling detection of hole-electron imbalance in superconductors. *Phys. Rev. B*, 6(5):1747–1756, Sep 1972.
- [69] Allen Rothwarf and B. N. Taylor. Measurement of recombination lifetimes in superconductors. *Phys. Rev. Lett.*, 19(1):27–30, Jul 1967.
- [70] W. H. Parker. Modified heating theory of nonequilibrium superconductors. *Phys. Rev. B*, 12(9):3667–3672, Nov 1975.
- [71] S. B. Kaplan, C. C. Chi, D. N. Langenberg, J. J. Chang, S. Jafarey, and D. J. Scalapino. Quasiparticle and phonon lifetimes in superconductors. *Phys. Rev. B*, 14(11):4854–4873, Dec 1976.
- [72] P. Hu, R. C. Dynes, and V. Narayanamurti. Dynamics of quasiparticles in superconductors. *Phys. Rev. B*, 10(7):2786–2788, Oct 1974.
- [73] C. M. Wilson and D. E. Prober. Quasiparticle number fluctuations in superconductors. *Physical Review B (Condensed Matter and Materials Physics)*, 69(9):094524, 2004.
- [74] V. Narayanamurti, R. C. Dynes, P. Hu, H. Smith, and W. F. Brinkman. Quasiparticle and phonon propagation in bulk, superconducting lead. *Phys. Rev. B*, 18(11):6041–6052, Dec 1978.
- [75] B. Pannetier, D. Huet, J. Buechner, and J. P. Maneval. Ballistic propagation of near-gap phonons in bulk superconducting tin. *Phys. Rev. Lett.*, 39(10):646–649, Sep 1977.
- [76] B. Pannetier and J. P. Maneval. Measurement of phonon lifetimes in bulk superconducting tin. *Phys. Rev. B*, 23(1):85–98, Jan 1981.
- [77] R. Yagi. Charge imbalance observed in voltage-biased superconductor–normal tunnel junctions. *Physical Review B (Condensed Matter and Materials Physics)*, 73(13):134507, 2006.
- [78] C. C. Chi and John Clarke. Quasiparticle branch mixing rates in superconducting aluminum. *Phys. Rev. B*, 19(9):4495–4509, May 1979.
- [79] J. Jochum, C. Mears, S. Golwala, B. Sadoulet, J. P. Castle, M. F. Cunningham, O. B. Drury, M. Frank, S. E. Labov, F. P. Lipschultz, H. Netel, and B. Neuhauser. Modeling the power flow in normal conductor-insulator-superconductor junctions. *Journal of Applied Physics*, 83(6):3217–3224, 1998.

-
- [80] A R Long. The attenuation of high frequency phonons in metals. *J. Phys. F: Met. Phys.*, 3:2023–2039, 1973.
- [81] T. Zijlstra, C.F.J. Lodewijk, N. Vercruyssen, F.D. Tichelaar, D.N. Loudkov, and Klapwijk T.M. Epitaxial aluminium nitride tunnel barriers grown by nitridation with a plasma source. *Applied Physics Letters*, 91(23):233102, 2007.
- [82] R. S. Keizer, S. T. B. Goennenwein, T. M. Klapwijk, G. Miao, G. Xiao, and Gupta A. A spin triplet supercurrent through the half-metallic ferromagnet CrO₂. *Nature*, 439(7078):825–827, 2006.

Résumé

Refroidissement électronique à base de jonctions tunnel supraconductrices

Au cours des dernières années, le refroidissement des électrons par effet tunnel dans des jonctions hybrides composés de métal Normal - Isolant - Supraconducteur (N-I-S) a suscité de plus en plus l'attention. Son principe repose sur un effet tunnel sélectif en énergie en raison de la présence d'une bande interdite Δ dans la densité d'états du supraconducteur. Avec une tension de polarisation inférieure à l'énergie du gap, seuls les électrons de plus haute énergie peuvent traverser l'interface du métal normal par effet tunnel, laissant derrière eux les électrons de moindre énergie.

Nous avons mesuré la conductance différentielle de jonctions S-I-N-I-S avec une grande résolution. Son analyse nous renseigne sur la température électronique du métal normal en fonction de la tension. Un modèle quantitatif est proposé qui inclut le couplage électron-phonon et la résistance dite de Kapitza, à l'interface avec le substrat. Avec ce modèle, nous avons réalisé une description détaillée du courant électronique et du flux de chaleur. Nous avons également montré que la température des phonons dans le métal normal baisse sensiblement au-dessous de la température du substrat.

À très basse température ($T < 200$ mK) et à faible tension de polarisation, le courant d'Andreev cohérent en phase domine le courant des quasi-particules. En analysant quantitativement l'équilibre thermique dans la jonction S-I-N-I-S, nous avons démontré que le courant d'Andreev transporte de la chaleur. Cette contribution thermique chauffe les électrons du métal normal.

Le refroidissement électronique à la tension de polarisation optimum ($V \sim 2\Delta/e$) dans la jonction S-I-N-I-S est un problème bien connu mais qui reste en suspens. L'effet de refroidissement dans la jonction S-I-N-I-S est accompagné par l'injection de quasi-particules dans les électrodes supraconductrices. Nous avons proposé un modèle simple pour la diffusion de l'excès des quasi-particules dans l'électrode supraconductrice possédant un piège métallique. Le modèle de diffusion a une solution analytique qui prédit la température minimum de refroidissement susceptible d'être atteinte.

Mots clés:

Supraconductivité – jonction S-I-N – effet tunnel quantique – refroidissement électronique – courant Andreev – nano-électronique quantique

Abstract

Electronic refrigeration using superconducting tunnel junctions

In the recent years, nano-refrigeration using electron tunneling in hybrid Normal metal - Insulator - Superconductor (N-I-S) junctions has gained increasing attention. Its basic principle is the energy selective tunneling due to the presence of an energy gap in the superconductor density of states. With a sub-gap voltage bias, only the most energetic electrons can tunnel out of the normal metal, leaving behind the electrons with less energy.

We have measured with a high resolution the differential conductance of S-I-N-I-S junctions, whose analysis gives us an access to the normal metal electronic temperature as a function of the voltage. A quantitative model is proposed, that includes the electron-phonon coupling and the Kapitza resistance at the interface with the substrate. With this model, we have achieved a thorough description of the charge and heat currents. We have also shown that the normal metal phonon temperature drops significantly below the substrate temperature.

At very low temperature ($T < 200\text{mK}$) and low bias, the phase coherent Andreev current dominates the quasi-particle current. By analyzing quantitatively the heat balance in the S-I-N-I-S junction, we demonstrate that the Andreev current does carry heat. This thermal contribution heats the normal metal electrons, overriding over a large voltage range the tunneling-based cooling.

The electronic cooling at an optimal bias ($V \sim 2\Delta/e$) in a S-I-N-I-S junction is a known pending issue. Cooling effect in S-I-N-I-S junction is accompanied by the injection of hot quasi-particles in the S electrodes. We have proposed a simple model for the diffusion of excess quasi-particles in a superconducting strip with an external trap junction. The diffusion model has a complete analytic solution and predicts the minimum attainable temperature of the coolers.

Keywords:

superconductivity - S-I-N junction - quantum tunneling - electronic cooling - Andreev current - quantum nanoelectronics